A BIOCOMPATIBLE FLOW CHAMBER TO STUDY THE HEMODYNAMIC PERFORMANCE OF PROSTHETIC HEART VALVES

By

EK CHING NGWE

Bachelor of Science in Mechanical Engineering

Oklahoma State University

Stillwater, Oklahoma

2008

Submitted to the Faculty of the
Graduate College of the
Oklahoma State University
in partial fulfillment of
the requirements for
the Degree of
MASTER OF SCIENCE
December, 2010

A BIOCOMPATIBLE FLOW CHAMBER TO STUDY

THE HEMODYNAMIC PERFORMANCE OF

PROSTHETIC HEART VALVES

Thesis Approved:

Dr. Wei Yin

Thesis Adviser

Dr. David A. Rubenstein

Dr. Ronald D. Delahoussaye

Dr. Mark E. Payton

Dean of the Graduate College

To my beloved family

ACKNOWLEDGMENTS

I would like to take this opportunity to thank my advisor, Dr. Wei Yin for her patient guidance, support, and providing me a good environment for doing research. She always gave me suggestion and instruction on my research. I would specially like to thank her for the time she spent on checking my thesis report.

I would like to thank Dr. Rubenstein for his suggestion and advice on my thesis. I also want to thank Dr. Ronald D. Delahoussaye for serving on my thesis committee.

I would like to thank my lab colleagues at BELOS, especially Saravan Kumar, who has always been sharing his ideas regarding my research.

I also want to thank my family for their love and support.

At last, I would specially thank Chiew San Yap, my dearest girlfriend for her supports all the times.

TABLE OF CONTENTS

LIST OF TABLES

Table Page

LIST OF FIGURES

Figure Page

CHAPTER I

INTRODUCTION

Heart valve diseases claim more than 250,000 victims each year in the United States. One treatment is to replace the diseased heart valves with prosthetic heart valves (PHVs). PHVs have a long history of saving people's lives - about 4 million PHV replacements have been placed into patients over the past 50 years. There are two commonly used PHVs, mechanical heart valves (MHVs) and bioprosthetic heart valves (BHVs). The advantage of BHVs is that patients do not need anticoagulant treatment, but the morphological changes and the structure failures have limited their viability. MHVs have stronger mechanical properties than BHVs, so they have longer durability which can lower the chance of second valve surgery. However, the changes of hemodynamics following the placement of MHVs can increase the risk of thromboembolism and other cardiac complications, which can lead to mortality. Patients with MHV are required to have anticoagulant treatment for the rest of their life. These insufficiencies of current PHVs have led to the development of new PHVs, either better in designs or using better materials. Polymer heart valves have attracted scientists' attention as a viable alternative to MHVs or BHVs. This is not a completely new idea and it has been under investigation for nearly 50 years. However, none of the proposed polymeric heart valves are suitable for patient use yet. An ideal polymer heart valve should be a good combination of MHV

and BHV, which should not suffer from morphological changes, have good durability and should not cause thrombogenicity.

To evaluate the dynamic performance of PHVs, numerical simulation (e.g., computational fluid dynamics, or CFD), *in vitro* experiments and *in vivo* experiments can all be used. CFD can give a good estimation of flow dynamics induced by the heart valves, as long as the model is constructed with realistic geometry and flow conditions. *In vitro* experiments usually require a flow chamber to hold the heart valves, which can mimic the hemodynamic performance of the heart. The most commonly used flow chamber for this purpose is a left ventricular assist device (LVAD). However, the cost of LVAD is relatively high. *In vivo* experiments are more complicated than *in vitro* experiment because it requires heart valve implant into living animals' heart. Usually, these animals have similar heart structure or size compared to the human heart. *In vivo* experiment provides a better way to study the overall effects on a living object. In this study, we designed and manufactured a flow chamber, following the design of a LVAD, and use it to evaluate novel polymeric heart valves. Numerical simulation and *in vitro* experiments would be conducted to evaluate the suitability of this flow chamber to perform heart valve studies.

Hemodynamics and flow pattern changes induced by the implantation of PHVs can increase mechanical stress and lead to blood damage. Platelets and red blood cells are sensitive to altered mechanical stresses. Shear stress is the major mechanical stress that can cause platelet activation. Elevated shear stress can lead to platelet activation and thromboembolism. Abnormal shear stress can break red blood cells membrane elasticity and cause membrane damage. Hemoglobin in the red blood cells will be released into

surrounding fluid which will lead to the reduction of oxygen transportation by blood to other tissues in the body.

The major goal of this thesis was to **design and fabricate a flow chamber suitable for heart valve studies. We would test its biocompatibility towards blood under static and dynamic conditions.**

The specific aims of this study are listed as the following.

Specific Aim 1: To design and fabricate a flow chamber following the concept of a left ventricular assist device to study the performance of prosthetic heart valves.

Specific Aim 2: To investigate the biocompatibility of the flow chamber to platelets and red blood cells *in vitro*.

Specific Aim 3: To perform numerical simulation to study the flow dynamics in the flow system.

The flow chamber designed and fabricated through this study can be used in the future to evaluate hemodynamic performance of various PHVs. Knowledge obtained from this study would help us to design better PHVs (i.e., a polymeric heart valve) and benefit more patients in a long run.

CHAPTER II

BACKGROUND

2.1 Anatomy of the heart

Human heart contains four chambers and the function of the heart is to pump blood to the whole body. Two upper chambers are the right atrium and the left atrium. The right atrium, receives blood from vena cava (systemic circulation) and the left atrium receives blood from pulmonary veins (pulmonary circulation). Two lower chambers are the right ventricle and the left ventricle. The right ventricle collects blood from the right atrium and pumps blood to pulmonary circulation. While the left ventricle collects blood from left atrium and pumps blood to systemic circulation. The left ventricular pressure is higher than that of the right ventricle because the left heart supplies blood to everywhere in the body. As a result, the left ventricle is much larger and has a thicker wall than the right ventricle. The heart also has four unidirectional valves that prevent the backflow of blood when the chambers contract. The atrioventricular valves, between the ventricles and the atria, prevent the backflow of blood from the ventricles to atria during the contraction of ventricles. The pulmonary valve prevents the backflow from the pulmonary trunk to the right ventricle, while the aortic valve prevents backflow from aorta to the left ventricles (Frederic H.Martini and Judi L.Nath, 2009). Figure 2.1 shows

the layout of the chambers and the valves of the heart as well as blood flowing direction in and out of the heart.

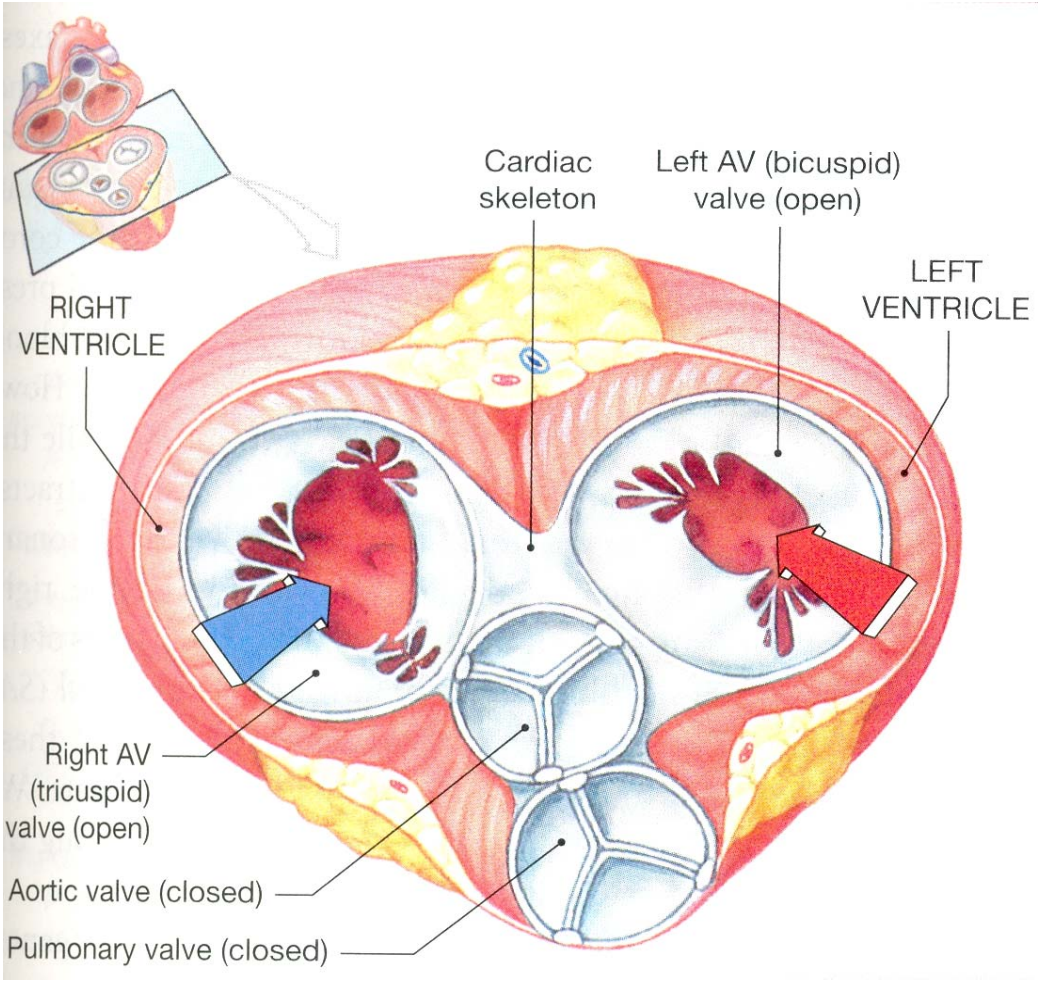

Figure 2.1: A model of transverse section of human heart which shows the location of different valves and blood flow direction (Frederic H.Martini and Judi L.Nath, 2009).

The cardiac cycle has two phases: diastole and systole. Diastole is part of the cardiac muscle relaxing, while systole is part of the cardiac muscle contracting during the cardiac cycle. The cardiac cycle usually takes about 800 msec and begins with atrial systole. When the atrial systole begins, about 70 percent of the normal ventricle capacities are already occupied by blood. As the atria contract, the pressure in the atrial increases and pushes the blood through AV valves to fill the remaining 30 percent. Each ventricle contains the maximum amount of blood at the end of atrial systole (end of ventricular diastole) and this amount is called the end-diastolic volume (EDV). The EDV for an adult standing at rest is about 130ml. Ventricular systole begins right after atrial systole ends. During this period, ventricular pressure keeps rising, until it is high enough to push open the valves (aortic valve and pulmonary valve), driving blood flow into the pulmonary and the aortic trunk. This is the beginning of ventricular ejection. When ventricular ejection starts, the left ventricle will eject 70 to 80ml of blood and this is known as stroke volume (SV) of the heart. During the end of ventricular systole, the pressure in the ventricular drops quickly. The amount of blood left in the ventricle when the pulmonary and aortic valve close is the end systolic volume (ESV). The ESV at rest is about 50ml and carries 40 percent of EDV (Frederic H.Martini and Judi L.Nath, 2009).

The relationship between the ventricular pressure and volume can be presented in Wiggers diagram (Krisnan B.Chandran et al., 2007a). Wiggers diagram is a standard diagram that used in cardiac physiology. It interprets the relationship of the volume changes in the ventricular chamber with the atrial and ventricular pressure. Wiggers diagram can be used as a standard research that is related to human heart. Figure 2.2 shows the Wiggers diagram in one cardiac cycle.

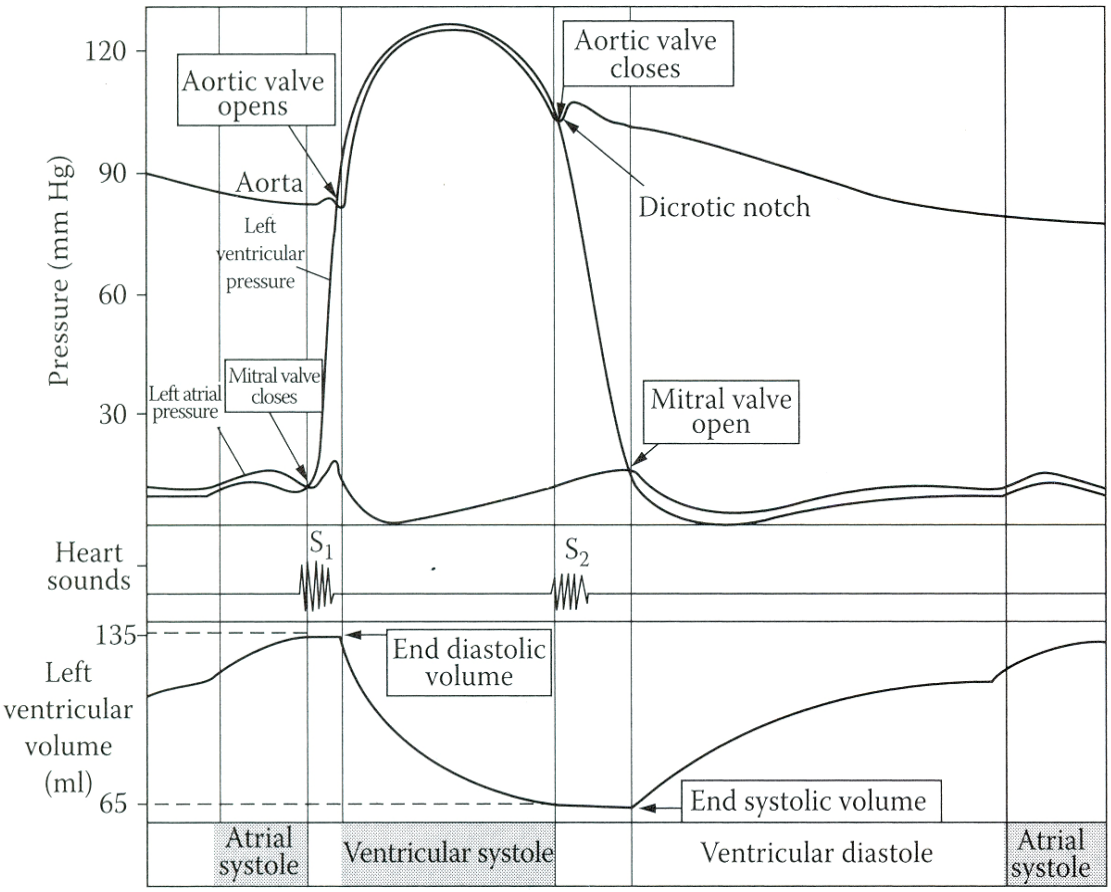

Figure 2.2: The Wiggers Diagram demonstrated the relationship between the pressure and volume changes in one cardiac cycle (Krisnan B.Chandran et al., 2007a).

2.2. Prosthetic heart valves

Heart valve disease is one of the major complications of the cardiovascular system and can lead to heart muscle disease. It can be caused by rheumatic fever, ischemic heart disease, bacterial or fungal infection, connective tissue disorders, trauma, and malignant carcinoid (Krisnan B.Chandran et al., 2007b). Any valve that causes the heart to unable to maintain normal circulatory flow is considered a diseased heart valve and the patient is called to have valvular disease (VHD). VHD always falls into two categories: stenosis and incompetence. The stenotic heart valve prevents the valve from opening fully due to the stiffened valve tissue. As a result, more work is required to push blood through the valve. On the other hand, the incompetent valve causes inefficient blood circulation and causes a backflow of blood into the heart. Both these conditions reduce the efficiency of the heart and increase stresses and strains on it. PHVs are commonly used today for replacing degenerated heart valves. About 4 million PHVs were used in patients over the past 50 years, and sometimes a heart valve replacement surgery is the only option for VHD patients. It is believed that the total number of replacement will increase to 850,000 per year by 2050 due to the higher rate of population increase (Yacoub and Takkenberg, 2005).

PHVs can be either mechanical, polymeric or bioprosthetic. Among all the PHVs used, about 55% of them are mechanical ones and the remaining 45% are biological (Butany et al., 2003).

Mechanical heart valves (MHV) have been in use since 1950s. The very first MHV implanted into a human patient was a Hufnagel Valve, placed in the descending

thoracic aorta in 1952 (Hufnagel et al., 1954). The disadvantage of this design is that it can only be placed in the descending thoracic aorta instead of the heart itself, so it did not really solve the problem. However, it was a great achievement because it showed that PHVs could be used to treat VHD. Based on the design of the Hufnagel Valve, Starr-Edwards caged ball valve was successfully implanted in 1960. The ball was trapped in a strut cage at both ends but could move freely (Figure 2.3A). The idea for the design was to reduce thrombus formation around the sewing ring (Grunkemeier et al., 2000). However, the ball blocked the center flow of blood and generated a wake of stagnant blood flow which led to a higher rate in thromboembolism (Yoganathan et al., 2004). In contrast, monoleaflet tilting valves and bileaflet valves can offer more physiological flow compared to Starr-Edwards caged ball valves. Single leaflet or tilting disk valves were introduced in later 1960s. These valves have a significant improvement compared to caged ball valves. They can provide more central flow of blood and reduce the risk of thromboembolism. Bjrok-Shiley was the first successful tilting-disk valve and was introduced to the world in 1969 (Bjork, 1969). The valve consisted of a single leaflet at the center which was held by a strut (Figure 2.3B). It provided good center flow and can prevent blood regurgitation. Unfortunately, strut fracture and thromboembolism were the main problems of the valve. Because of these problems, the production of the flat disc and convexo-concave disc Bjrok-Shiley valves was stopped in 1986 (Butany et al., 2003). St. Jude bileaflet MHV is the most commonly used MHV nowadays, which was introduced to the world in 1977. It was the first bileaflet valve that was made of pyrolitic carbon coated with graphite (Sun et al., 2009). It consists of two leaflets which can move around butterfly hinges (Figure 2.3C). This design provides the valve leaflets more

freedom in movement and helps to reduce the inertia for valve opening and closing. The advantages of bileaflet valves include that 1) the flow through the valve opening is symmetric, 2) there is little turbulence and more central flow compared to previous valves (Butany et al., 2003). However, patients with this type of valves still need lifelong anticoagulant treatment.

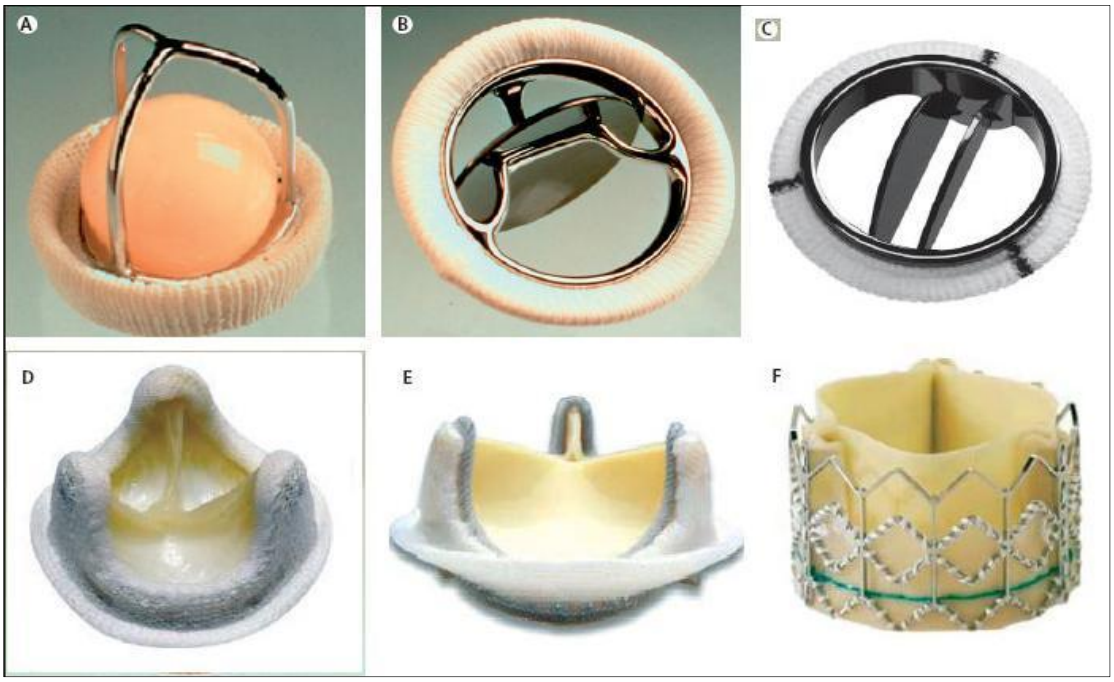

Figure 2.3: Different models of PHVs. (A) Starr-Edwards caged ball valve. (B) Bjork-Shiley tilting-disk valve. (C) St. Jude bileaflet valve. (D) Medtronic HK II ultra porcine valve. (E) Carpentier-Edwards Perimount bovine pericardial valve. (F) Edwards SAPIEN transcatheter pericardial aortic valve (Sun et al., 2009).

Bioprosthetic heart valves (BHV) were the solution to the thromboembolism problem faced by MHVs. BHVs are valves that are taken from animals. After certain chemical processes, they are suitable to be placed into human patients. Porcine valves are the most widely used BHV in the market because their structure is the closest to a human valve (Figure 2.3 D). Potential risks associated with BHV implantation include calcification and possible immune responses. Compared to MHVs, BHVs provide better hemodynamics since they are natural valve and can provide a better central flow. Patients with BHVs do not need anticoagulant treatments. Hancock valve is the first porcine valve that was manufactured commercially in 1970. It solved the hemodynamics problems that MHVs cannot solve in many years. However, morphological failure has limited the success of the valve. Research has shown that tissue calcification was the main reason for the valve failure (Bortolotti et al., 1988). Calcification makes leaflet cusp stiff, resulting in stenosis and valve failure. It was also suggested that that porcine BHVs should be removed until a better bioprosthetic with better durability appear. Carpentier-Ewards Perimount valve has improved the design by minimizing leaflet cusp stress and durability (Figure 2.3E). However, studies have shown that the valve was a good BHV for mitral valve replacement but only for patients older than 60 years old of age (Marchand et al., 2001). As a result, it limited the implantation for patients of certain age. Stentless bioprosthetic valves are different from stented bioprosthetic valves (Figure 2.3F). Stentless valves have no frame on the structure, which can increase orifice area and provide better central flow. But a meta-analysis study has found that patients with stentless valve would have larger left ventricular mass regression compared to the patients with stented valve (Kunadian et al., 2007).

Due to the limitations in MHVs and BHVs, people have turned their attention to polymeric heart valves. Researchers have hoped that with our advanced knowledge in new synthetic biomaterials and hemodynamics, we may be able to achieve a polymeric heart valve with better hemodynamic performances and mechanical properties. However, the early design of polymeric heart valves was not very successful because of the degradation of the materials. Polymeric heart valves are usually designed to mimic the natural heart valve structure so they generally have suitable hemodynamic properties. Material is a critical factor for the success of a polymeric heart valve, in terms of biocompatibility and durability. In theory, synthetic polymeric heart valves have the potential to overcome the problem faced by MHVs and BHVs. However, low biostability, poor hemocompatibility, potential thrombogenicity and durability (Daebritz et al., 2004) are the major concerns that prevent polymeric heart valves from becoming an alternative option in heart valve replacement surgeries. If these problems can be solved, polymeric heart valves can serve as a good alternative to MHVs and BHVs.

2.3 Left ventricular assist device

Since the early 19th century, researchers have sought after a mechanical device that can mimic the activities of human heart to help or replace the heart with problems. However, it was only in 1950s that people started to use the mechanical devices to help patients with heart problems. In 1960s, the first ventricular assist device (VAD) was used on a human patient (Frazier, 2010). The initial function of VAD was to serve as a bridge to transplant, which means that it can help the patient survive until the donor heart becomes available. Nowadays, the number of patients with heart failure problems is increasing year by year and the heart donors are not sufficient to fulfill the patients' need

for a heart transplant. Mechanical circulatory support through a VAD has become an option to the patients who do not have a candidate for heart transplant. VAD also can be used as a destination therapy and provide long term support for the patients. However, the cost of a left VAD for destination therapy is a high burden for patients. According to REMATCH, the average cost for VAD destination therapy from surgery to hospital discharge was about $210,187 (Oz et al., 2003).

A VAD is usually connected between the heart and a major artery. It helps the patient's heart to pump blood throughout the whole body, by decreasing the workload of the heart. VADs are good mechanical circulatory devices. They provide a good flow environment for blood and are made with biocompatible materials.

VADs can also be used to study the *in vitro* performance of PHVs since they can provide a similar flow environment as what a normal heart can generate. However, the cost for the left VAD itself has prevented researchers from using them widely in their research laboratories. VADs that have a diaphragm are fairly commonly used. They generally consist of two fluid chambers separated by a flexible diaphragm. One of the fluid chambers contains blood and connects to the body with one inlet and one outlet. While another fluid chamber is filled with water or other fluid and connected to a pump. When the pump starts moving, it can generate pulsatile pressure upon the diaphragm. As the diaphragm deforms towards blood chamber, it pushes the blood to circulate. If a flow chamber with similar properties can be constructed, it will be ideal for researchers to conduct PHV studies at a low cost.

2.4 Computational fluid dynamics (CFD)

CFD uses numerical methods and computational calculations to analyze complex fluid problems. It can provide detailed, two or three dimensional, and time varying information on flow conditions in complex geometries. In recent years, CFD has been widely used to investigate the hemodynamic performance of PHVs. Using CFD, the flow pattern changes induced by the implantation of a PHV can be estimated. For most of the studies of this type, the major focus is usually placed on the flow downstream of the valve, turbulence formation, shear stress produced and velocity field.

Simon et al studied the three-dimensional hinge flow fields of a bileaflet mechanical heart valve under aortic conditions (Simon et al., 2010). They conducted the simulation by using Cartesian sharp-interference immersed-boundary methodology combined with a second-order accurate fraction step method. Their results indicated that the three dimensional and unsteady flow fields near the hinge area were the major risk for platelet aggregation and thrombosis during systole. Their results suggested that the design of the leaflet ear, the upstream section of the leaflet edge, and the hinge recess wall curvature is of particular importance in achieving better hemodynamic performance and less thromboembolic complications for prosthetic heart valves. Smadi et al studied the pulsatile blood flow pattern through a dysfunctional mechanical heart valve (Smadi et al., 2010). They constructed five 2D numerical models with 0%, 25%, 50%, 75%, and 100% malfunction by Fluent 6.3.26 to study the velocity field, vortex formation and potential negative effects on blood components at the flow downstream. The results showed that the downstream of the malfunctioned valve, both the flow velocity and shear stress increased abnormally and there was a large number of vortices formation, which would

lead to the damage of the blood cells. These results indicated that the lateral velocity is as important as the central velocity, in the case of a dysfunctioned heart valve. King et al studied the effect of two leaflet opening angles on time-dependent 3D flows through a bileaflet mechanical heart valve (King et al., 1997). They constructed transient laminar 3D CFD models to study the hemodynamic performance of the bileaflet valve opening at 78 and 85 degree. The results indicated that the smaller the angle between leaflets the more shed vortices and flow separation would form, as well as higher shear stress. The results suggest that the orifice area for the central flow is also a very important factor to be considered for the valve design. Indeed, CFD models can provide detailed information on flow fields around the heart valves, and provide insight into new valve designs.

2.5 Platelets and prosthetic heart valves

Platelets are blood cells that look like flattened discs, with an average diameter of 4 μm and a thickness about 1 μm. Platelets usually circulate for 9 to 12 days before being digested by phagocytes. The average concentration of platelets in blood is roughly 350,000/μl. Platelets play an important role in hemostasis and thrombosis. They are the most important players in coagulation. .

Platelets are sensitive to mechanical forces, non-physiology flow patterns or contact with foreign materials. Flow factors that can cause the platelet activation include high shear and deformation rate, turbulence, and recirculation. Activated platelets enlarge in size and their shape become irregular with pseudopods sticking out. They express negative charge on their surface and release a lot of coagulant proteins from alpha granules and dense bodies. Among many other activation proteins, P-selectin are

expressed on activated platelet surface, and is usually considered platelet activation marker.

Implantation of MHV into a human heart can alter the fluid dynamics and induce platelet activation (Bluestein et al., 2004). Alemu et al studied the flow-induced platelet activation and damage accumulation in a mechanical heart valve by numerical simulation (Alemu and Bluestein, 2007). They found that on the pathways that platelets repeatedly pass through, they are exposed to increased stress around MHV leaflet and can be trapped in the wake of the valve. These will increase the potential of platelets activation. Smadi et al reported that the velocities and shear stress downstream of a dysfunctional valve increased abnormally as large numbers of vortices formed around the location (Smadi et al., 2010). All these factors can damage blood cells, especially platelets. Therefore, it is very important for us to pay attention to platelet behavior (especially platelet activation) when a new prosthetic heart valve is introduced.

2.6 Red blood cells and prosthetic heart valves

Red blood cells (erythrocytes) are the most abundant cells in blood, accounting for about 99.9 percent of the formed elements. Red blood cells are flexible and they look like biconcave disks. A red blood cell can circulate in the body for 100-120 days before digested by macrophages. Hemoglobin is the major component and its primary function is to transport oxygen to tissues everywhere in the body. When the cell membrane of the red blood cell breaks, hemoglobin and other internal components are released into plasma. This is known as hemolysis. Hemolysis can lead complications like anemia, jaundice and congestive heart failure.

Hemolysis after PHV replacements has been recognized as one of the serious complications (Mecozzi et al., 2002). Elevated mechanical forces on red blood cells are known to be the primary cause of hemolysis in patients with PHVs. High shear stress, pressure changes, contact with foreign materials and turbulent flow can all cause hemolysis. Among these factors, turbulence flow through PHVs is known to be the major factor that causes hemolysis due to the excessive shear force generated on the surface of red blood cells (Rodgers and Sabiston, Jr., 1969). Garcia et al studied the mechanisms of hemolysis with mitral prosthetic regurgitation (Garcia et al., 1996). They found that hemolysis with prosthetic heart valves was related to the flow disturbance in the jet flow and high shear stress. They also suggested that hemolysis was not related to the site of origin of the regurgitation and types of PHV implanted. Mild hemolysis occurs quite often in patients with PHV (Shapira et al., 2009). A study investigated on 170 patients with St. Jude Medical valves and 80 patients with Medtronic-Hall valves, and the results showed that the subclinical hemolysis rate was 51.2 percent for St. Jude heart valve and 17.8 percent for Medtronic-Hall heart valves (Shapira et al., 2009).

However, studies have shown that chance of hemolysis in patients with PHVs can be decreased by improving the design of heart valves (Maraj et al., 1998). Therefore, hemolysis should be used as a factor to determine the performance of a newly designed PHV.

CHAPTER III

MATERIALS & METHODS

3.1 Flow chamber design

3.1.1 Design of the flow chamber

The goal of this study was to build a biocompatible flow chamber similar to a left ventricular assist device to study hemodynamic performance of PHVs. The materials chosen to construct the flow chamber must be biocompatible. Ideally, the flow chamber would provide a similar flow environment to that of a heart. The flow chamber consists of three major parts: water chamber, testing fluid chamber (for whole blood, plasma and washed platelets), and transparent valve sockets.

3.1.2 Computer aided design (CAD) of flow chamber

We designed the three-dimensional water chamber, testing fluid chamber, and transparent valve sockets by using CAD software Pro-E Wildfire 4.0 PTC. A key design of the flow chamber was that the connections of the parts have to be as smooth as possible to minimize turbulent flow. Based on the computer aided design, the physical flow chamber was fabricated at OSU Physics machine shop.

3.1.3 Testing fluid chamber

The testing fluid chamber was the most important part in the flow chamber because this was the location where whole blood, plasma or washed platelets were stored and circulated. It serves as the left ventricle in the human heart. The testing fluid chamber was made from Teflon (Regal Plastic). From outside, the testing fluid chamber looks like two flat cylinders stacked together (Figure 3.1). The bigger (bottom) cylinder had a diameter of 6 inches and the smaller (top) cylinder had a diameter of 4.6 inches. The thickness of the bigger cylinder was 0.78 inches and smaller cylinder 1.18 inches. On the inside of the chamber, it was shaped as a half sphere with a diameter of 3.7 inches. The volume of the semispherical space was about 7.75 cubic inches which was equivalent to 127 milliliters. Two holes (1 inch in diameter) were drilled all the way through the semispherical space. These holes served as channels for testing fluid to circulate through PHVs. In each channel, a step with a height of 0.125 inch and a diameter of 1.315 inch was made for the placement of a PHV. An O-ring groove (4.28 inches external diameter, 0.13 thickness) at the opening of the semi sphere provided room for a sealing o-ring. Similarly, two O-rings were placed on the valve steps to prevent leaking. Six screw holes (0.25 inches) were made on the bottom cylinder, to connect it with the water chamber. On the top cylinder, 6 screws holes (0.20 inches) were drilled for the connection with the Valve Sockets. Figure 3.2 shows the detailed dimensions of the testing fluid chamber.

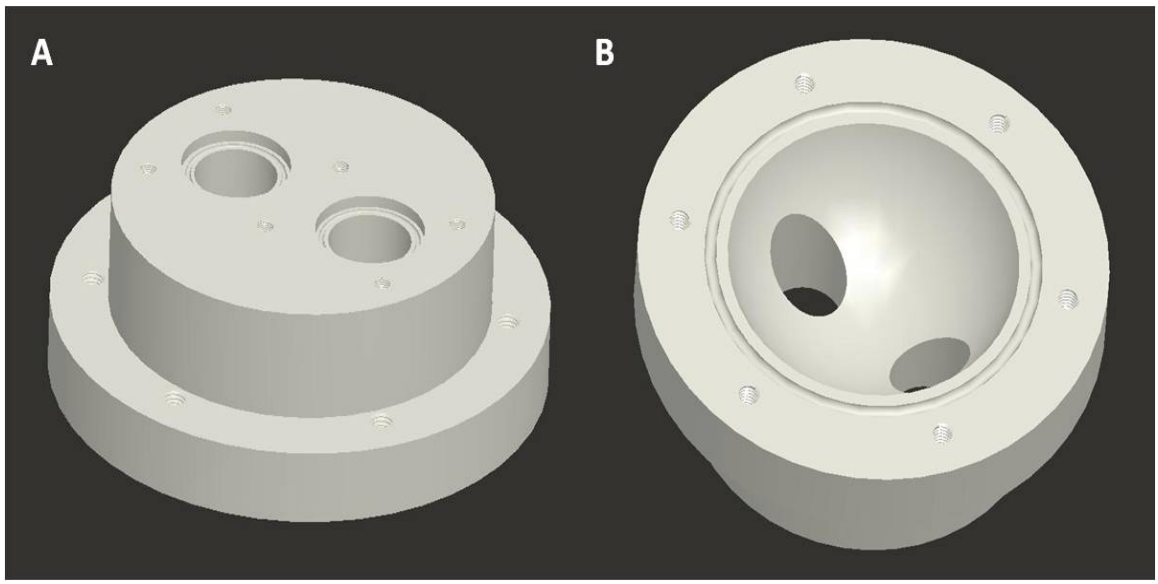

Figure 3.1: 3D CAD model of the testing fluid chamber. (A) The top surface of the testing fluid chamber. (B) The bottom surface of the testing fluid chamber.

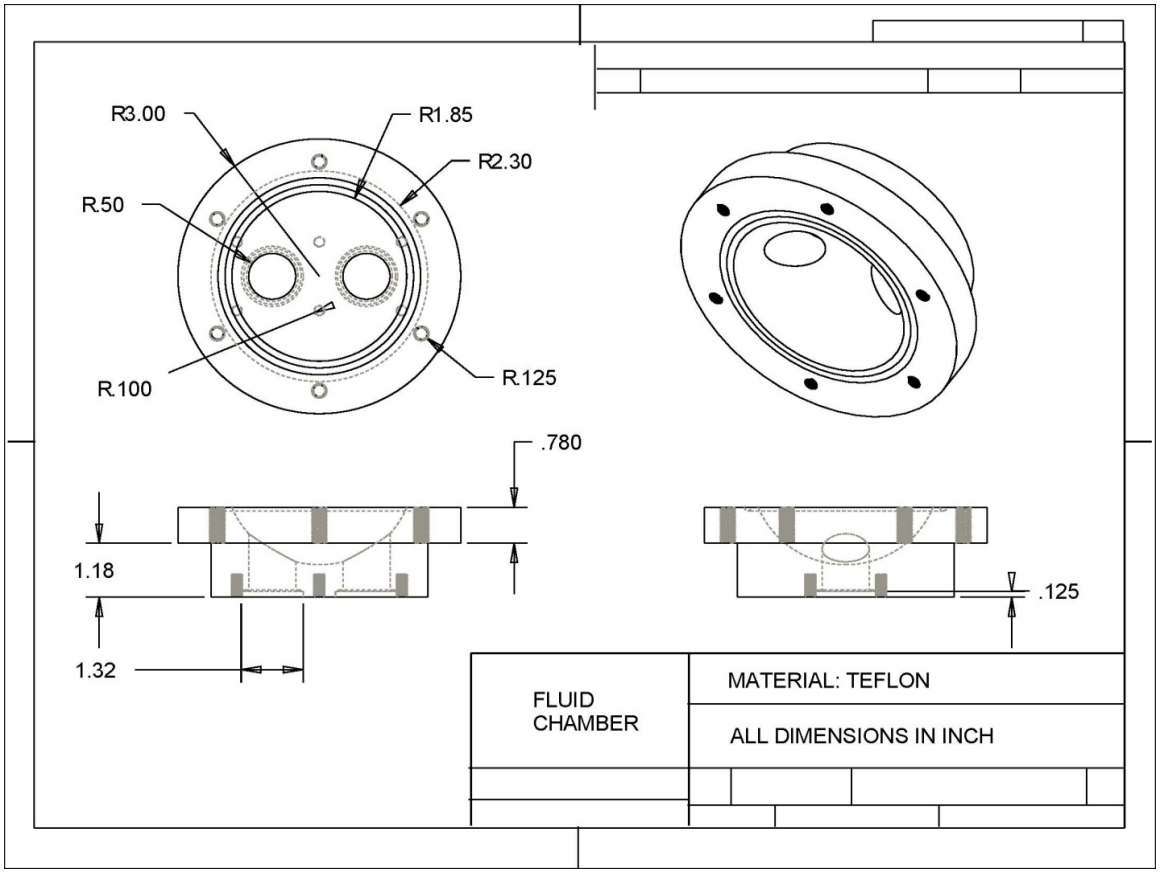

Figure 3.2: 2D CAD model of the testing fluid chamber with detailed dimensions. Figures are presented as the top, front, right hand and isometric views.

3.1.4 Water chamber

The water chamber had a similar design compared to the testing fluid chamber. This was the place where water is stored and connected to the reciprocating pump. Since this chamber does not have any contact with blood, plasma or blood cells, biocompatility is not required for the chamber material. However, for convenience, Teflon was used to build the housing of the water chamber as well. The inside and outside structures of the water chamber are the same as that of the testing fluid chamber as described above (Figure 3.3). On the bottom of the water channel, there were two threaded channels, to connect to two PVC pipes (average inner diameter 1.033", average outer diameter 1.315", Alsco Industrial Products, Inc.) The PVC pipes were threaded externally at one end and internally at the other. The externally-threaded end was connected to water chamber, while internally-threaded was connected to Brass Tapped Hose Adapter (A-665, ¾" MH x ¾" MIP x ½" tapped FIP, Lowe's). Teflon tape was used on the threaded surfaces to prevent leaking. Clear PVC was chosen because it can provide the visibility of the water flow and simplify the task of water filling. Six holes were made on the water chamber to match the holes on the testing fluid chamber so the two chambers could be attached together. Figure 3.4 provides the dimensions of the water chamber.

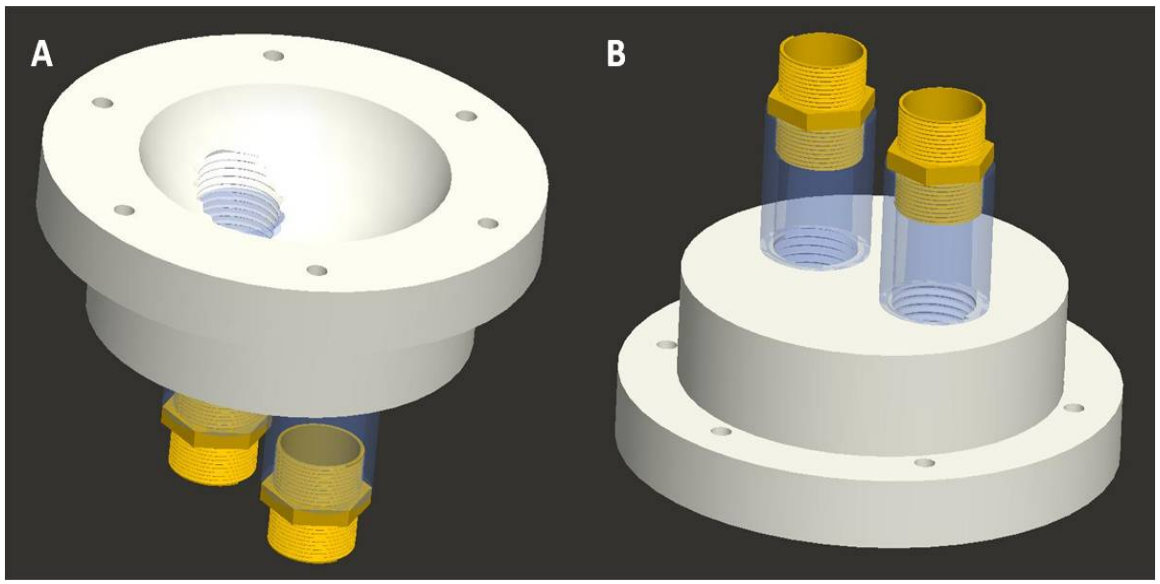

Figure 3.3: 3D CAD model of water chamber. (A) The top surface of the water chamber. (B) The bottom surface of the water chamber.

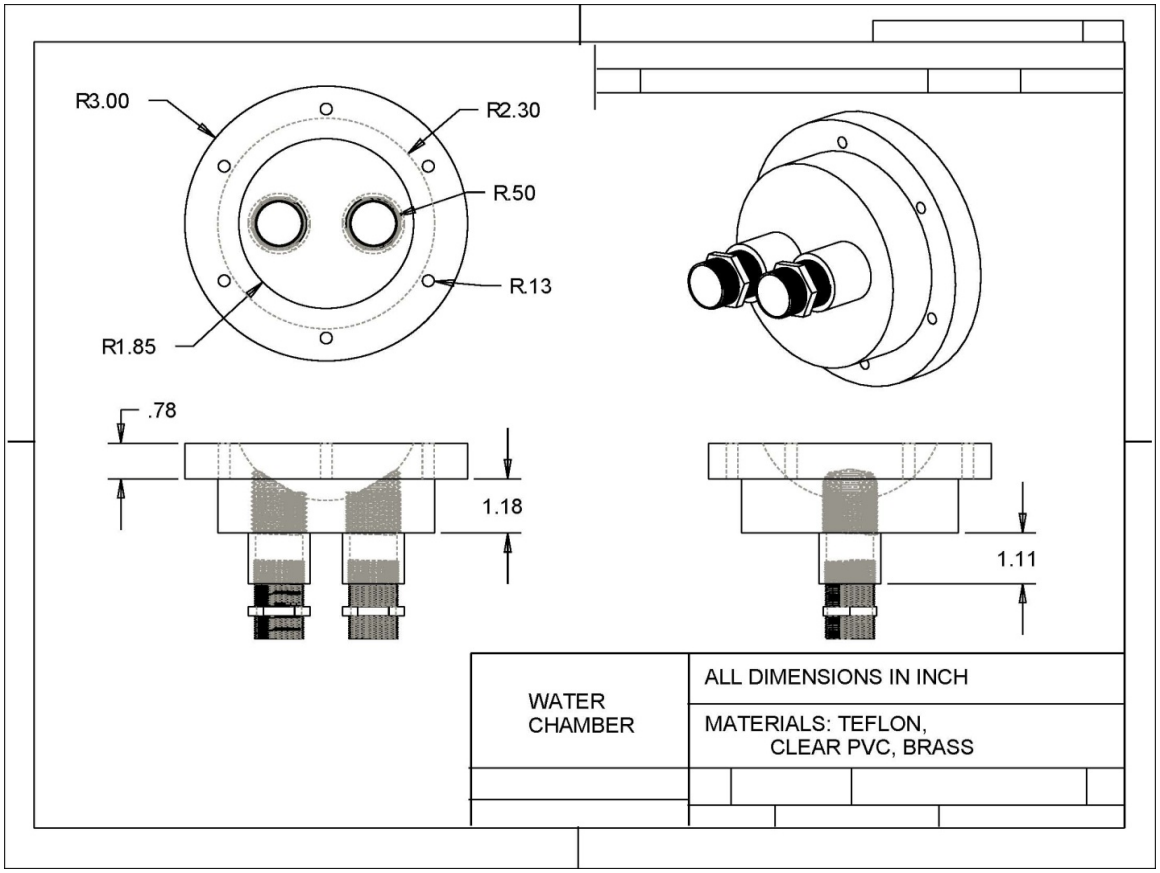

Figure 3.4: 2D CAD model of water chamber with detailed dimensions. Figures are presented as the top, front, right hand and isometric views.

3.1.5 Transparent valve socket

A transparent valve socket was connected to the top surface of testing fluid chamber and consisted of two small spaces to place PHVs. The two major parts of transparent valve socket were a clear plate and a pair of clear connecting tubings. Clear plate (Figure 3.5) was made from transparent PVC and the dimensions were 4 inches long, 2.5 inches wide, and 0.65 inches thick. There were two 1.125-inche holes in the middle of the plate and they were 2 inches apart, measuring from the center of the holes. The depth of the two holes was 0.25 inch. Two slightly bigger holes with a diameter of 1.315 inches with same centers were made at the bottom of the plate and the depth of these holes was 0.4 inches. Six holes that match the threaded holes on the surface of testing fluid chamber were made on the plate so that the plate and the testing fluid chamber can be screwed together. Figure 3.6 shows the 2D CAD design of clear plate with detailed dimensions. Clear connecting tubings (Figure 3.7) were made from clear PVC with a length of 1.5 inch. The internal diameter of the tubings was 1 inch. One Female Luer (female Luer thread style with ¼" Hex, Small Parts) connector was placed on each connecting tubing for filling and sampling. Figure 3.8 shows the 2D CAD design of clear connecting tubing with detailed dimensions. The transparent valve socket (Figure 3.9) was the combination of the clear connecting tubings and the clear plate. Both clear connecting tubings would insert into the holes of the clear plate. Figure 3.10 shows the 2D CAD design of transparent valve socket (combination of clear connecting tubings and clear plate) with dimensions.

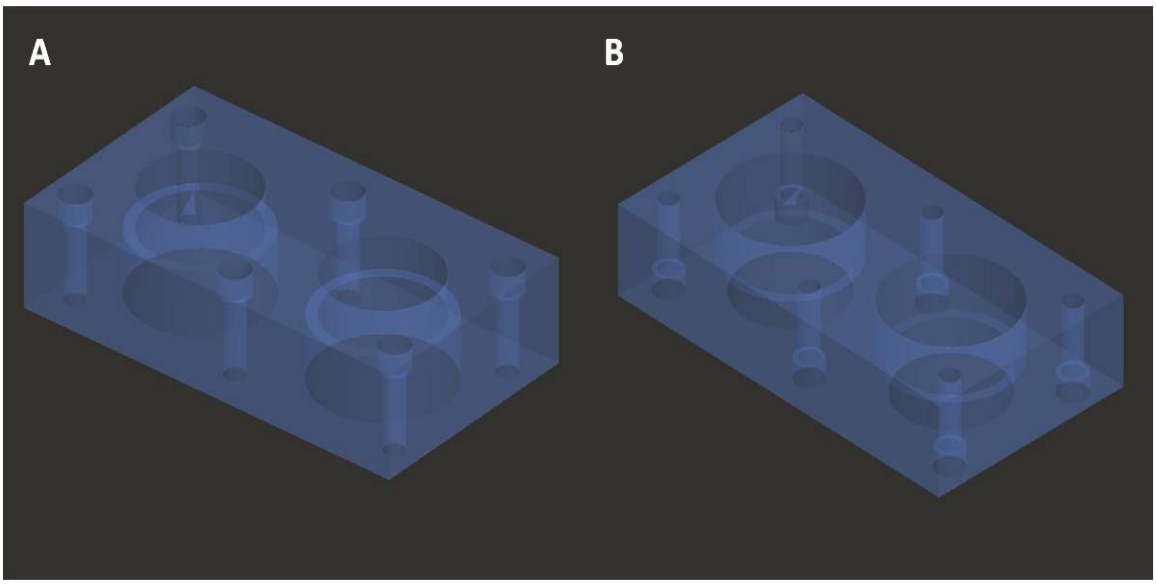

Figure 3.5: 3D CAD model of clear plate. (A) The top surface of the clear plate. (B) The bottom surface of the clear plate.

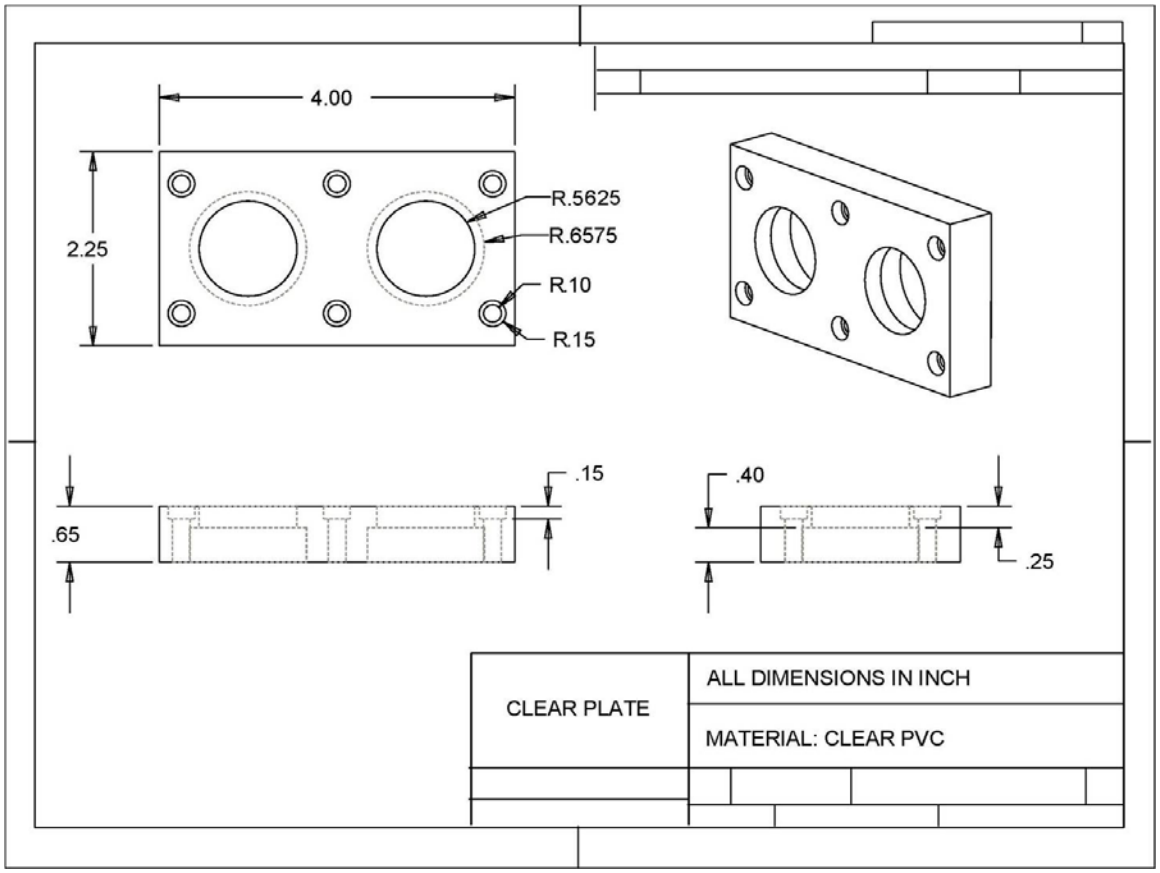

Figure 3.6: 2D CAD model of clear plate with detailed dimensions. Figures are presented as the top, front, right hand and isometric views.

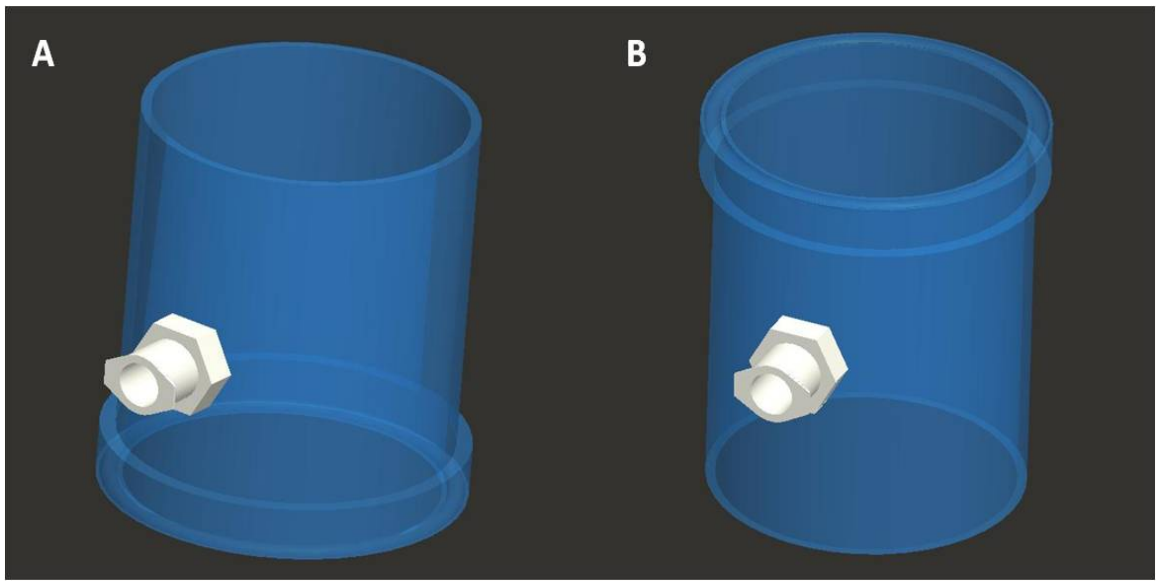

Figure 3.7: 3D CAD model of clear connecting tubing. (A) The top surface of the clear connecting tubing. (B) The bottom surface of the clear connecting tubing.

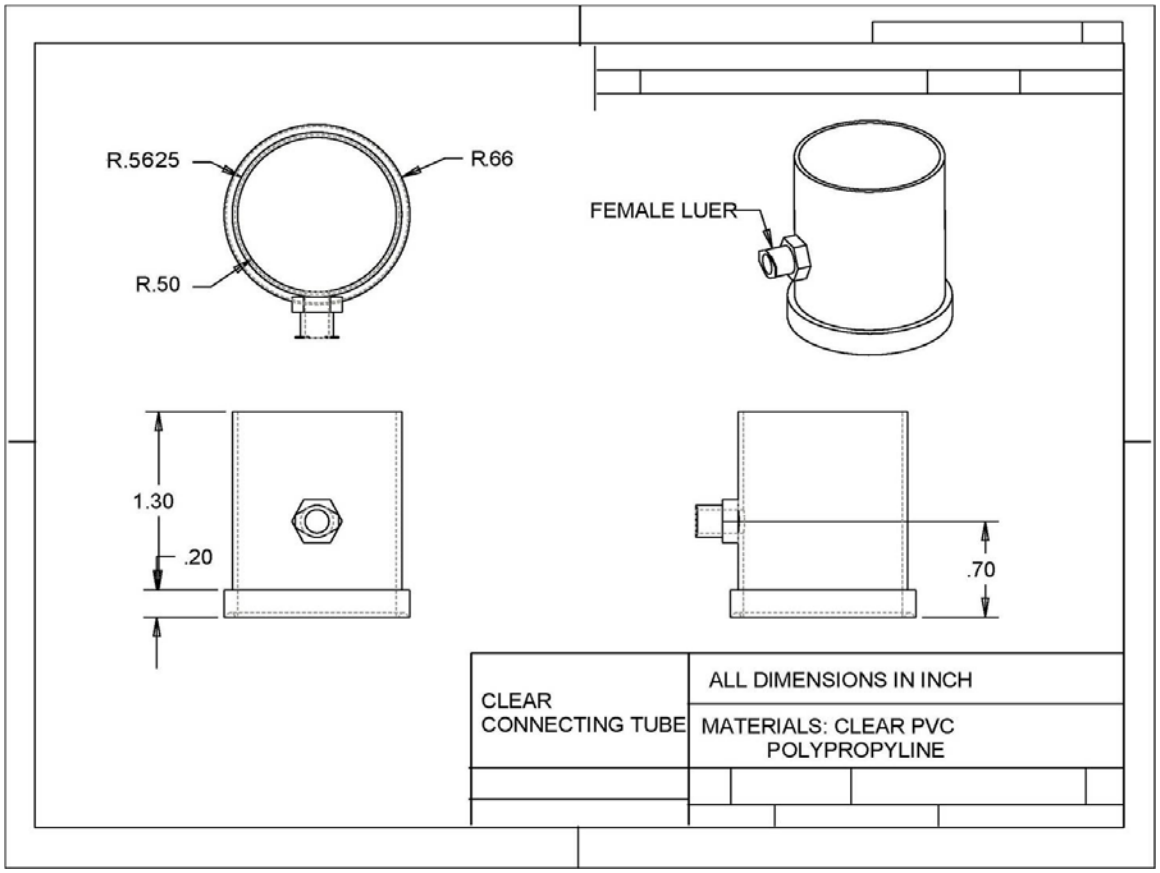

Figure 3.8: 2D CAD model of the clear connecting tubing with detailed dimensions. Figures are presented as the top, front, right hand and isometric views.

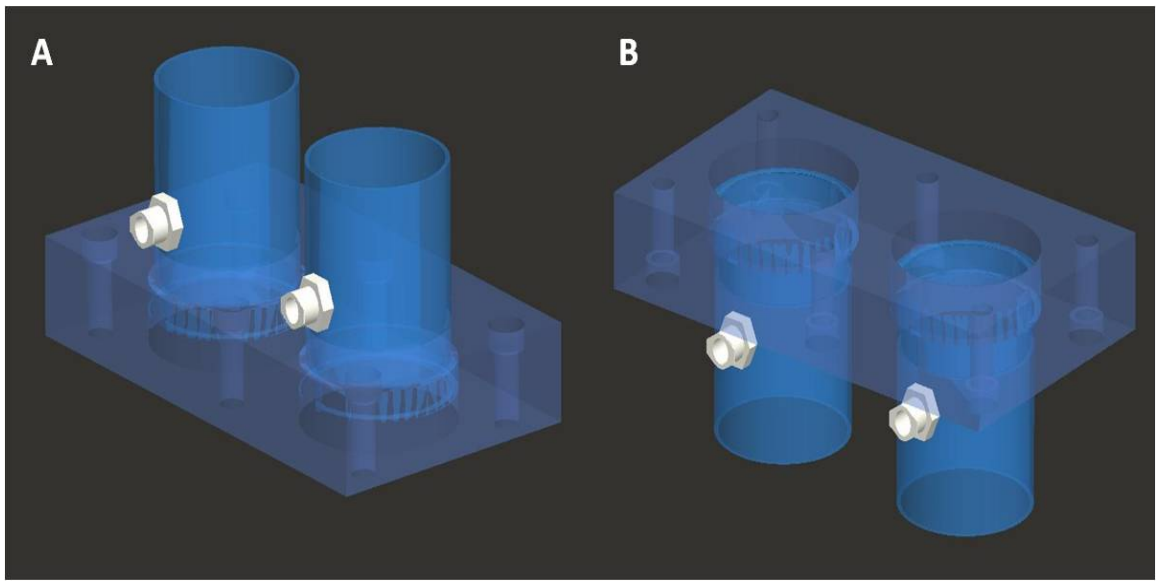

Figure 3.9: 3D CAD model of transparent valve socket. (A) Shows the top surface of the transparent valve socket. (B) Shows the bottom surface of the transparent valve socket.

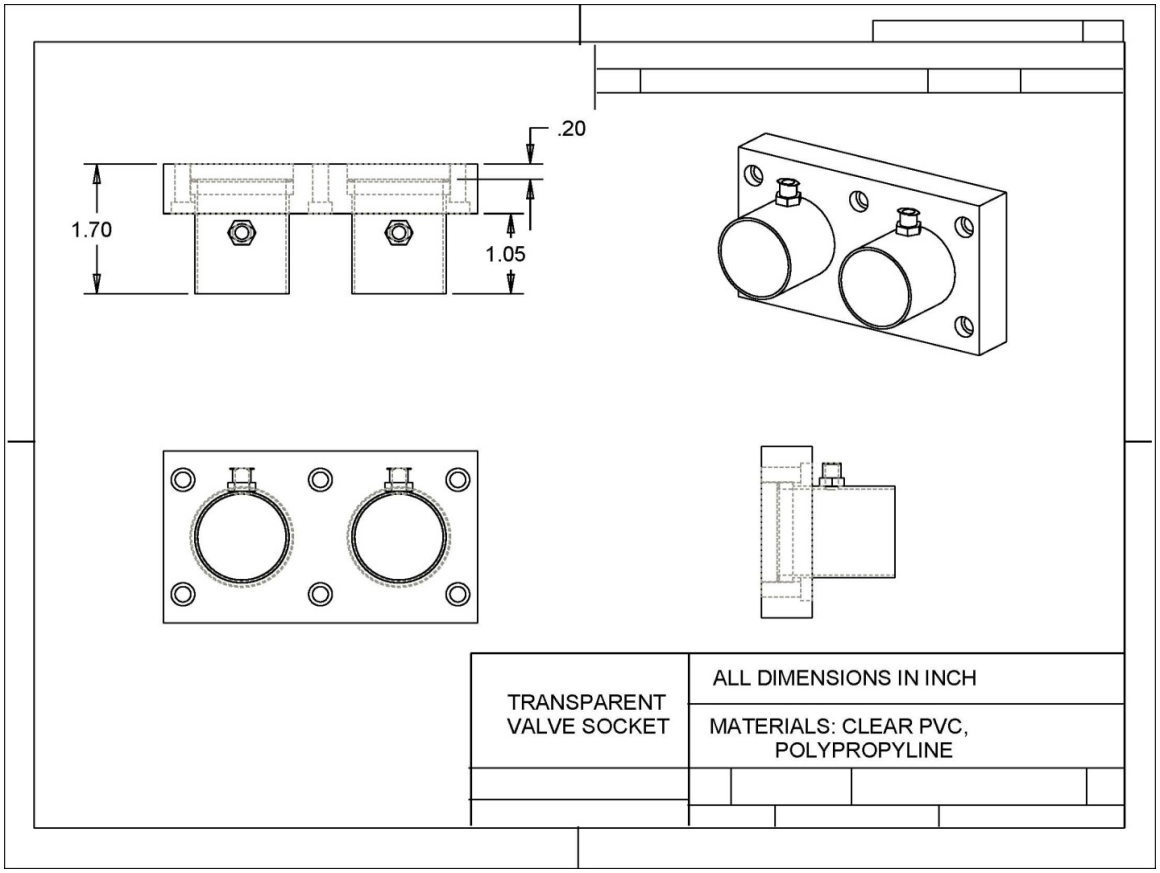

Figure 3.10: 2D CAD model of the transparent valve socket with detailed dimensions. Figures are presented as the top, front, right hand and isometric views.

3.1.6 Valve housing, diaphragm, O-rings, and Penrose tubing

Two St. Jude bileaflet mechanical heart valves (St. Jude Medical Inc.) were used as the control valves to test the dynamic performance of the flow chamber. The external diameter of the valve was 0.9913 inches without housing. The valve housing (Figure 3.11) was made from clear PVC (same material as the clear connecting tubing) and constructed in a ring shape with a thickness of 0.25 inch. The internal diameter of the valve housing was 1 inch, which allowed for the valve to be placed within it; the external diameter of the valve housing was 1.315 inch, which allowed the housing to sit tightly between the testing fluid chamber and the transparent valve socket. The valves were slightly smaller than the internal diameter of the valve housing, so a Teflon tape was used to wrap around the valves to ensure better fitting between them. Figure 3.12 shows the detailed dimension of the valve housing.

Diaphragm (Figure 3.13) of the flow chamber was made from Latex (Natural Latex Rubber Sheet, 0.025" thickness, Small Parts, Inc.). It was made to fit between the testing fluid chamber and the water chamber. Figure 3.14 shows the 2D CAD design of diaphragm with detailed dimensions.

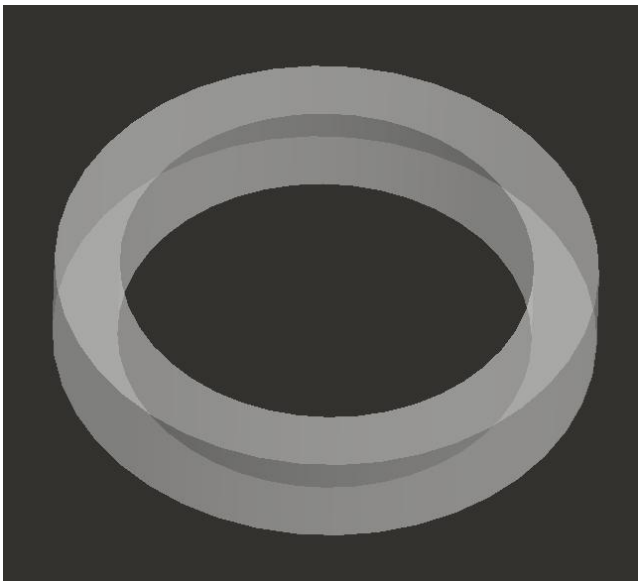

Figure 3.11: 3D CAD model of the valve housing.

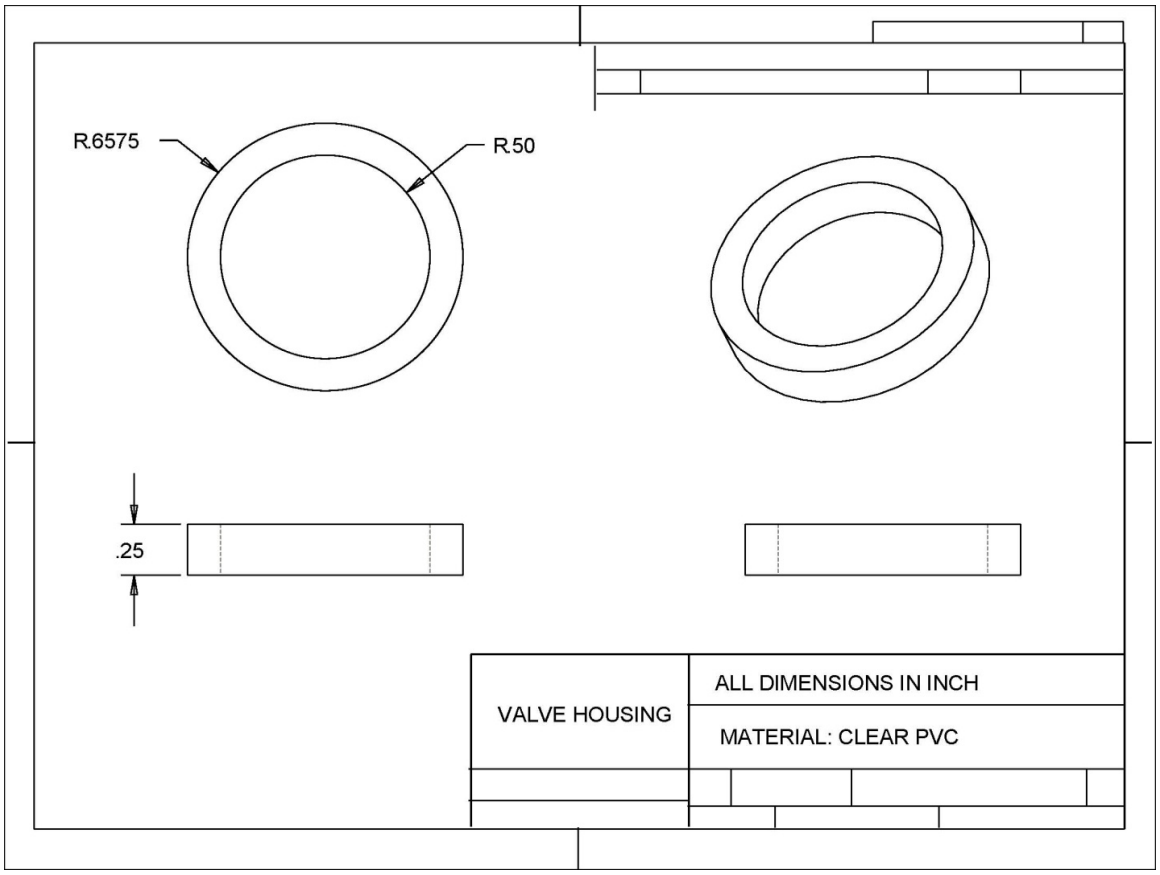

Figure 3.12: 2D CAD model of valve housing with dimensions and top, front, right hand and isometric views.

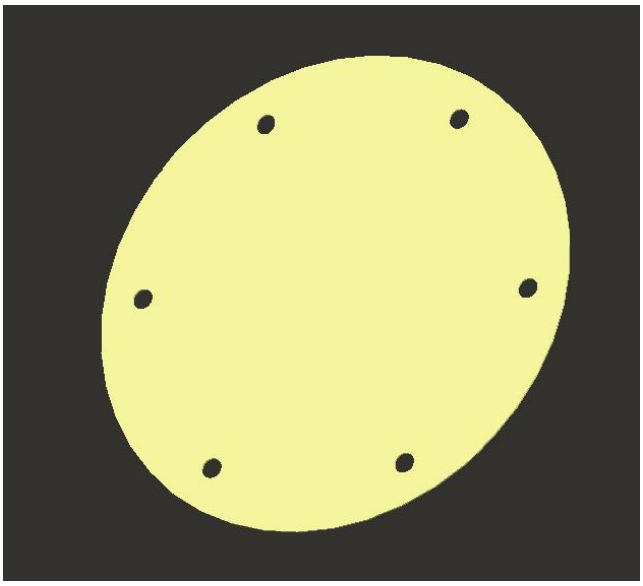

Figure 3.13: 3D CAD model of the diaphragm.

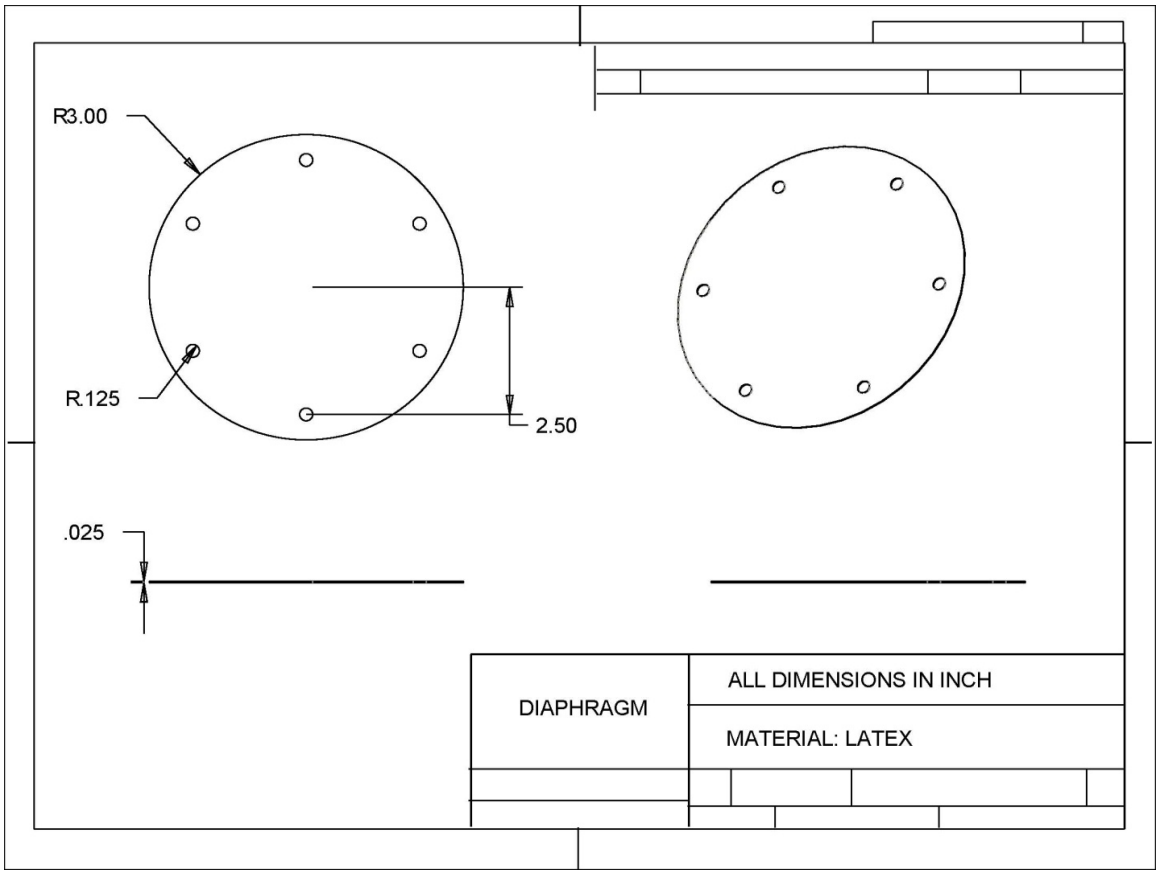

Figure 3.14: 2D CAD model of diaphragm with dimensions and top, front, right hand and isometric views.

The flow chamber had a total of five O-rings to prevent leaking. Two different sizes of O-rings were used: one bigger O-ring (internal diameter 4", external diameter 4.25", Small Parts) was placed between the testing fluid chamber and the water chamber; four smaller O-rings (internal diameter 1.125", external diameter 1.25", Small Parts) were placed between the testing fluid chamber and the valve housing, and between the valve housing and the transparent valve socket.

A 5.5-inch surgical Penrose tubing (Penrose Drain, 1" x 0.12" x 18", GF Health Products, Inc.) was used to connect the inlet and outlet of the testing fluid chamber.

3.1.7 Assembly

All the parts described above were assembled by screws and clamps. Two different sized screws were used. Six big screws (vented socket cap screw, inch thread size: ¼"-20, length: 1- ½", McMaster-Carr) were used to attach the testing fluid chamber and the water chamber. Stainless steel washers (round hole washer, internal diameter ¼", external diameter 0.6", McMaster-Carr) were used. Six small screws (vented socket cap screw, inch thread size: 10-32, length: 1", McMaster-Carr) were used to attach the transparent valve socket and the testing fluid chamber.

Silicon tubing (Peroxide-cured silicon tubing, internal diameter: ½", external diameter: 5/8", Cole-Parmer) was used to connect the flow device to the reciprocating pump (Harvard Apparatus Pulsatile Blood Pump for Large Animal, Harvard Apparatus) through the water chamber inlet/outlet. One end of the silicon tubing was connected to a brass machine female hose nut (½" FH x ¾" Flare, Lowe's). This fitting had a threaded adapter that can fit into the nipple of the water housing and the other end can fit in with

the silicon tubing that was connected to the reciprocating pump. In order to prevent leaking, when the pressure changed, hose clamps were used at the connection between the pump and the tubing. Stainless steel hose clamps (Murray #8 adjustable clamp, Lowe's) were used on the connection of silicon tubing and brass hose barbs; and acetal hose clamps (acetal snapper type hose clamp, for 5/8" outer diameter, 0.569-0.65 clamp internal diameter) were used on the connection of silicon tubing and the nozzle of the pump. Other bigger acetal hose clamps were placed at the connection between clear connecting tubing and Penrose tubing to prevent leaking when whole blood or plasma were circulated in the system. Figure 3.15 shows the assembling of all the components. Figure 3.16 shows the CAD assembled of the flow chamber. Figure 3.17 shows the desired flow direction in the flow device.

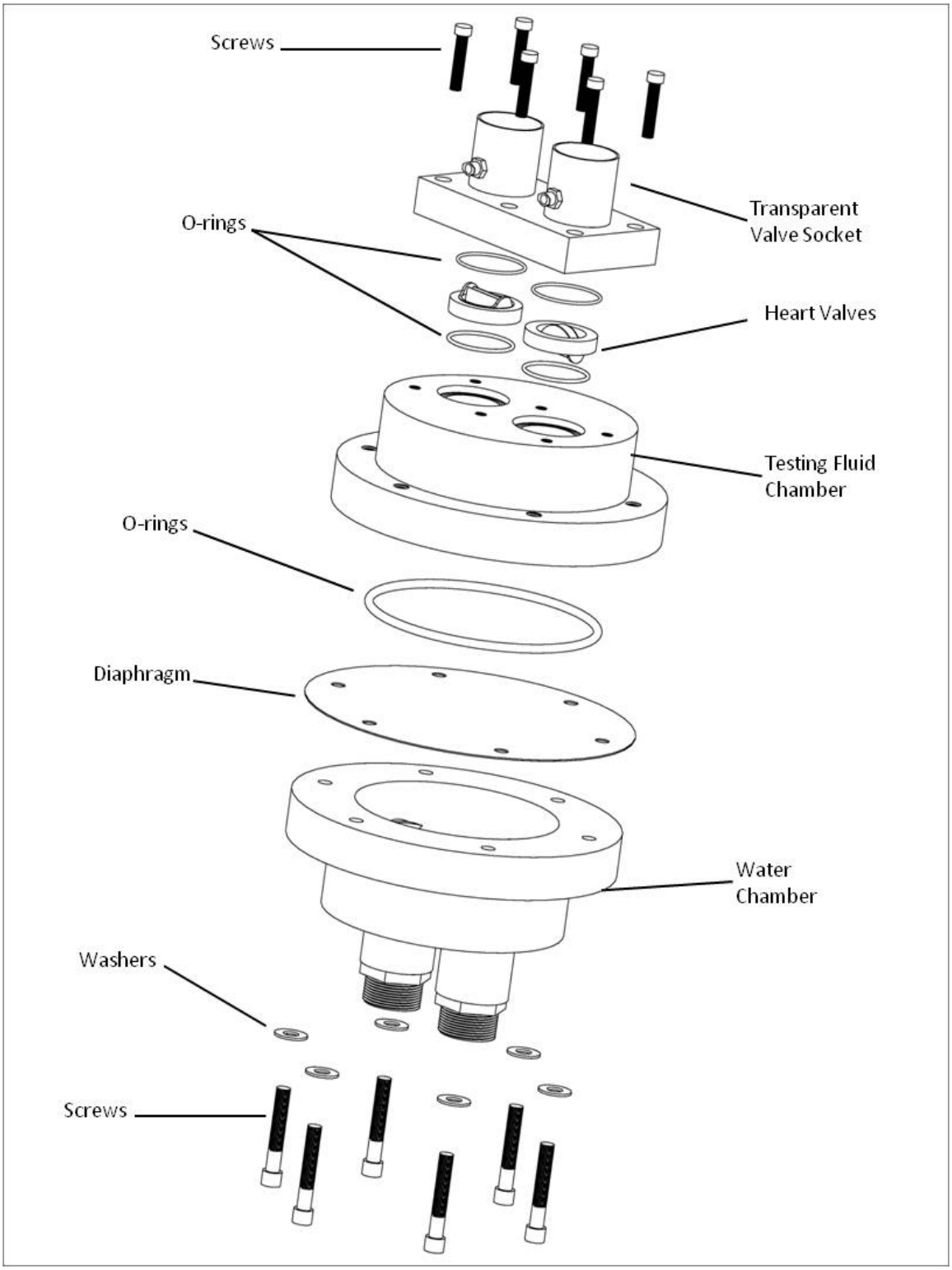

Figure3.15: CAD model of assembling of different components.

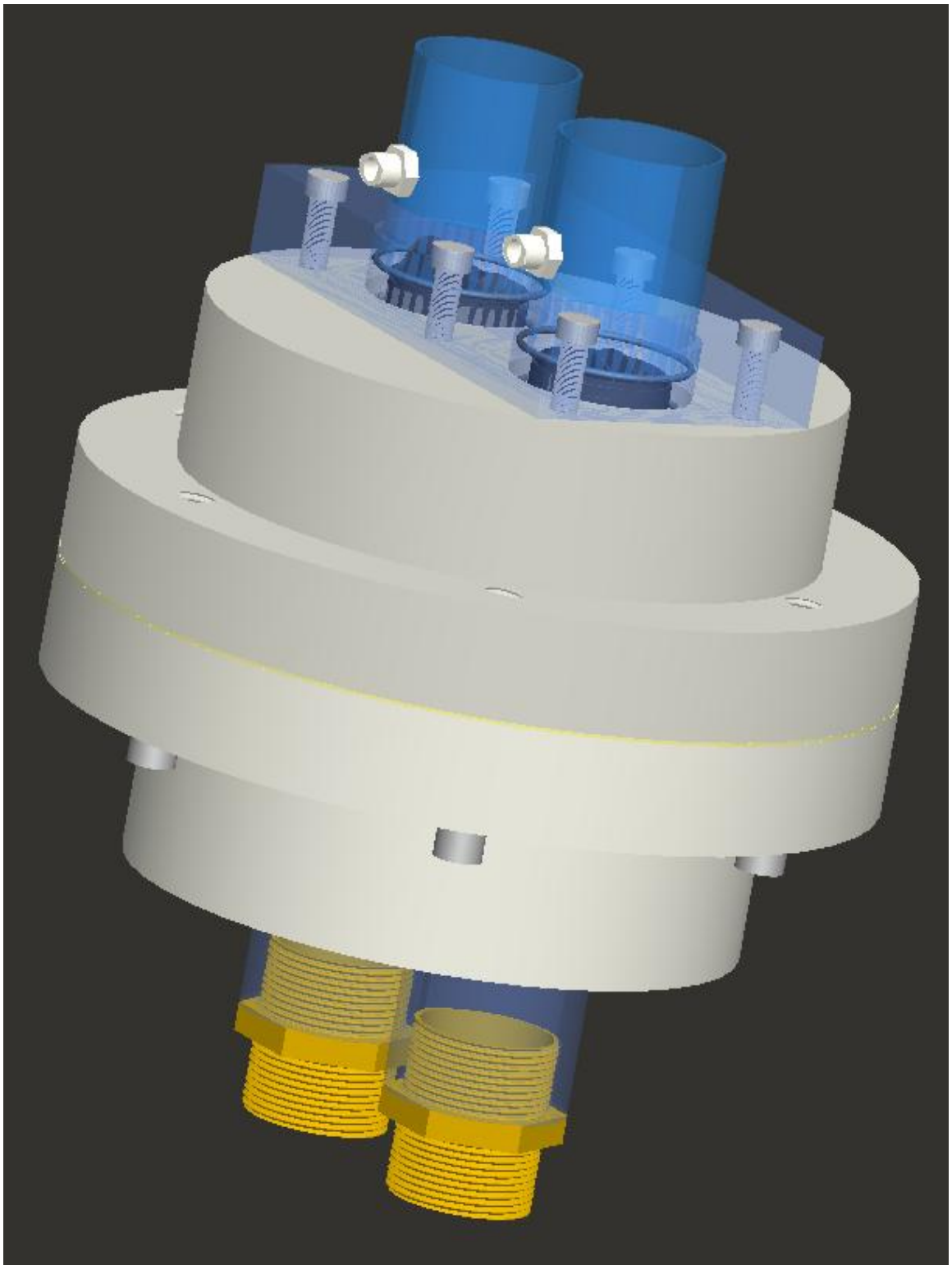

Figure 3.16: 3D CAD model of the assembled flow chamber

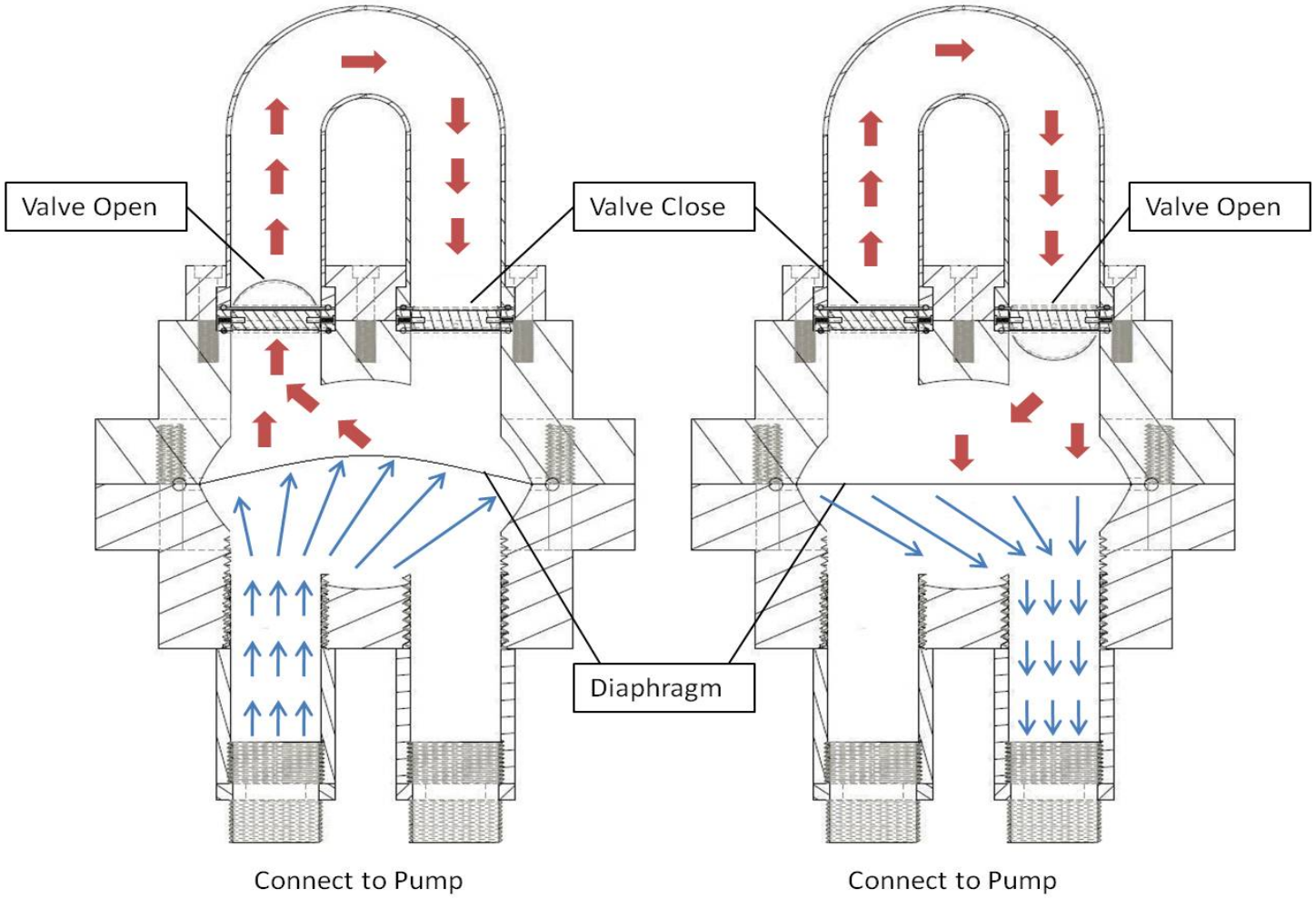

Figure 3.17: Desired flow direction in the flow chamber. Thin blue arrows indicate the flow direction of water and thick red arrows indicate the flow direction in the testing fluid chamber.

3.2 *In vitro* studies

3.2.1 Biocompatibility of the flow chamber towards washed platelets

Both foreign materials and altered shear stress induced by disturbed flow can trigger platelet activation. Therefore, platelet activities within the flow chamber was the first to be examined, under both static and dynamic conditions.

3.2.1.1 Platelets preparation

Platelet rich plasma (PRP) was obtained from Oklahoma Blood Institute. To make washed platelets, PRP was centrifuged at 1000xg for 9 minutes. Cell pellets were resuspended in platelet buffer, which contains 135 mM NaCl, 5 mM D-(+)-Glucose, 2.7 mM KCl, 0.5 mM Na_2HPO_4, 1 mM $MgCl_2$, 1 mM Sodium Citrate, 0.1% Bovine Serum Albumin, and 10 mM HEPES (pH 7.4, adjusted by adding NaOH). The final concentration of washed platelets was 100,000 cells/μl.

3.2.1.2 Platelet activation (CD62P expression) under static conditions

Before filling washed platelets into the testing fluid chamber, the flow system was rinsed with distilled water and platelets buffer for about 5 minutes. After that, washed platelets were filled into the testing fluid chamber through the filling port (with the sampling port open to remove the air bubbles). After all air bubbles were removed, both the sampling and filling ports were closed. For 5 hours, 10 ml platelet samples were taken every hour from the testing fluid chamber (the chamber was gently shake to prevent platelet settling) for P-selection expression measurement. To measure P-selection expression, FITC conjugated murine anti human CD62P (Ancell Corp.) (1:50) antibody

was added to platelet samples (100 µl) and incubated at room temperature for 30 minutes. Then 400µl of platelet buffer was added to each sample and analyzed by flow cytometry. Washed platelets that were kept in a test tube (without exposure to the flow chamber) served as the negative control. Positive control was achieved by Ionophore A23187 (200 µM, 5 minutes at 37ºC).

3.2.1.3 Platelet activation under dynamic conditions

The setup of dynamic experiments was similar to that of static experiments except that two St. Jude bileaflet mechanical heart valves were placed oppositely in the system to control flow direction. The water chamber was filled with water and connected to a Harvard reciprocating pump. About 250 ml washed platelets (100,000/µl) were placed in the testing fluid chamber. The flow rate of the system was fixed at 5 L/min with a stroke volume of 80 ml and stroke rate of 72 min^{-1}. The systolic/diastolic ratio was fixed at 0.375. The experiment was for 90 minutes and platelet samples were taken out from the circulation every 15 minutes by syringe through the sampling port. Platelet surface P-selectin expression was measured as discussed above. On average, one platelet stays approximately 7 days in circulation and passes through the aortic valve once every 90 seconds in its lifetime (Bluestein et al., 2004). Therefore, it is about 6700 valve passages for a normal platelet in its lifetime. The time chosen for the dynamic experiments was 90 minutes, corresponding to 8400 passages through the valves. The passages of the platelet in the chamber were sufficient to test the platelet activity *in vitro*.

3.2.2 Hemolysis measurement under static conditions

Biocompatibility of the red blood cells towards the testing fluid chamber was tested through hemolysis. Fresh whole blood (with dextrose, EDTA and Sodium citrate) was obtained from Oklahoma Blood Institute. 250 ml whole blood was placed into the testing fluid chamber under static conditions. 10 ml of blood samples were taken from sampling port every hour. Hemolysis was measured using a spectrophotometer (Beckman Coulter) at 540 nm. The hemoglobin concentration was calculated by:

Hemoglobin concentration = absorbance x concentration of hemoglobin standard/absorbance of hemoglobin standard, where the absorbance values were obtained from spectrophotometer measurements, and the hemoglobin standard (11.6g/dl) was purchased from Pointe Scientific Inc. Whole blood that was not exposed to the flow chamber served as negative control. Positive control was achieved by homogenizing whole blood (at 20,000 RPM, 55 Hz for 30 sec).

3.2.3 Red blood cells dynamic test

Similar experiments were conducted under dynamic conditions. For this set of experiments, two St. Jude bileaflet mechanical heart valves were placed in the testing fluid chamber to control flow direction. The experiment was run for 90 minutes and 10 ml of blood samples were taken from the sampling port every 15 minutes by a syringe. Hemolysis was measured and blood hemoglobin concentration was calculated as previously described.

At the end of the each experiment, all the components and valves were cleaned with caution. The flow chamber was dissembled to separate pieces and the valves were

taken from housing as well. Every single part was rinsed thoroughly with large amounts of distilled water, followed by 10% of bleach. After that, all the parts were rinsed with large amounts of distilled water again and washed with 0.01 M HCL. At the end, all parts were rinsed again with distilled water to ensure they were thoroughly cleaned. Penrose tubing was discarded after each use.

3.3 Numerical simulation

3.3.1 3D numerical model of the testing fluid chamber

The model of the flow device was constructed in ANSYS ICEM CFD 12.0. In this study we developed a 3D numerical model of the testing fluid chamber (the only part that is in contact with blood or plasma) with St. Jude bileaflet mechanical heart valves in the device to examine the fluid dynamics of the system.

The dimensions and geometrical information were based on the models constructed in Pro-E. The simulation was aimed to mimic and help us to visualize the realistic flow conditions in the flow chamber. The original driving force of the chamber circulation came from the reciprocating pump, whose movement induced a pressure difference in the water chamber, which in turn caused the flexible diaphragm to move up and down. The movement of the diaphragm caused the opening and closing of the heart valves, i.e., the circulation in the testing fluid chamber. Therefore, only the diaphragm, semispherical space of the testing fluid chamber, and the two flow channels with the valves were included in the model. The diaphragm was defined as the inlet of the fluid chamber and the two valves were constructed in fully opened or fully closed position. The maximum angle (compared to the horizontal plane) for the fully opened valve was 10

degree and the maximum closing angle was 85 degree (Figure 3.18). Two half circles (0.05 inches diameter) were used to mimic the hinge area of the St. bileaflet valve (Figure 3.19). Five dynamic positions were used to monitor the flow conditions during the outlet valve opening: when 0, 20, 40, 60, and 80 ml of fluid was pushed out the outlet valve. Table3.1 listed the height of the diaphragm with different volume change.

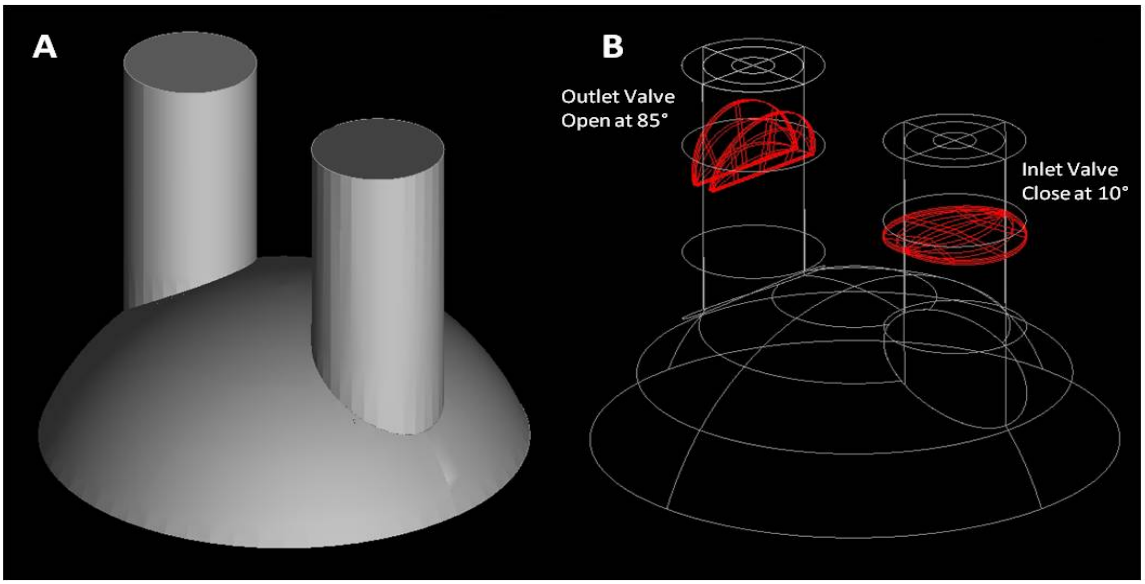

Figure 3.18: 3D numerical model of the testing fluid chamber. (A) 3D model of the flow system. (B) Valve location in the system, one valve was at fully opened position and the other valve at fully closed position.

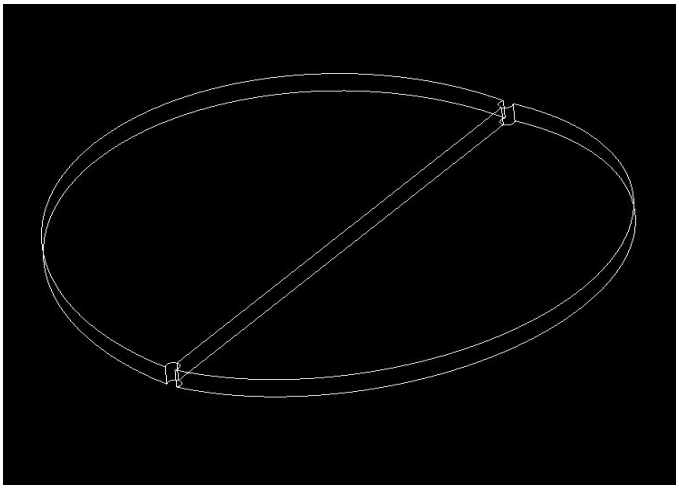

Figure 3.19: 3D model of fully closed valve with two small hinge areas at both ends.

Table 3.1- Diaphragm height (from equilibrium location) and the number of elements in different volumes.

Volume (ml)	Diaphragm height (inch)	Number of elements
0	0	781,207
20	0.17	782,083
40	0.34	781,535
60	0.51	777,681
80	0.68	776,801

3.3.2 Meshing

The model with the above discussed geometry was meshed with hybrid mesh using hexahedral and tetrahedral elements in ANSIS ICEM CFD 12.0.1. The areas of valves and the surfaces between the two channels and chamber were finely meshed because these were the regions of interest (total elements-298,562, average element size-0.03 inches). The reason of having different mesh sizes in the model was to compensate for the technical insufficiency of computational memory, especially when turbulent solver was used. Table 3.1 also shows the complete list of element numbers at different volume and diaphragm height. All results from the simulation were proved to be independent of mesh density. Figure 3.20 shows the meshing of the fluid chamber (at volume = 0 ml) and one valve (with two leaflets).

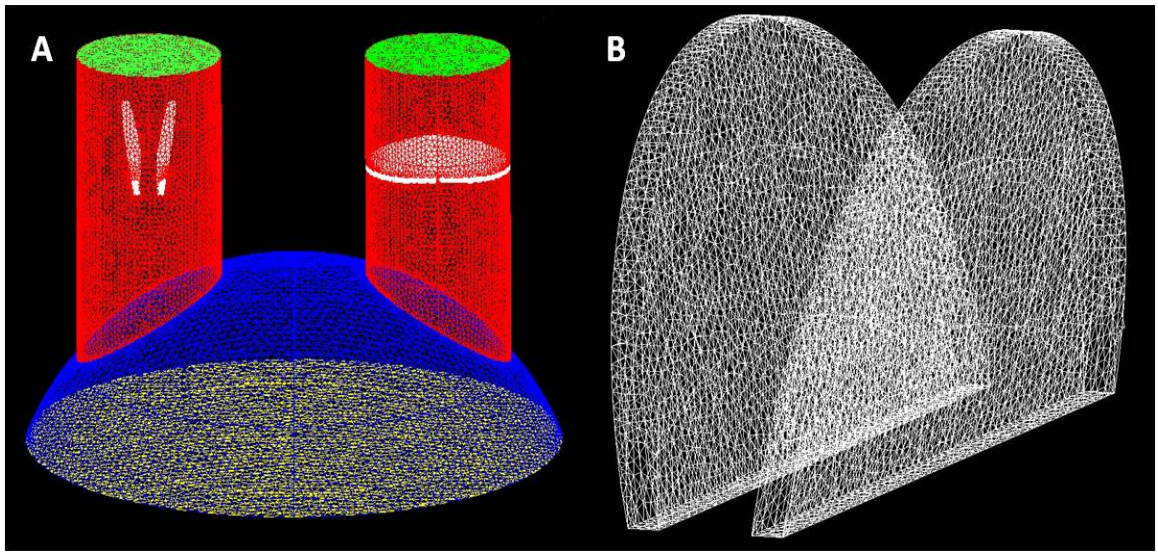

Figure 3.20: (A) Meshing of the testing fluid chamber with diaphragm at 0" height. (B) Meshing of the valve leaflets when the fully open position.

3.3.3 Computational fluid dynamics

3.3.3.1 Basic theory

The fundamental theory of computational fluid dynamics (CFD) is governed by Navier-Stokes equations. The basic idea is to transform the flow domain into finite numbers of small computational elements and apply Navier-Stokes equations to every single element. Every element in the entire domain would have a solution and the computational calculation would keep calculating until it reached the required accuracy (convergence criteria for velocity components-1.0E-04, continuity-1.0E-04). Navier-Stokes equations are derived from Newton's Second Law, conservation of mass. The general form of fluid motion equation is:

$$\rho\left(\frac{\partial v}{\partial t} + v \cdot \nabla v\right) = \rho g - \nabla p + \nabla T \qquad (3.1)$$

where ρ is fluid density, v is fluid velocity, g is gravitational force, p is pressure, and T is tensor.

For incompressible Newtonian fluid with constant viscosity, the equation further changes to a vector form:

$$\rho\left(\frac{\partial v}{\partial t} + v \cdot \nabla v\right) = \rho g - \nabla p + \mu\nabla^2 v \qquad (3.2)$$

where μ is fluid viscosity. In our case, blood or plasma to be tested in the testing fluid chamber were considered incompressible fluids.

The Cartesian form of the equation can be written as the following:

$$\frac{\partial u}{\partial x} + \frac{\partial v}{\partial y} + \frac{\partial w}{\partial z} = 0 \qquad (3.3)$$

$$\rho\left(\frac{\partial u}{\partial t} + u\frac{\partial u}{\partial x} + v\frac{\partial u}{\partial y} + w\frac{\partial u}{\partial z}\right) = \rho g_x - \frac{\partial p}{\partial x} + \mu\left(\frac{\partial^2 u}{\partial x^2} + \frac{\partial^2 u}{\partial y^2} + \frac{\partial^2 u}{\partial z^2}\right) \qquad (3.4)$$

$$\rho\left(\frac{\partial v}{\partial t} + u\frac{\partial v}{\partial x} + v\frac{\partial v}{\partial y} + w\frac{\partial v}{\partial z}\right) = \rho g_y - \frac{\partial p}{\partial y} + \mu\left(\frac{\partial^2 v}{\partial x^2} + \frac{\partial^2 v}{\partial y^2} + \frac{\partial^2 v}{\partial z^2}\right) \qquad (3.5)$$

$$\rho\left(\frac{\partial w}{\partial t} + u\frac{\partial w}{\partial x} + v\frac{\partial w}{\partial y} + w\frac{\partial w}{\partial z}\right) = \rho g_z - \frac{\partial p}{\partial z} + \mu\left(\frac{\partial^2 w}{\partial x^2} + \frac{\partial^2 w}{\partial y^2} + \frac{\partial^2 w}{\partial z^2}\right) \qquad (3.6)$$

where u, v, and w are the velocities on x, y, and z direction in Cartesian coordinate system, and g is the gravitational force.

3.3.3.2 Laminar flow model

The flow field in the numerical model was firstly estimated by laminar models, to check the validity of model structure and geometry, meshing as well as the basic flow patterns. The viscosity is 1 cP, the inlet velocity was given in Table 3.2, and boundary conditions were discussed in the following section.

3.3.3.3 Turbulent flow model

To examine the complex flow patterns in the testing fluid chamber, a k-ω turbulent model was used. Reynolds number was obtained for the whole flow field to examine if turbulence exists in the chamber under dynamic flow conditions.

3.3.4 Flow analysis

The meshed models of the fluid chamber form ANSYS ICEM CFD 12.0.1 was imported to ANSYS CFX-Pre 12.0 for boundary setup and surface definition. Every element was checked for proper meshing (CFX-Pre 12.0). The model was simulated by ANSYS CFX-Solver Manager 12.0 and exported to ANSYS CFD-Post 12.0 for the results.

Assumptions:

The following assumptions were used to solve the numerical model:

- Fluid Medium: Water was defined as the fluid medium in both the laminar and turbulent flow model.
- Inlet Velocity: The flow was fully developed before entering the chamber.

Boundary conditions:

The boundary conditions were defined as the following:

- Inlet: During systole, fluid was pushed out of the outlet valve, so diaphragm was defined as the inlet surface. The complete list of velocities at different chamber volume was given in Table 3.2. Outlet: The outlet surfaces were defined as pressure outlets.
- Walls: Housing, channels, and valve leaflets were defined as rigid walls. During diastole, fluid was pushed into the fluid chamber through the inlet valve, so the diaphragm was defined as a rigid wall.
- Turbulent parameters: Turbulent intensity was defined as 3% in the turbulent model.
- Steady condition: The simulation was run under the steady condition.

Table 3.2-The different inlet velocity of systolic/diastolic at different volumes.

	Systolic	Diastolic
Volume (ml)	Inlet Velocity (cm/s)	Inlet Velocity (cm/s)
0	0	0
20	0.3460	4.7365
40	0.6919	9.4731
60	1.0379	14.2096
80	1.3839	18.9458

CHAPTER IV

RESULTS

4.1 Flow chamber

After the design of the flow chamber in Pro E has been completed, all the components were fabricated at OSU physics machine Shop. All the components were manufactured following the dimensions designed in Pro E. Figure 4.1 shows all the finished components and some readymade parts used in the flow chamber. The volume of both the water and the testing fluid chamber was about 125 ml, which was close to the desired volume. The two channels (inlet and outlet) in the testing fluid chamber each had 1-inch diameter, which perfectly matched the size of the valves. All the components were put together by screws. Teflon tape was used to wrap around the valves to ensure a better fitting into the valve housing. Figure 4.2 shows the assembled flow chamber with the valves.

Silicon tubing was used to connect the flow chamber to the pump. One end of the silicon tubing with the female hose adapter was used to connect with the water chamber and the other end was connected to the nozzle of the pump. There was a T-connector in one of the silicon tubings to provide an extra path for the water filling port.

All the connections were fixed by stainless steel hose clamps. Figure 4.3 shows the setup of the connecting silicon tubing.

Before each dynamic experiment, the system was assembled properly as designed. Then it was connected to the pump through the silicon tubing and water was slowly filled into the water chamber from water filling port until the water chamber was full (no more bubbles). Washed platelet or whole blood was then filled into the testing fluid chamber through the filling port with the sampling port open to remove bubble. The assembled system is shown in Figure 4.4.

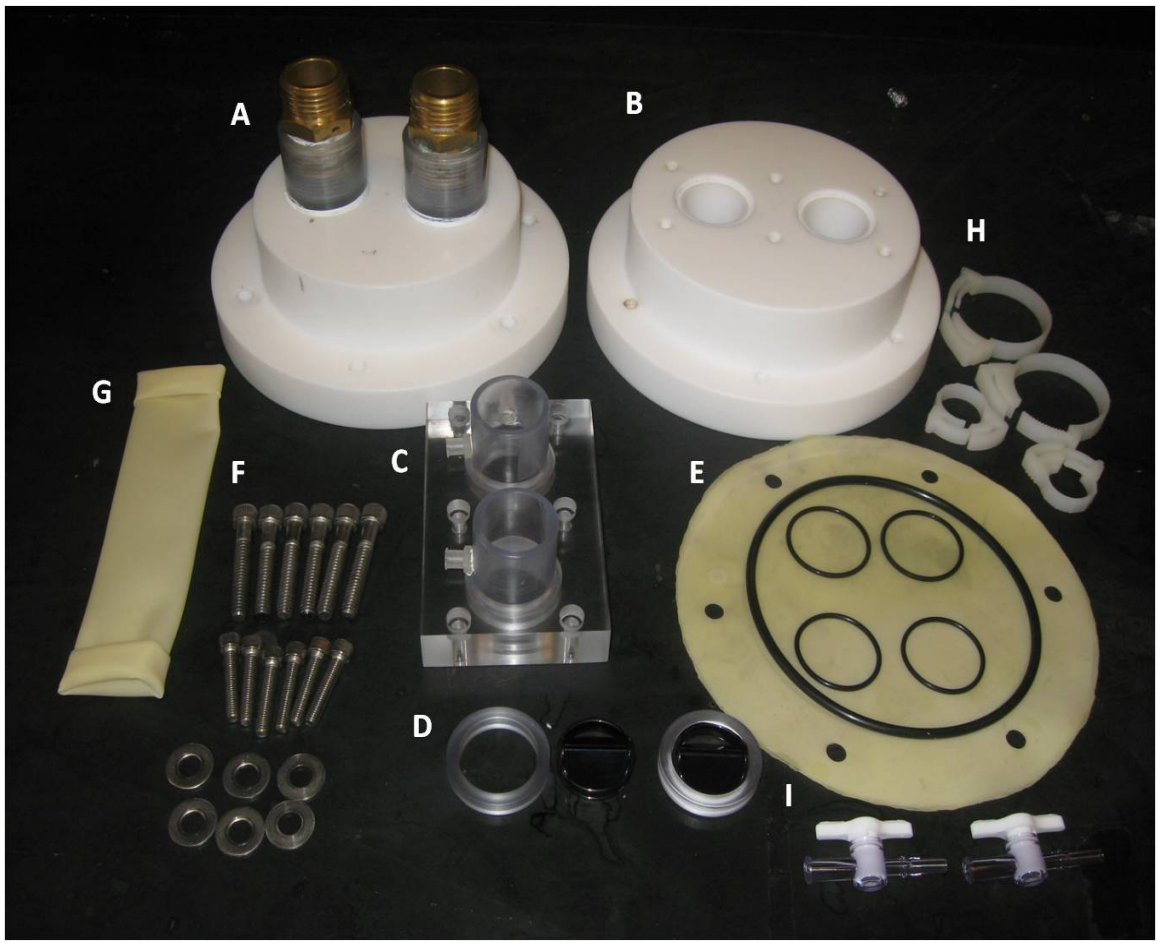

Figure 4.1: Finished components and readymade parts of the flow chamber. (A) Water chamber. (B) Testing fluid chamber. (C) Transparent valve socket. (D) From left to right, valve housing, St. Jude bileaflet mechanical heart valve, and valve with housing. (E) Diaphragm and different sizes of O-rings. (F) Screws and washers. (G) Folded Penrose tubing. (H) Acetal clamps with different sizes. (I) Luer fittings inserted at filling and sampling ports.

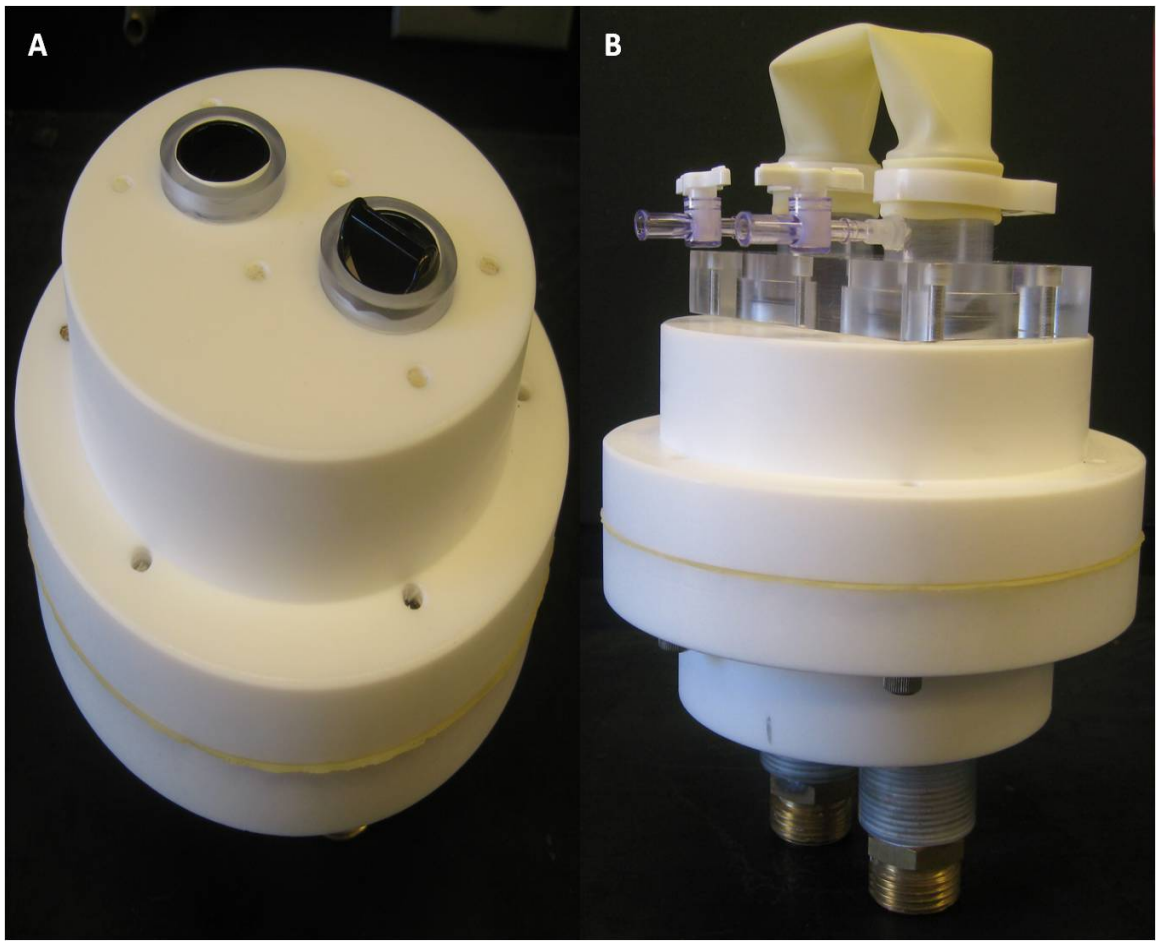

Figure 4.2: Assembled components. (A) Installation of the valves in the fluid chamber before transparent valve socket was connected. The valves were placed on opposite side of the channel to control flow direction. (B) Final assembled of the flow chamber with the penrose tubing tied with acetal clamps and Luer fittings inserted in the sampling and filling ports.

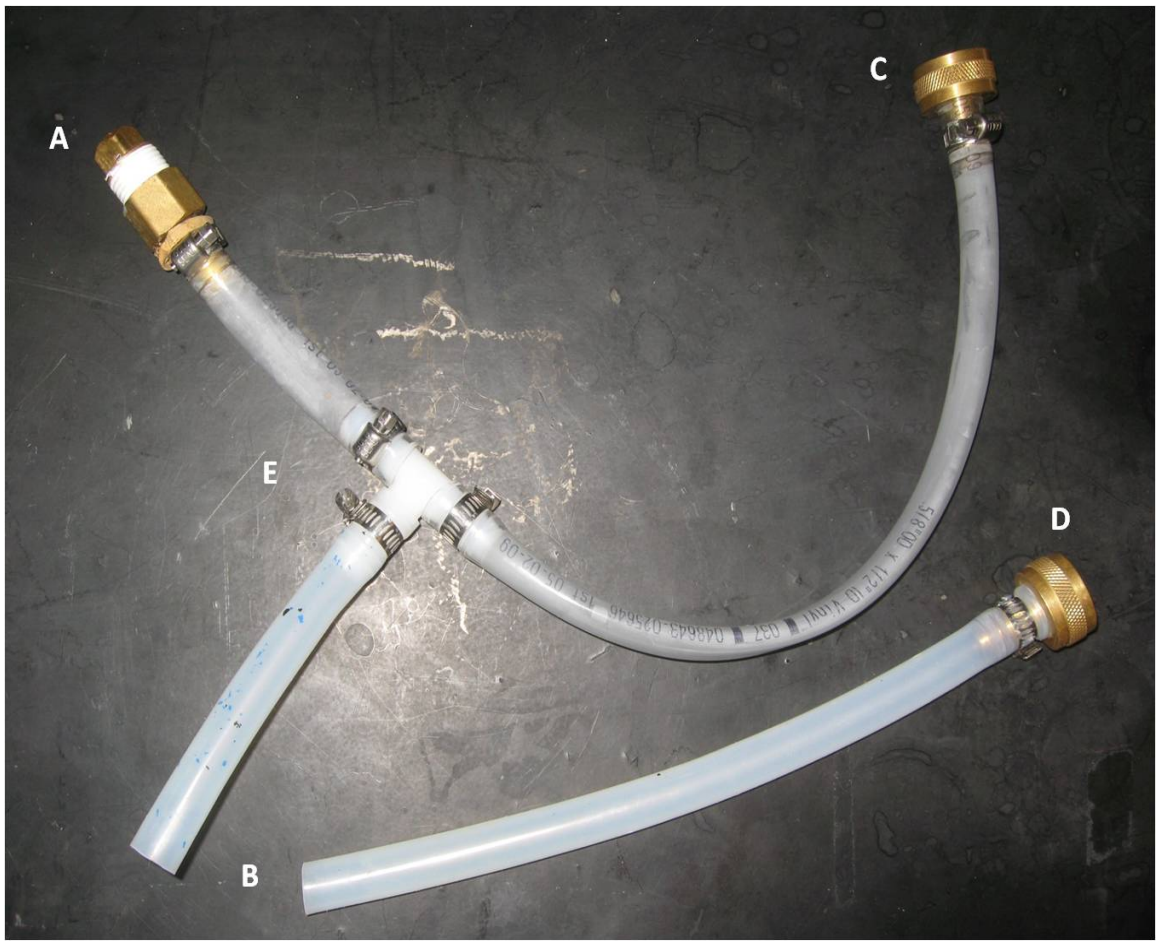

Figure 4.3: The tubing to connect the reciprocating pump and the flow chamber, which was made from Silicon. (A) Filling port of the water chamber and pump. (B) Locations where the tubings connected to the pump and were fixed by Acetal clamps to prevent leaking. (C, D) Brass machined female hose nut to hose barbs connected to water chamber. (E) T-connector connected to pump, water chamber, and water filling port.

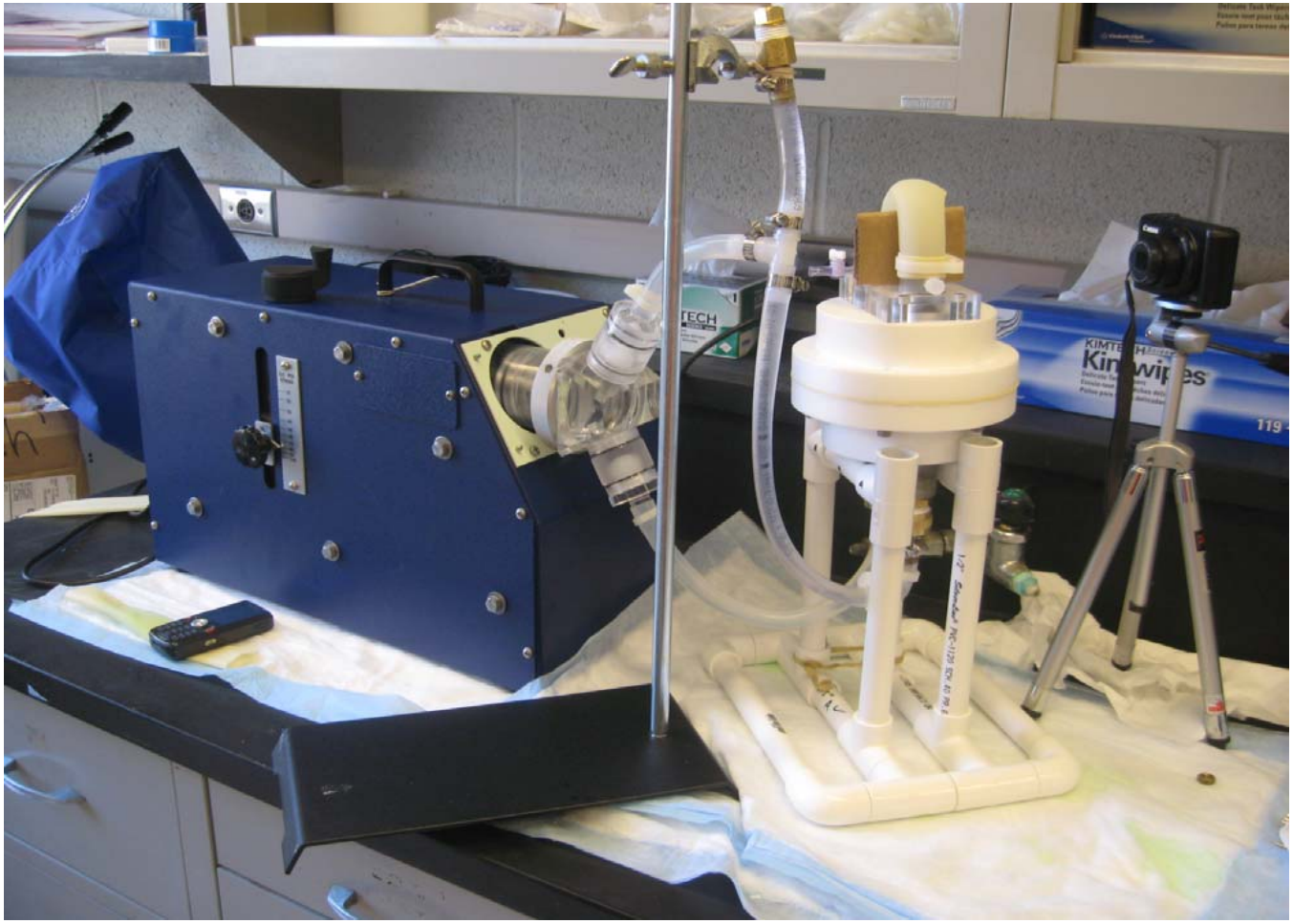

Figure 4.4: Complete experimental setup with a stand to hold the flow chamber. The stand was made from ½ " PVC tubing. The camera was used to record the experiment to observe the valve movements.

4.2 Results from *in vitro* experiments

4.2.1 Platelets activation experiments (CD62P expression)

4.2.1.1 Platelet activation measurement under static conditions

CD62P expression on platelets that were placed in the flow chamber was compared to that from control platelets (platelet sitting on bench without any treatment). Due to the variance in platelet activation from different donors and on different days, CD62P expression from both control platelets and flow chamber platelets were normalized to that of control platelets at time 0. Figure 4.5 shows the typical flow cytometry results of CD62P expression on control platelets, platelets in the flow chamber, and platelets treated with Ionophore A23187 (positive control). Experiments under static conditions were repeated 6 times. Paired Student's *t*-test was used to detect if there was any significant difference ($P<0.05$) between treated and control (bench) platelets. The results indicated that the elongated contact with the Teflon testing fluid chamber and the latex diaphragm induced a significant increase in platelet surface CD62P expression (Figure 4.6) after 3 hour contact. While before 3 hours, the testing fluid chamber did not induce any platelet activation. Two-way ANOVA was also used to examine if there were any significant effects from treatment (bench or chamber) or time. The results demonstrated that both treatments and time affect platelet surface P-selectin expression significantly ($P<0.05$). Then two separate single-classification ANOVA and Student-Newman-Keuls post-test were used to compare platelet activation at every time step when they were placed in the chamber or on the bench. The results indicated that without treatment (bench), platelet activation did not change with time. While in the flow

chamber, platelet activation at 5 hours was significantly different from that at 1, 2 and 3 hours, matching the Student's *t*-test results reported above.

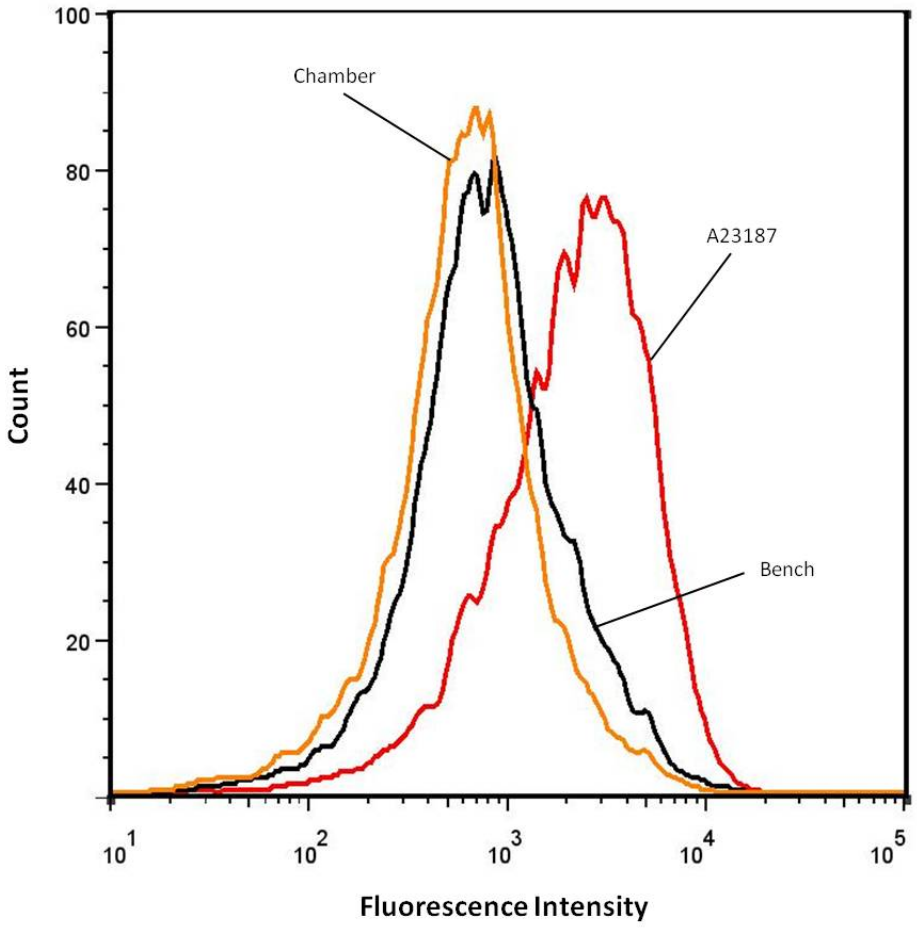

Figure4.5: Flow cytometry results of CD62P expression on control platelets and platelets in flow device at 5 hours. A23187 was Ionophore that used to activate platelets.

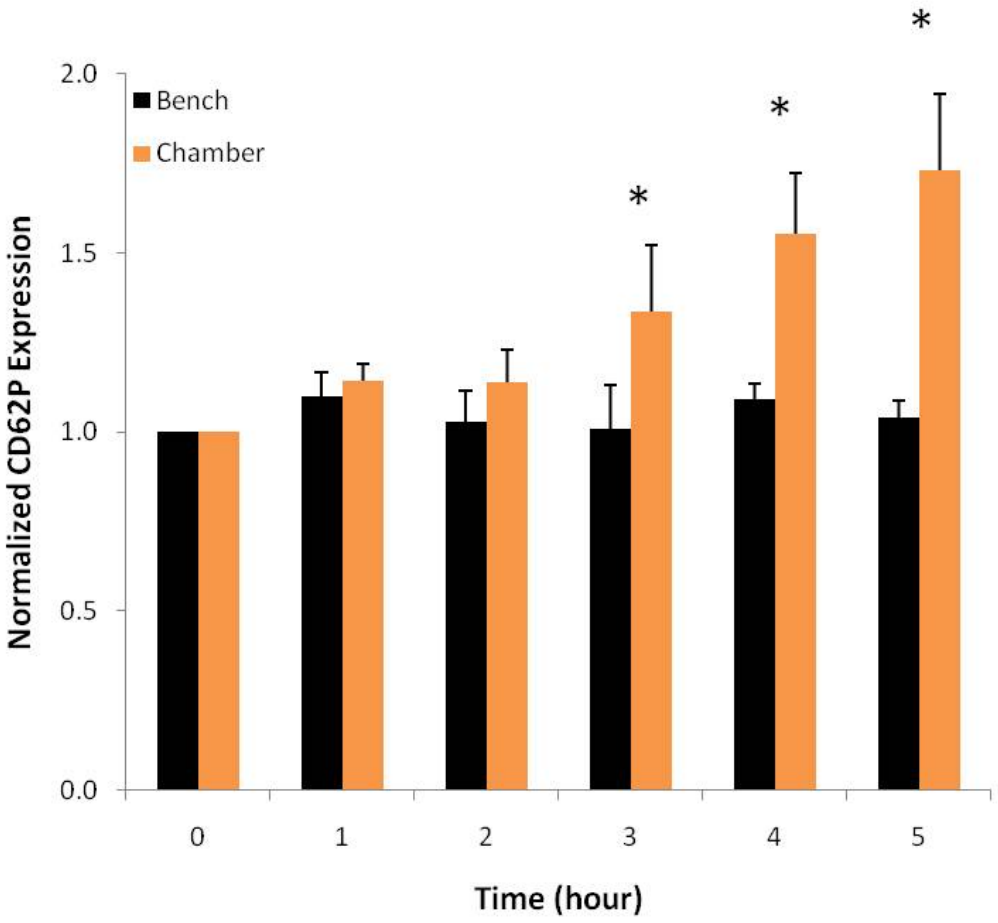

Figure 4.6: The platelet activation between bench and chamber during 5 hours of static experiments. Washed platelet with the concentration of 100,000/µl was taken every hour from bench and chamber for P-selectin measurement. It shows CD62P Expression ± SEM, normalized to the bench CD62P expression at time 0. The data demonstrated that no significant change of CD62P expression in the first 2 hours but a detectable change of CD62P expression from 3 hours. The difference between the two was significant (n=6, * - $P < 0.05$ by paired Student's *t*-test).

4.2.1.2 Platelet activation measurement under dynamic conditions

CD62P expression was measured on control platelets and platelets that were placed in the flow chamber under dynamic conditions. All data were normalized to that of control platelets at time 0. Figure 4.7 demonstrated that circulation in the flow chamber through the two St. Jude bileaflet mechanical heart valves did not induce any significant change in platelet activation. Again, paired Student's *t*-test and two-way ANOVA were used to conduct the statistical analysis.

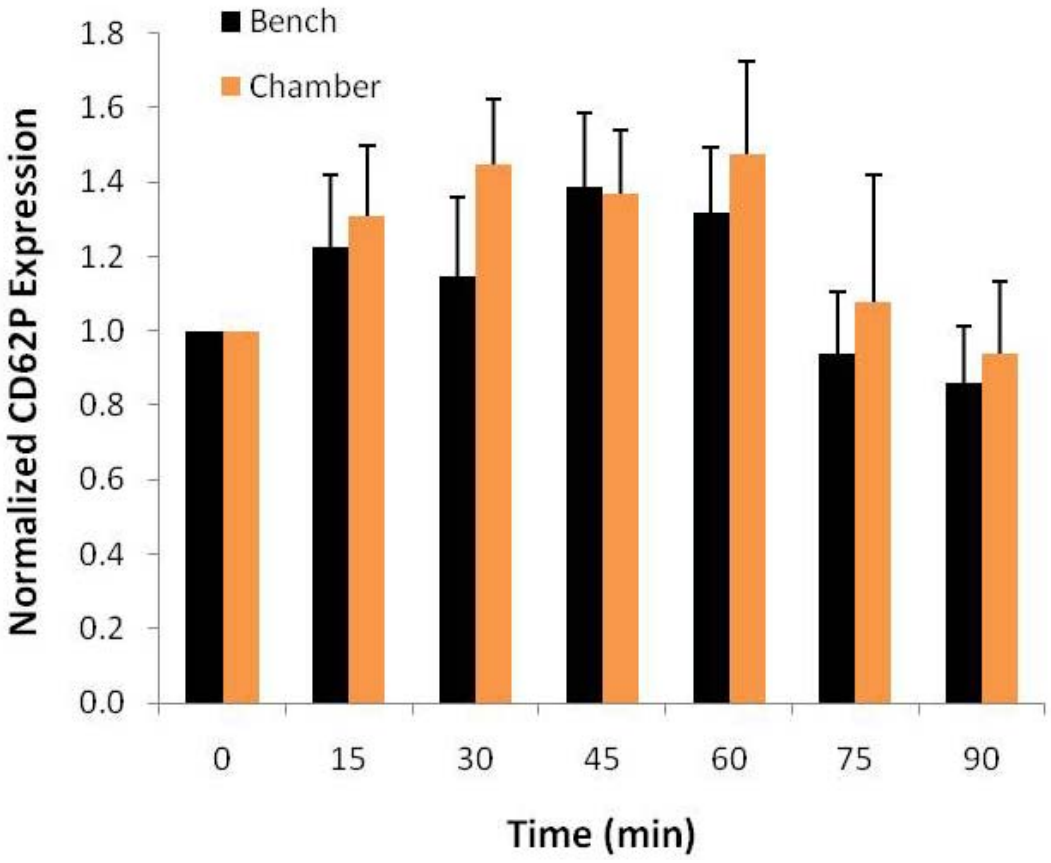

Figure 4.7: Platelet activation comparison between bench and chamber during 90 minutes of dynamic experiments. Washed platelet with the concentration of 100,000/µl was taken every 15 minutes from bench and chamber for P-selectin measurement. It shows CD62P Expression ± SEM, normalized to the bench CD62P expression at time 0. The data demonstrated that no significant change of CD62P expression over the period of 90 minutes in 15 minutes intervals (n=6).

4.2.2 Hemolysis measurements

4.2.2.1 Hemolysis measurement under static conditions

A comparison study of blood hemolysis of control (bench) red blood cells and red blood cells that were placed in the testing fluid chamber under static conditions was conducted. Both control and chamber blood sample absorbance was measured by spectrophotometer at 540 nm. Hemoglobin concentration (g/dl) in whole blood was determined based on the formula below:

$$\frac{Absorbance\ of\ Sample}{Absorbance\ of Satndard} \times Concentration\ of\ Standard\ (^{g}/_{dl}) = Hemoglobin(^{g}/_{dl}) \quad (4.1)$$

where the absorbance of standard is the absorbance from hemoglobin standard, the concentration of standard is equal to 11.6 g/dl, and absorbance of sample is the absorbance from the sample.

All measured values of control and chamber blood samples were applied to the formula (4.1) to calculate the hemoglobin concentration. Both bench and chamber hemoglobin concentrations were normalized by the bench hemoglobin concentration at time 0. Figure 4.8 demonstrates the comparison between the bench blood samples and chamber blood samples for 6 hours. The data was examined by paired Student's *t*-test and two-way ANOVA. The results showed that no statistically significant difference significance was detected in hemolysis between control and chamber blood samples. In this set of experiments, measured hemoglobin concentration varied between 14.71 g/dl

and 17.45 g/dl (only male blood was used), and the normal hemoglobin concentration is 11-16 g/dl for adult female and 13-18 g/dl for adult male.

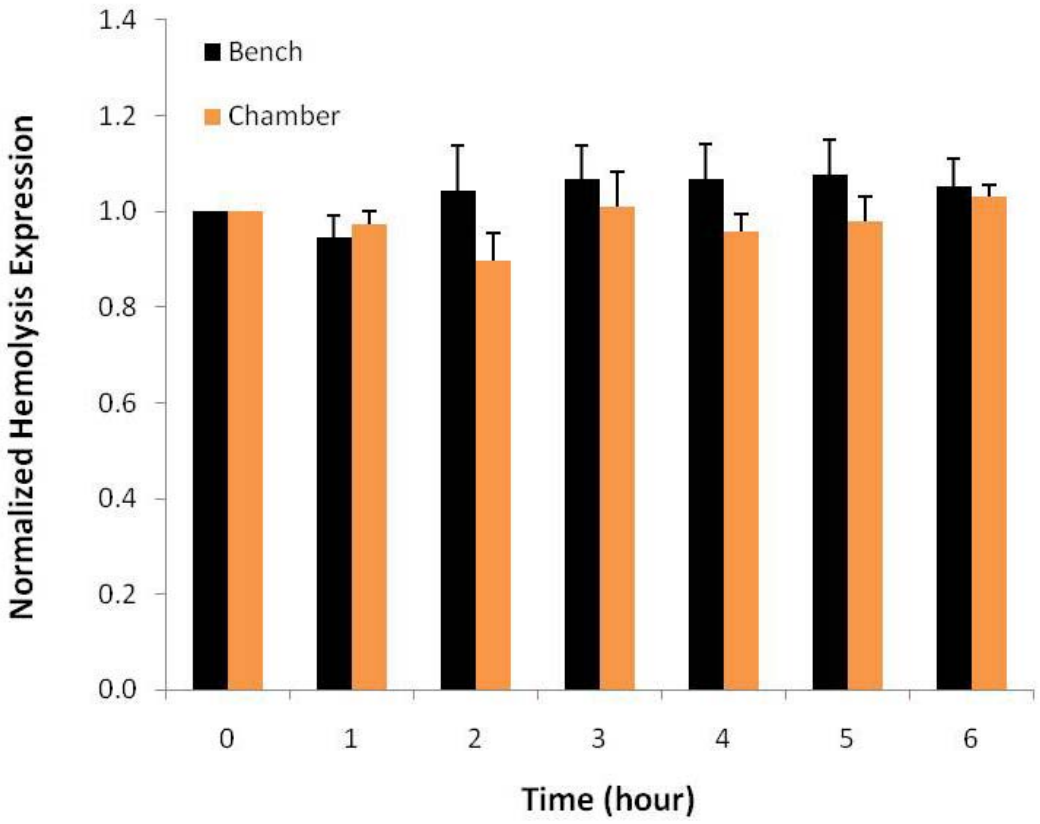

Figure 4.8: The hemolysis between bench and chamber during 6 hours of static experiments. Whole blood was taken every 1 hour from bench and chamber for absorbance measurement at 540 nm. It shows hemoglobin concentration ± SEM, normalized to the bench hemoglobin concentration at time 0. The data demonstrated that no significant change of hemolysis over the period of 6 hours in every hour intervals (n=5).

4.2.2.2 Hemolysis measurement in dynamic experiments

Similar experiments were conducted under dynamic conditions. Whole blood was circulated in the testing fluid chamber for 90 minutes and samples were taken out every 15 minutes for hemoglobin concentration measurement using a spectrophotometer at 540 nm. Blood samples that were not treated were used as the negative control. Both control and chamber hemoglobin concentrations were normalized by the control hemoglobin concentration at time 0. Paired Student's *t*-test was used to detect if there was any significant difference between bench blood samples and chamber blood samples. The results (Figure 4.9) indicated that there was no statistically significant difference between control blood and that were circulated in the testing fluid chamber. Two-way ANOVA was used to further investigate the effects on hemolysis from treatment (bench or chamber) and time. The results demonstrated that only time has effect. Therefore, a single-classification ANOVA followed by Student-Newman-Keuls post-test were used to compare every timed sample for bench and chamber blood. The results indicated there was no significant change in hemolysis induced by time. However, paired *t-test* showed that bench blood samples had a significantly increased hemoglobin concentration at 15, 30, 45, and 90 minute compare to bench. Since hemolysis induced by chamber was lower than that in the control blood at those time points, we can conclude that the chamber did not induce any increase in hemolysis.

In this set of experiments, measured hemoglobin concentration varied between 12.25 g/dl and 17.75 g/dl (female blood); between 14.45 g/dl and 17.71 g/dl (male blood) indicating there was no hemolysis occurring during the dynamic experiments.

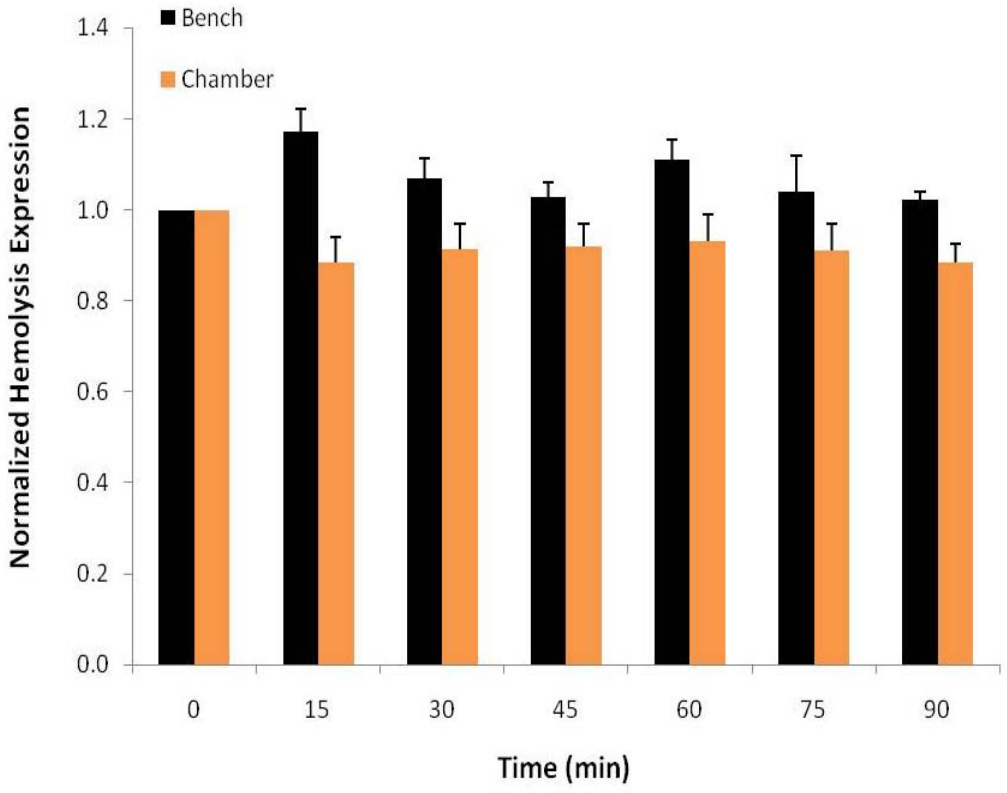

Figure 4.9: The hemolysis between bench and chamber during 90 minutes of dynamic experiments. Whole blood was taken every 15 minutes from bench and chamber for absorbance measurement at 540 nm. It shows hemoglobin concentration ± SEM, normalized to the bench hemoglobin concentration at time 0. The data demonstrated that no significant change of hemolysis over the period of 90 minutes in every 15 minutes intervals (n=4).

4.3 Numerical results

CFD studies were conducted to examine the flow field in the testing fluid chamber with two St. Jude bileaflet mechanical heart valves. During systole, fluid was pushed out of the outlet valve as the diaphragm moved up; during diastole, fluid was pushed into the chamber through the inlet valve as the diaphragm moved down. The model was conducted under both laminar and turbulent conditions.

4.3.1 Laminar flow model

The main purpose of the laminar model was to examine if the geometry, structure and meshing were proper. The laminar model provided a general view of the flow patterns in the flow chamber and was used as the base for our turbulent model. 2D and 3D velocity distributions were presented in Figure 4.10 through Figure 4.13.

Figure 4.10 shows 2D velocity vectors of systole and diastole under laminar flow conditions in the testing fluid chamber. The maximum velocity during systole was 0.5086 m/s (end of systole), while the maximum velocity during diastole was 0.4209 m/s (end of diastole). Figure 4.11 shows the 3D velocity vectors during systole and diastole under laminar flow conditions. Figure 4.12 shows velocity contours of the flow fields under both systolic and diastolic conditions. Figure 4.13 shows velocity stream lines in the chamber. All these results indicated that the highest velocity occurred near the valve region at the end of systole and diastole. Therefore, pressure difference (or gradient) across the valve was examined at that time. Figure 4.14 depicted the pressure distribution contour at the valve area. At the end of systole, the pressure difference across the open outlet valve was 57.2 Pa (0.43 mm Hg), and at the end of diastole, the pressure difference

across the open inlet valve was 37.8 Pa (0.28 mm Hg). The average pressure around the outlet valve at the end of systole was 21358.5 Pa (160.2 mmHg), while the average pressure around the inlet valve at the end of diastole was 10689.9 Pa (80.2 mmHg).

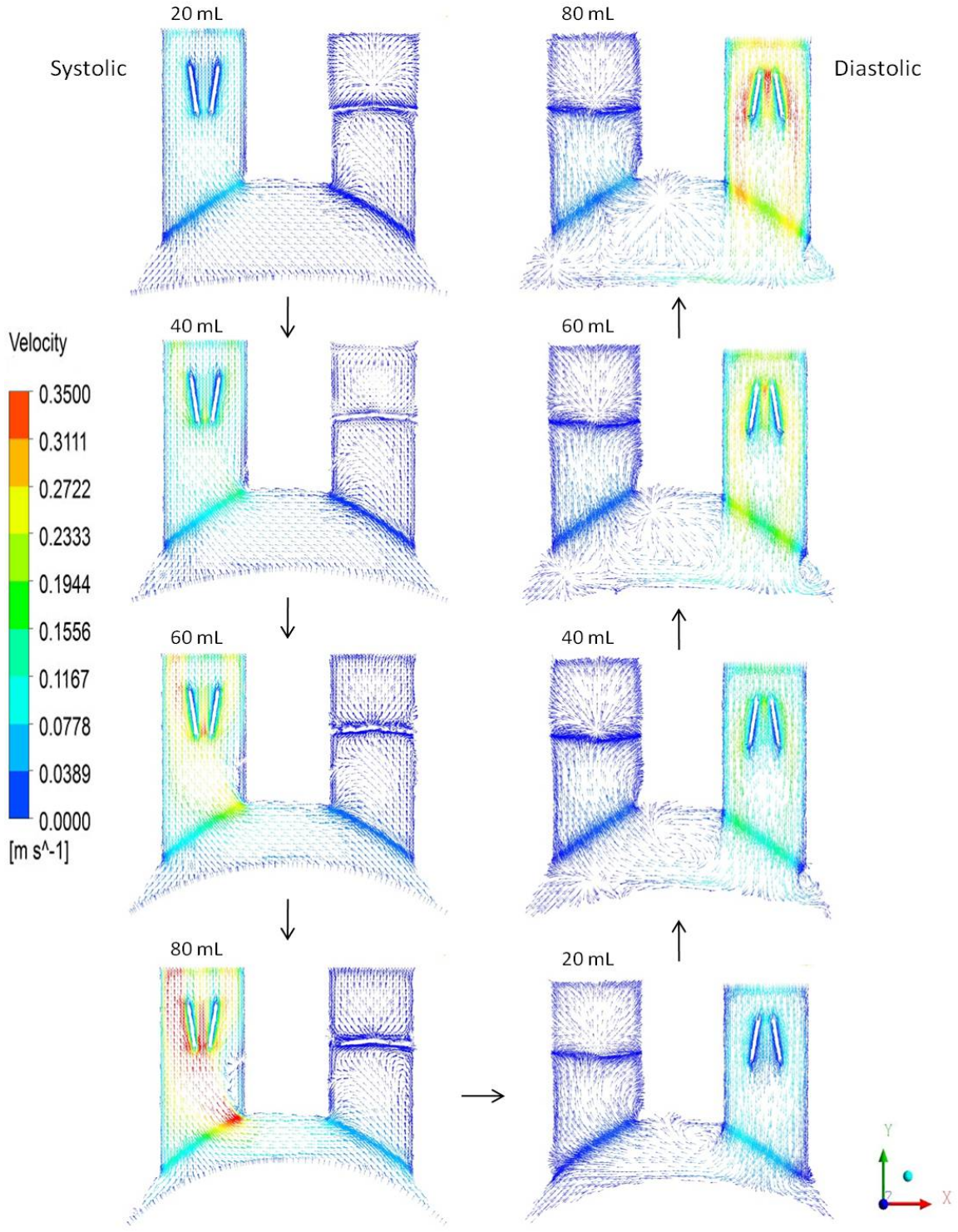

Figure 4.10: Velocity vectors in the testing fluid chamber during systole and diastole under laminar conditions. Images are presented in 2D views. The left side of the figure shows the flow fields as the diaphragm was moving up with a 20ml increment (systole). The right side of the figure shows the flow fields as the diaphragm was moving down with a 20ml increment. Arrows indicate the sequence in occurrence.

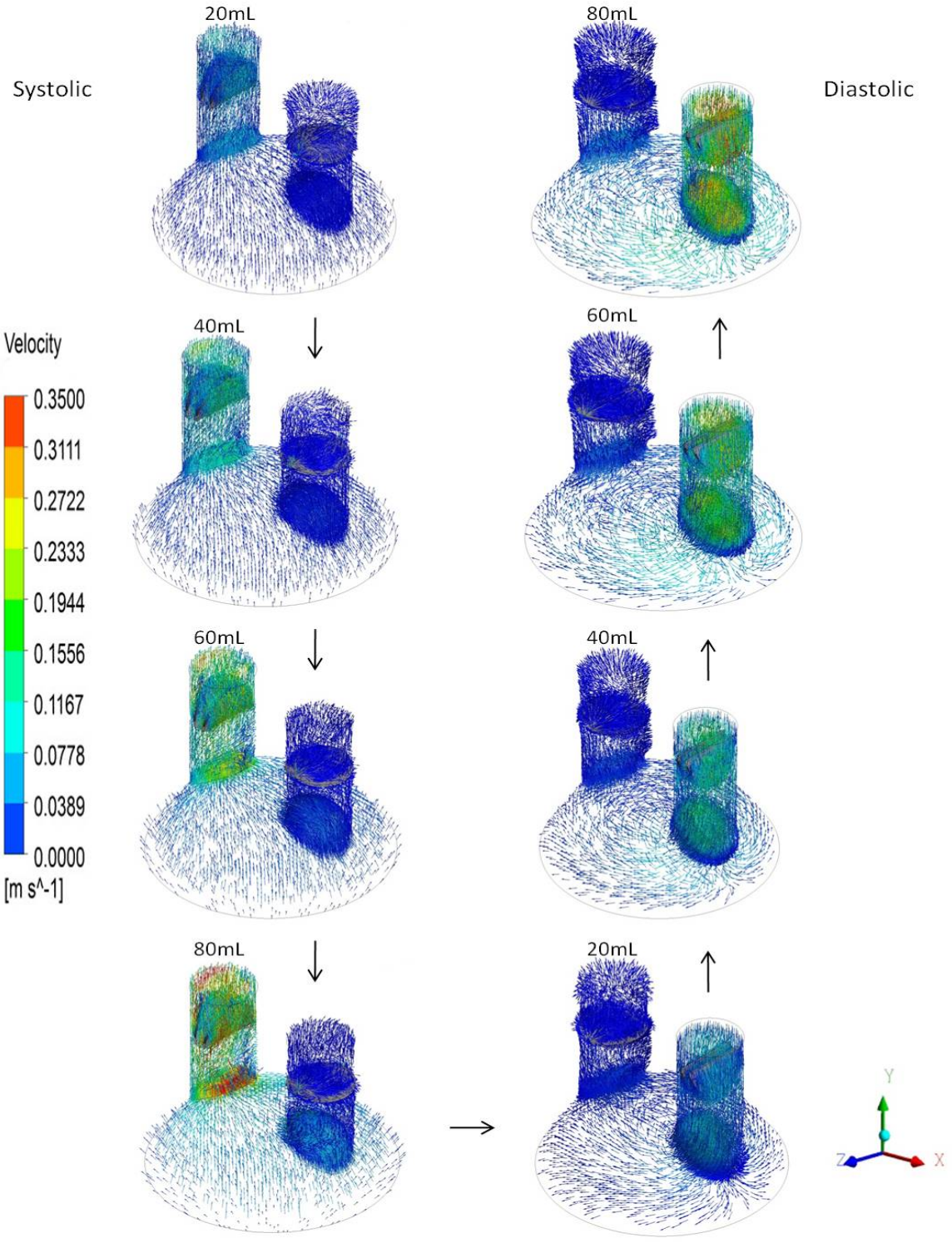

Figure 4.11: Velocity vectors in the testing fluid chamber during systole and diastole under laminar conditions. Images are presented in 3D views. The left side of the figure shows the flow fields as the diaphragm was moving up with a 20ml increment (systole). The right side of the figure shows the flow fields as the diaphragm was moving down with a 20ml increment. Arrows indicate the sequence in occurrence.

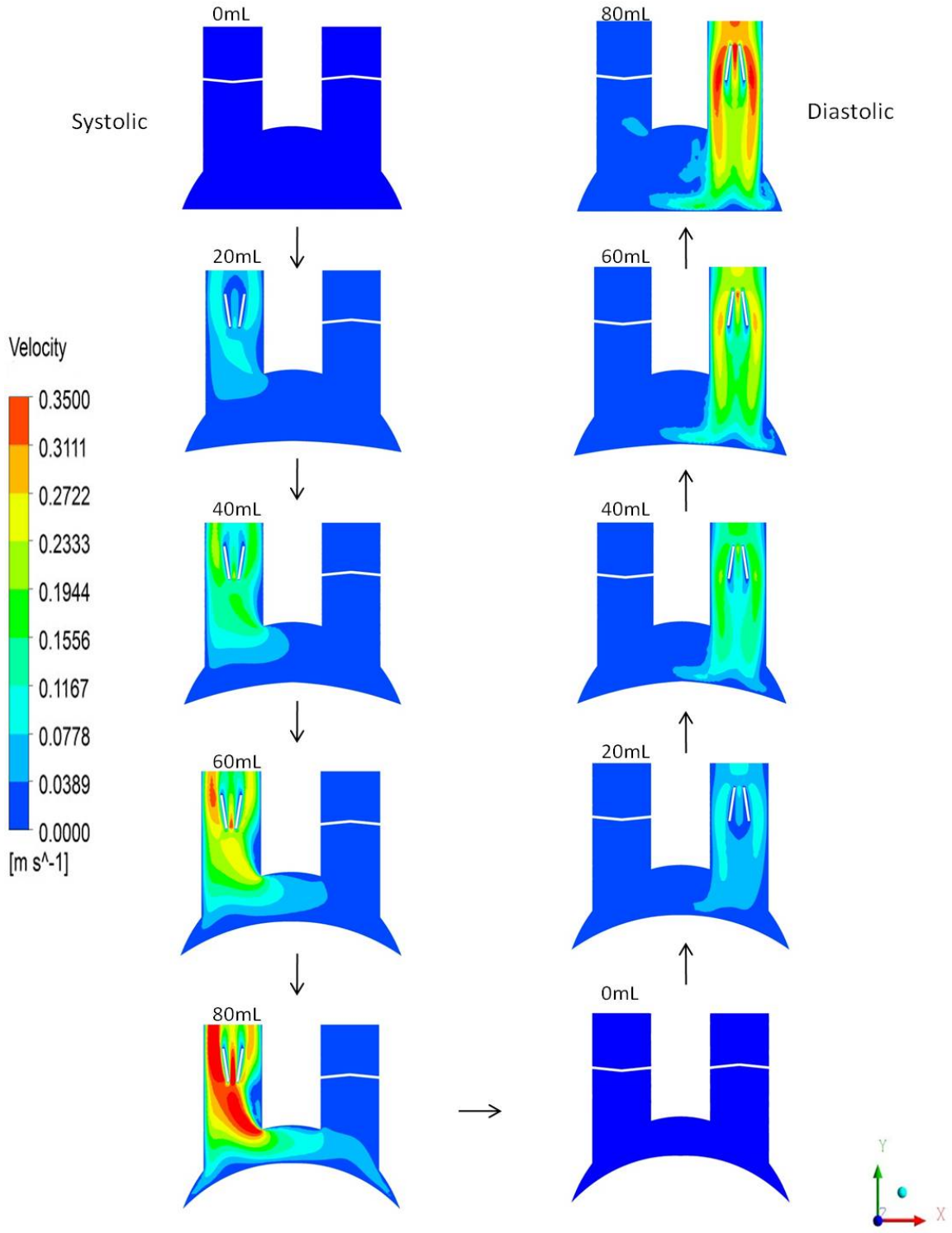

Figure 4.12: Velocity contour in the testing fluid chamber during systole and diastole under laminar conditions. Images are presented in 2D views. The left side of the figure shows the velocity contour as the diaphragm was moving up with a 20ml increment (systole). The right side of the figure shows the flow fields as the diaphragm was moving down with a 20ml increment. Arrows indicate the sequence in occurrence.

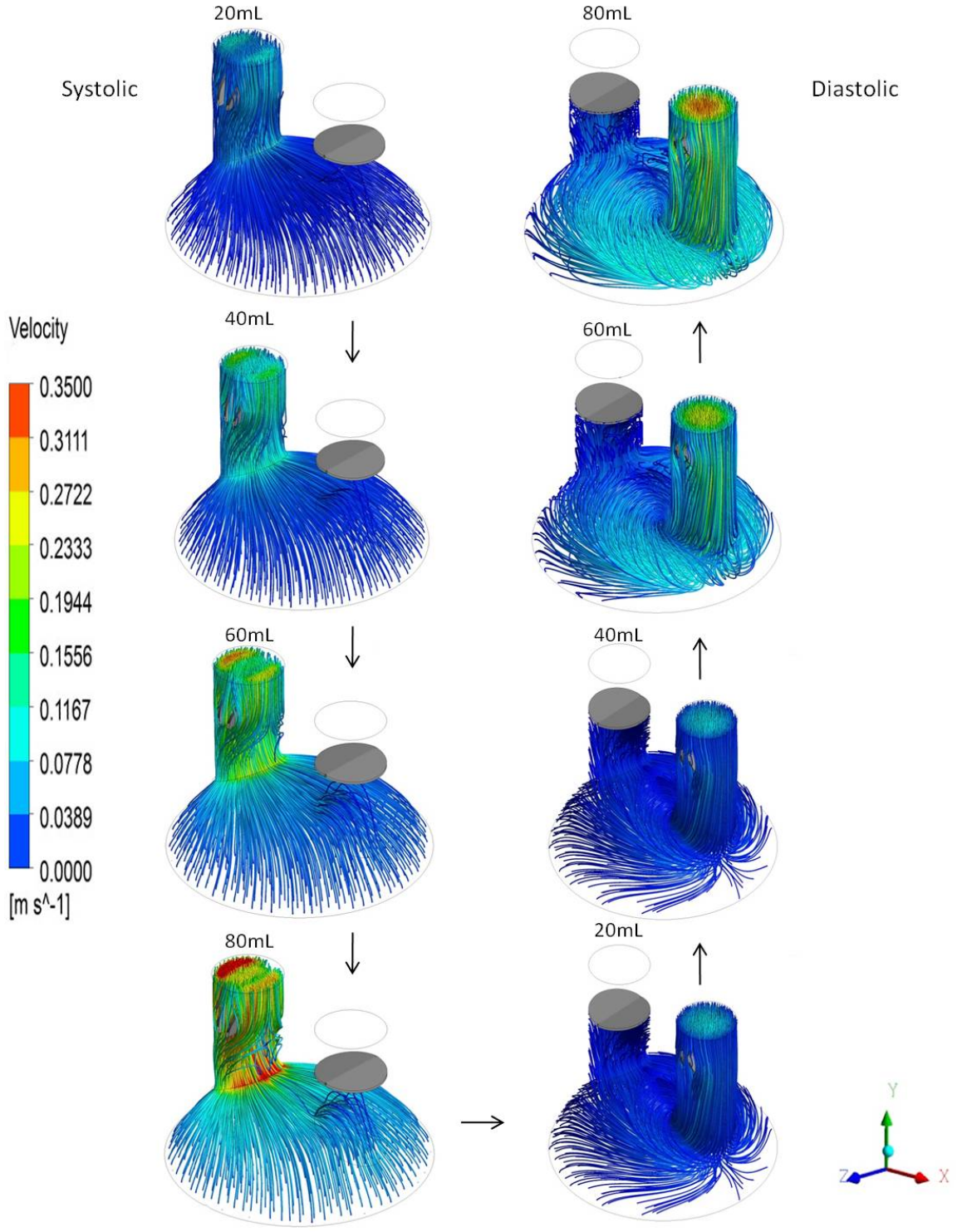

Figure 4.13: Velocity stream lines in the testing fluid chamber during systole and diastole under laminar conditions. Images are presented in 3D views. The left side of the figure shows the stream lines as the diaphragm was moving up with a 20ml increment (systole). The right side of the figure shows the flow fields as the diaphragm was moving down with a 20ml increment. Arrows indicate the sequence in occurrence.

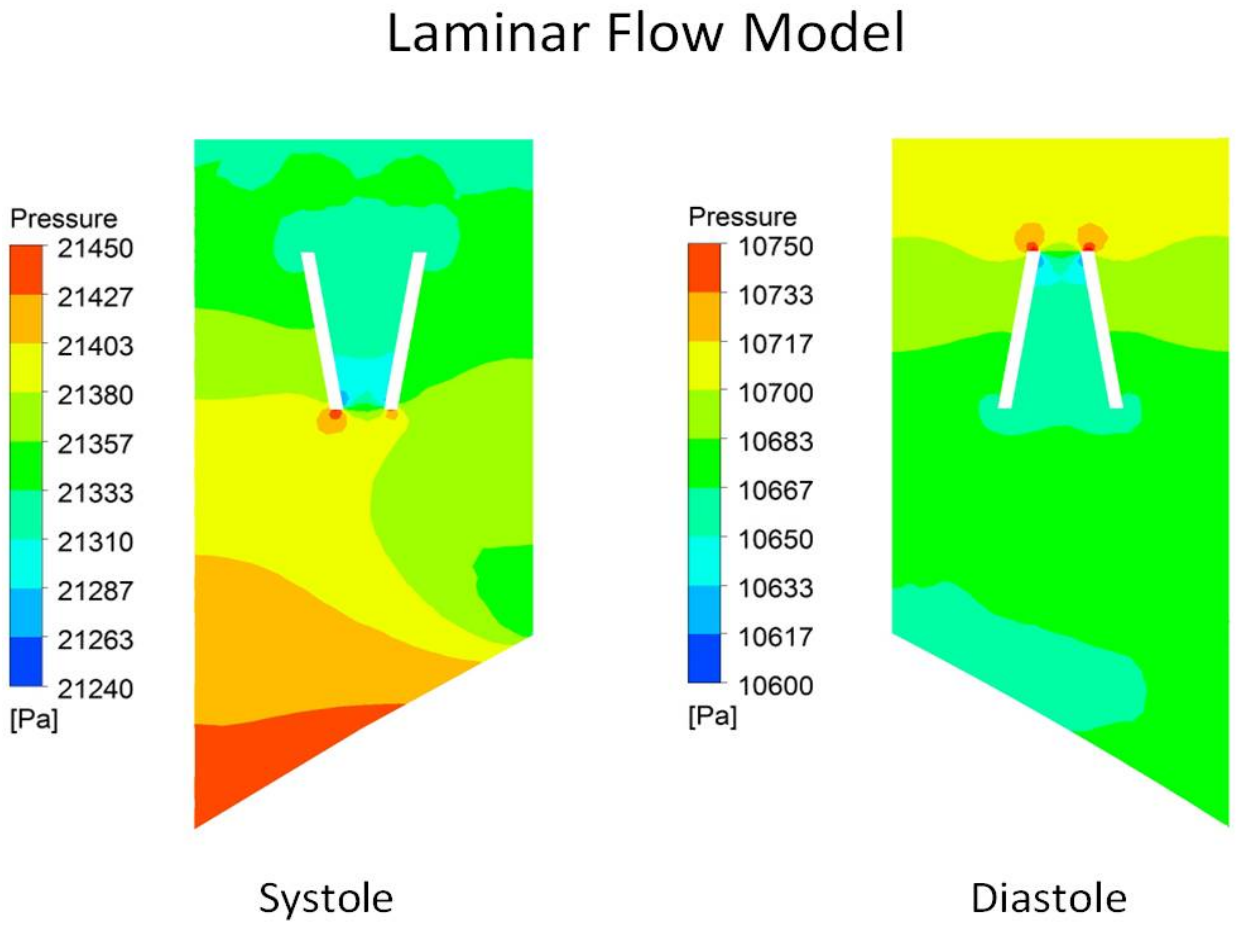

Figure 4.14: Pressure distribution contours at the valve area during systole and diastole under laminar conditions. Images are presented in 2D views. The left side of the figure shows the pressure contour as the outlet valve was fully opened (systole). The right side of the figure shows the pressure contour as the inlet valve was fully opened (diastole). (1 Pa = 0.007501 mmHg)

4.3.2 Turbulent flow model

Based on the laminar model, a 3D k-ω turbulence model was conducted to examine the flow field in the testing fluid chamber. Similar flow patterns were observed with the turbulent model, compared to that of the laminar model. Flow patterns were presented in velocity distributions in Figure 4.15 through Figure 4.18. Figure 4.15 shows the 2D velocity vectors during systole and diastole under turbulent flow conditions in the testing fluid chamber. The maximum velocity during systole was 0.5106 m/s (end of systole), while the maximum velocity during diastole was 0.4321 m/s (end of diastole). Figure 4.16 shows the 3D velocity vectors during systole and diastole under turbulent flow conditions. Figure 4.17 shows the velocity contours of the flow under both systolic and diastolic conditions. Figure 4.18 shows the velocity stream lines of the flow field in the chamber. Again, it was clear that the maximum velocity and biggest velocity gradient occurred at the end of systole and diastole around the valve area. Therefore, pressure distribution was examined (Figure 4.19). The results indicated that the average pressure around the outlet valve at the end of systole was 21357.3 Pa (160.2 mm Hg) and the average pressure around the inlet valve was 10691.6 Pa (80.2 mm Hg) at the end of diastole. For both systole and diastole conditions, the pressure difference across the open valve was similar to that observed under laminar flow conditions (53.8 Pa/0.40 mmHg for systole and 45.4 Pa/0.34 mmHg for diastole).

To examine if turbulence existed under flow conditions, Reynolds number was calculated for every single fluid element. The highest Reynolds number occurred at the end of systole and the value was 2127.69. The average Reynolds number during systole was 558.23 and the average Reynolds number during diastole was 385.06. Table 4.2

summarized the minimum and maximum Reynolds number during systole and diastole when various volumes of fluid was ejected or filled into the testing fluid chamber.

Table 4.1-Minimum and maximum Reynolds number in different systolic and diastolic volumes.

Volume (ml)	Systolic		Diastolic	
	Minimum	Maximum	Minimum	Maximum
20	0.0007	366.54	0.0824	308.39
40	0.0031	765.63	0.0630	614.18
60	0.0062	1205.96	0.1660	910.83
80	0.0263	2127.69	0.1230	1247.11

In summary, both the laminar model and the turbulent model demonstrated similar flow field and flow conditions in the testing fluid chamber. No turbulence was observed. The highest flow velocity (velocity gradient) occurred at the end of systole and diastole, while the associated pressure difference (gradient) was physical. Therefore, the results obtained from the numerical simulated demonstrated that the structure of the testing fluid chamber did not induce complex flow conditions and the flow environment generated by the chamber was suitable for heart valve dynamic performance studies.

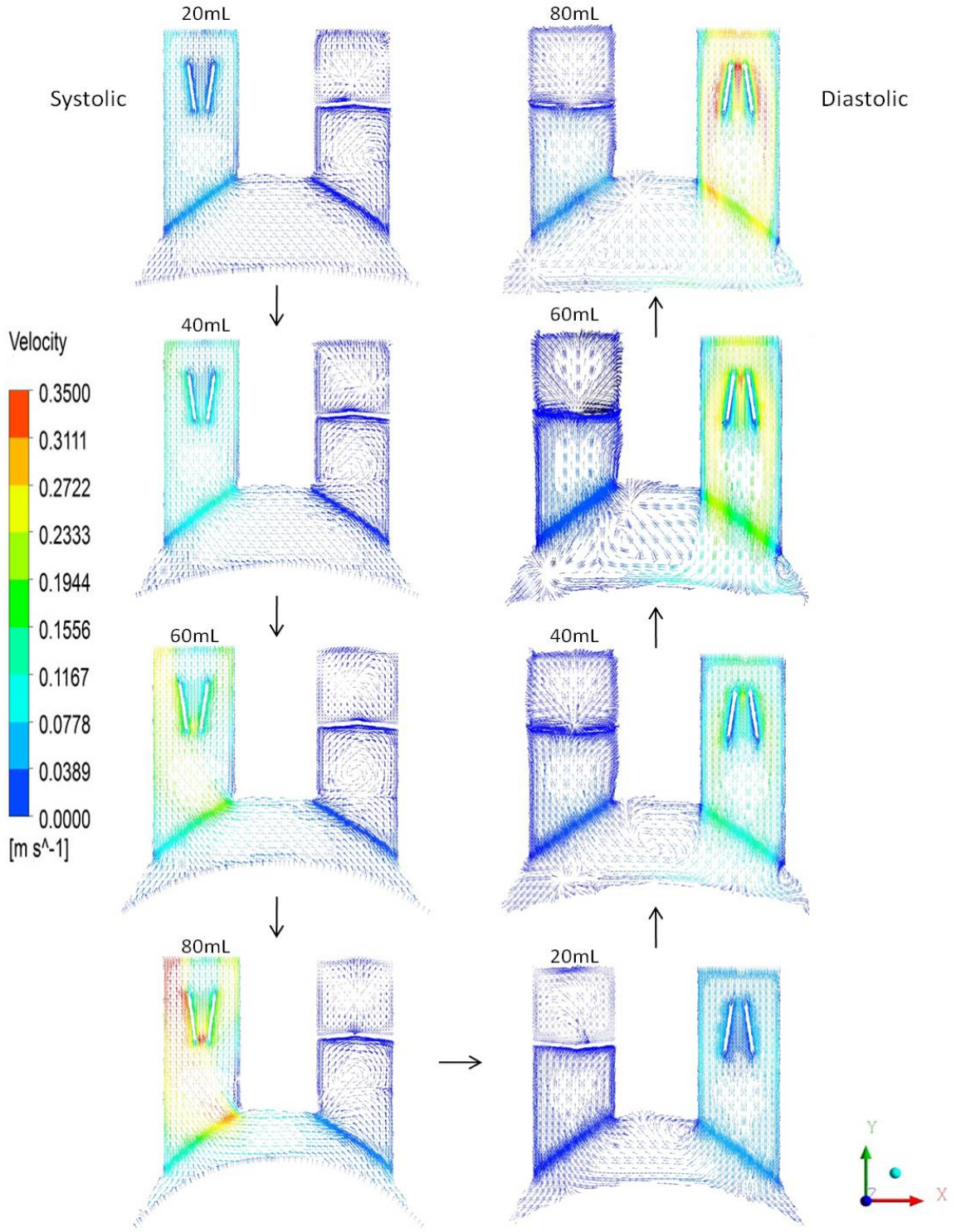

Figure 4.15: Velocity vectors in the testing fluid chamber during systole and diastole under turbulent conditions. Images are presented in 2D views. The left side of the figure shows the flow fields as the diaphragm was moving up with a 20ml increment (systole). The right side of the figure shows the flow fields as the diaphragm was moving down with a 20ml increment. Arrows indicate the sequence in occurrence.

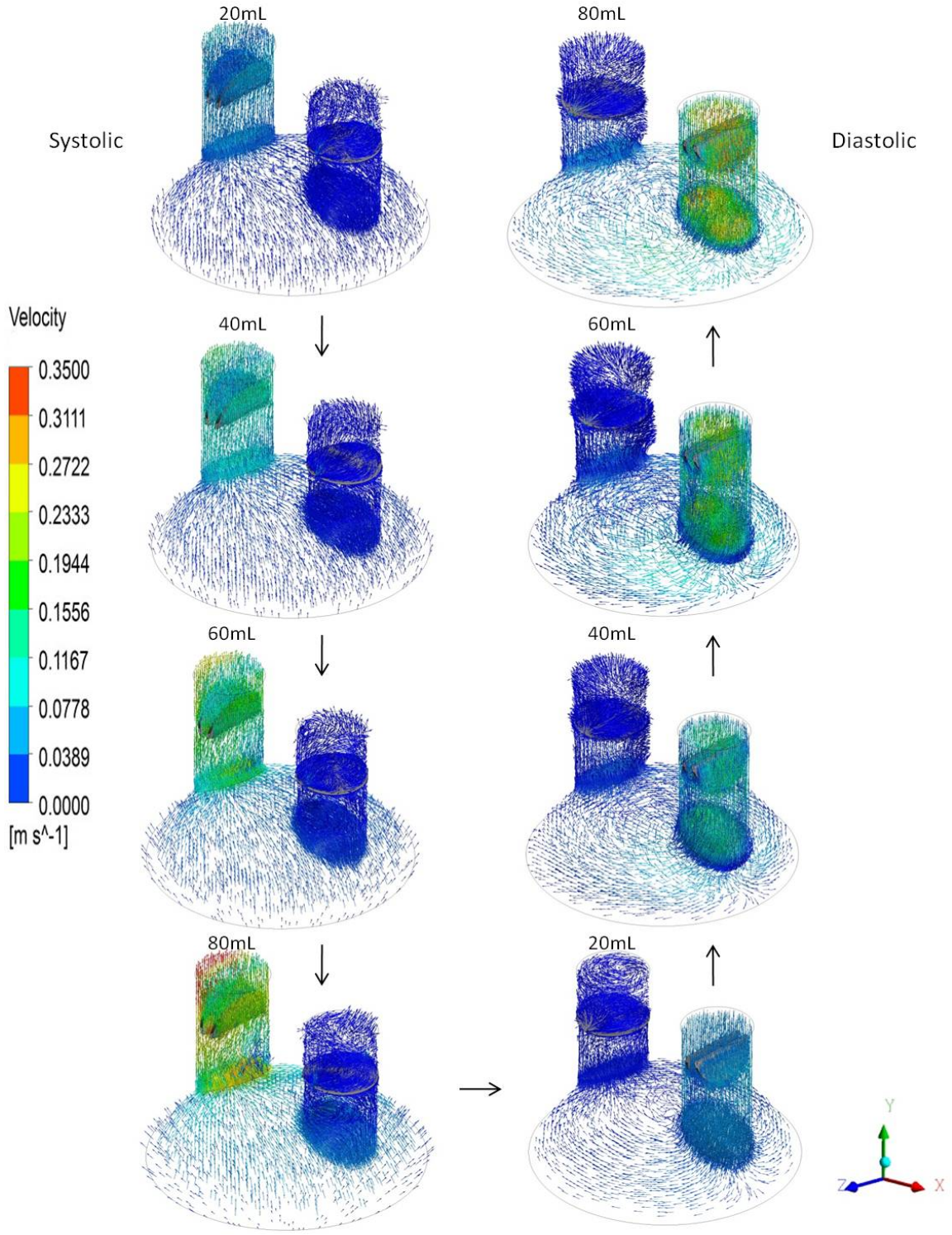

Figure 4.16: Velocity vectors in the testing fluid chamber during systole and diastole under turbulent conditions. Images are presented in 3D views. The left side of the figure shows the flow fields as the diaphragm was moving up with a 20ml increment (systole). The right side of the figure shows the flow fields as the diaphragm was moving down with a 20ml increment. Arrows indicate the sequence in occurrence.

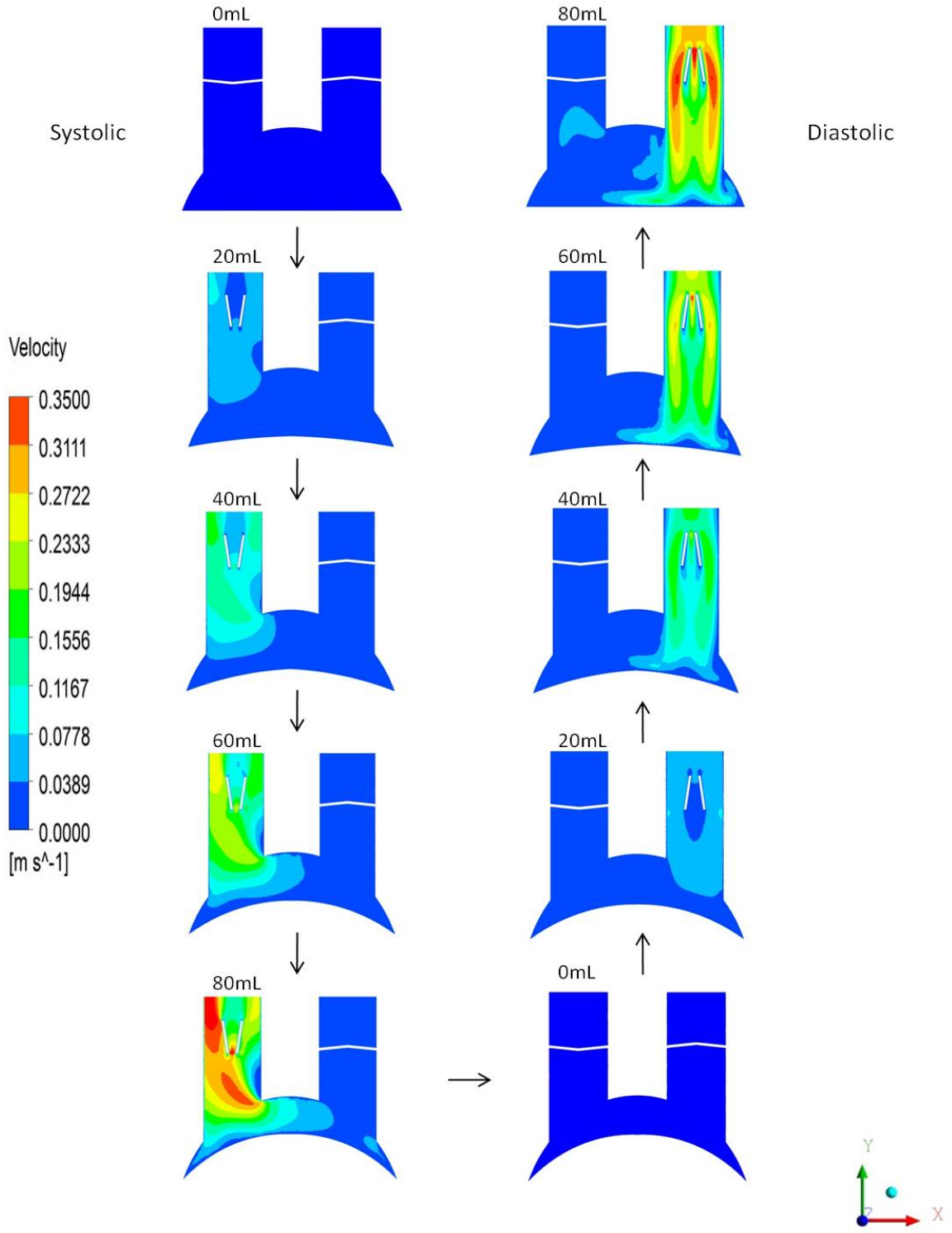

Figure 4.17: Velocity contour in the testing fluid chamber during systole and diastole under turbulent conditions. Images are presented in 2D views. The left side of the figure shows the velocity contour as the diaphragm was moving up with a 20ml increment (systole). The right side of the figure shows the flow fields as the diaphragm was moving down with a 20ml increment. Arrows indicate the sequence in occurrence.

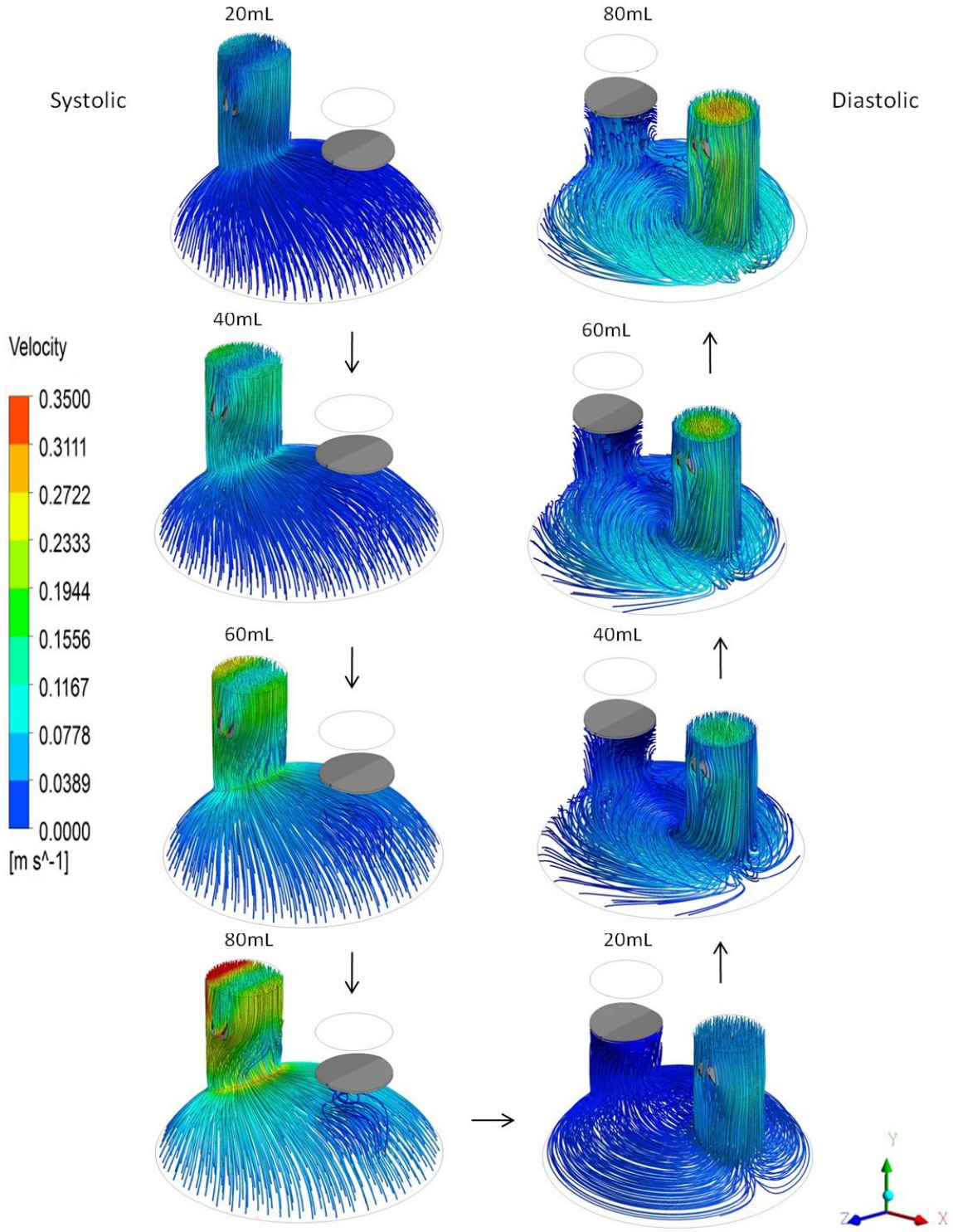

Figure 4.18: Velocity stream lines in the testing fluid chamber during systole and diastole under turbulent conditions. Images are presented in 3D views. The left side of the figure shows the stream lines as the diaphragm was moving up with a 20ml increment (systole). The right side of the figure shows the flow fields as the diaphragm was moving down with a 20ml increment. Arrows indicate the sequence in occurrence.

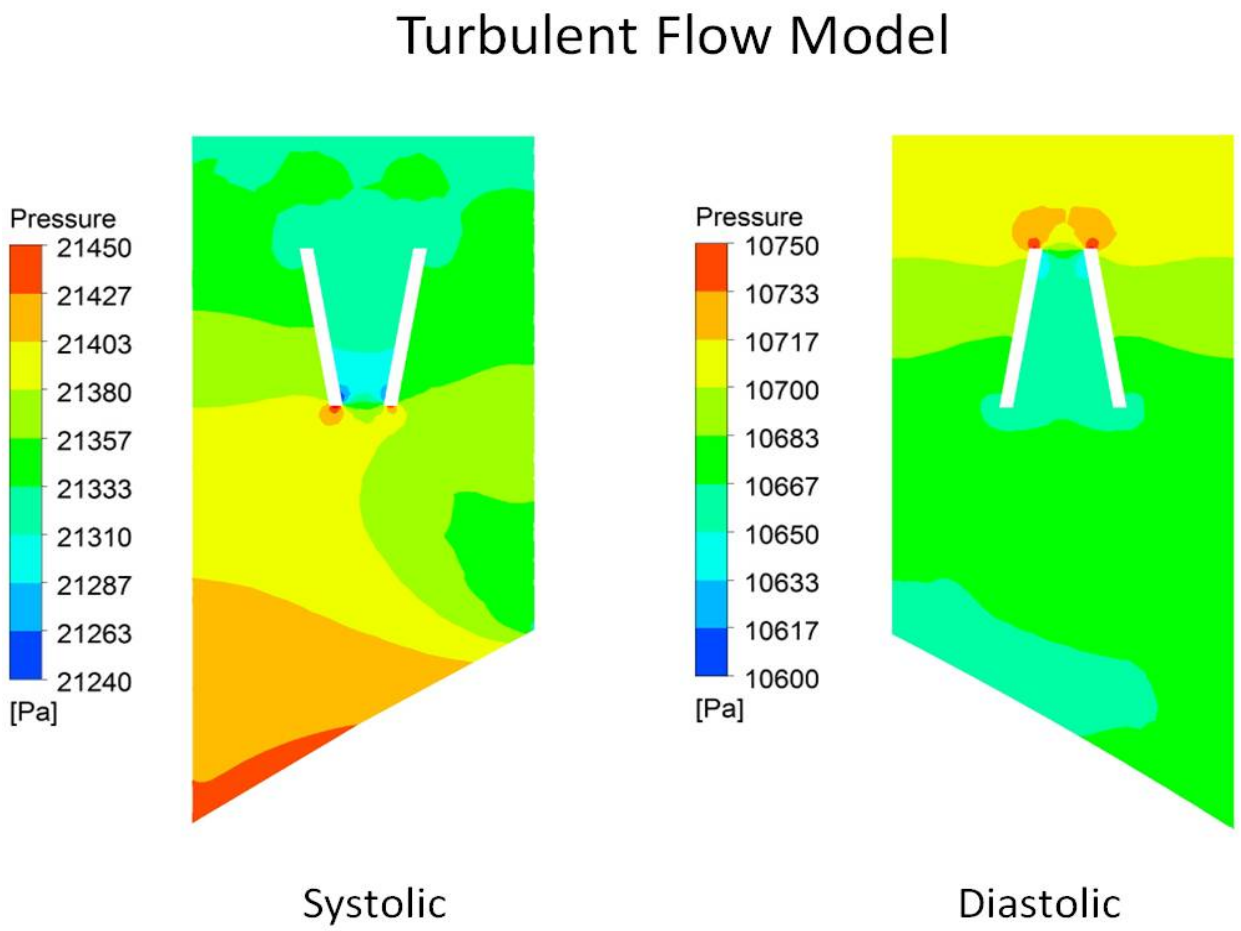

Figure 4.19: Pressure distribution contours at the valve area during systole and diastole under turbulent conditions. Images are presented in 2D views. The left side of the figure shows the pressure contour as the outlet valve was fully opened (systole). The right side of the figure shows the pressure contour as the inlet valve was fully opened (diastole). (1 Pa = 0.007501 mmHg)

CHAPTER V

DISCUSSION

In this study, we designed and fabricated a flow chamber to study the performance of prosthetic heart valves (PHVs). The biocompatibility of the flow chamber was tested through the responses from platelets (platelet activation, i.e. CD62P expression) and red blood cells (hemolysis). Both static and dynamic experiments with platelets and red blood cells were conducted. Also, the dynamic flow patterns inside the testing fluid chamber as investigated using numerical simulations.

5.1 Flow chamber design

Compared to the commercially available left ventricular assist devices (LVADs), this custom-built flow chamber provided a more economic experimental setup to study the performance of PHVs. (Oz et al., 2003). The other major advantage of this flow chamber is that it can be used to study PHVs of different designs and different sizes. The major components of the flow chamber include a testing fluid chamber, a water chamber, and a transparent valve socket. Both the testing fluid and water chambers were made from Teflon. Teflon is a well known biocompatible material and has been used in many blood implantable devices. In some cases, Teflon had also been used to make some parts of implantable heart devices (Akutsu and Kantrowitz, 1967).

The testing fluid chamber was carefully designed such that the chamber volume (127 ml) matched physiological end diastolic volume, 130 ml.

The Water chamber was connected to an external reciprocating pump (Harvard Apparatus Pump) which was used widely to provide physiologically relevant flow environments (Bluestein et al., 2004). The pump setting can be adjusted in order to mimic the flow rate, stroke volume (80 ml), stroke rate (72 min^{-1},) and systolic/diastolic ratio (0.375), etc. of a normal human heart. The ability of the pump to replicate physiological flow conditions provided a desirable environment for *in vitro* experiments. The testing fluid chamber and the water chamber were separated by a diaphragm, whose movement drove the flow in the testing fluid chamber by transmitting the pressure gradient from the water chamber. In dynamic experiments, the diaphragm was subjected to a maximum deformation of 0.68 inches (in height) for about 6,500 times (in 90 minutes). So, the thickness of the diaphragm was chosen at 0.025 inches, which can undergo a 750 percent elongation and withstand up to 4,000 psi of tensile strength. The mechanical property of the chosen diaphragm was strong enough to withstand the loading conditions required by the experiments.

The transparent valve socket was designed to hold two heart valves at the other end of the testing fluid chamber. The socket was made from PVC. PVC has been widely used in biomedical applications. It is one of the most common materials used for catheters (Spilezewski et al., 1988). In addition, clear PVC was selected so as to enable a direct visualization of the movement of the valves. Inside the socket, the two valves were placed parallel to each other but in opposite directions to control flow direction. The valve used in this study was the St Jude bileaflet mechanical heart valve, which was the

most commonly used mechanical heart valve in the US market. Since St. Jude bileaflet mechanical heart valves were well designed and would not induce flow disturbance, the experiments with these valves (control valves) were able to help us to evaluate the performance of the flow chamber and its direct effect on the flow field. The socket was tailor made to house the valves that are under consideration, so as to provide a smooth flow without any disturbance. The smooth and non-turbulent design of the testing flow chamber and valve holder provided a suitable dynamic environment to study valve functions.

5.2 Experimental studies

PHVs are primarily in contact with blood and so their performance greatly depends on the compatibility with platelets and red blood cells. In other words, PHVs should not induce any damage to red blood cells (hemolysis) or activate platelets. In this study, we measured platelet activation and hemolysis induced by the flow chamber under both static and dynamic conditions.

Hemolysis is the breaking of the red blood cell membrane and the release of hemoglobin into to the blood. During hemolysis, the concentration of the red blood cells (hemoglobin) decreases in blood which reduces the oxygen supply. Hemolysis has been used as a standard to determine the performance of PHVs or similar devices (Mecozzi et al., 2002). In our experiments, at different time points, the hemoglobin concentration in whole blood inside the testing fluid chamber was measured by a spectrophotometer at an absorbance wavelength of 540 nm. Our results demonstrated that under static conditions, there was no significant (n=5) change in hemoglobin concentration for a period of 6

hours. This indicated that the flow device did not induce hemolysis. The results obtained from dynamic experiments indicated that the addition of the St. Jude bileaflet mechanical heart valves and the dynamic flow environment induced significant (n=4) changes in hemoglobin concentration by using pair *t-test*, after blood was circulated in the device for 90 minutes, compared to the control. However, the results obtained from single-classification ANOVA indicated that no significant change of hemoglobin concentration in the chamber. The significant change showed in the pair *t-test* might come from the change in the bench blood sample itself. Together, these data demonstrated that the flow chamber itself and the flow environment in the device did not induce hemolysis.

Non-physiological blood flow can trigger platelet activation. Activated platelets will change in shape and start to adhere to other platelets and form a clot. In addition, activated platelets can lead to thrombosis and contribute to the development of atherosclerosis. (Bluestein et al., 2004; Davi and Patrono, 2007). In our experiments, platelet activation was measured by CD62P expression, using flow cytometry. Under static conditions, an increased CD62P expression (n=6, $P < 0.05$) was observed on platelets that were placed in the flow chamber after 3 hours of incubation. However, no change was observed on these platelets during the first two hours when incubated in the flow chamber. This result was not expected. It might come from the slow self-activation of platelets when a large amount of platelets (100,000/μl at 250 ml) were kept stagnant together. The results from dynamic experiments indicated that with the presence of the St. Jude bileaflet mechanical heart valves, the flow conditions in the testing fluid chamber did not induce any platelet activation (n=6) after 90 minutes of circulation, which was corresponding to 8400 valve passages. These data demonstrated that the

materials and the flow dynamics of the flow chamber were suitable for circulating platelets. In summary, the flow chamber, especially under dynamic flow conditions, can provide a physiologically relevant environment to study heart valve functions, without damaging circulating red blood cells and platelets.

5.3 Numerical simulation

Numerical simulations were conducted to evaluate the flow patterns in the flow chamber. Computational fluid dynamics (CFD) is an effective tool to estimate the flow patterns when direct measurement was not available, provided the usage of closely matched geometry of the model and boundary conditions. In this study, the flow patterns inside the chamber at various instances during systole and diastole were analyzed. To simplify the modeling process, the performance of the testing fluid chamber was modeled under 4 different conditions, depending on the volume of fluid ejected out of the outlet valve: 20 ml, 40 ml, 60 ml, and 80 ml. In addition, valve geometry replicating the St. Jude bileaflet mechanical heart valve was designed and included in the analysis. For simplification, the valve configuration was such that one of them was fully open while the other was closed, chosen based on systole or diastole. In other words, the valve in the flow direction was always open, while the other was always closed. Physiologically, it takes 20 to 30 msec for the aortic valve to open or close (Krisnan B.Chandran et al., 2007b). When fully open or closed, the valve will stay in that status (open or closed) for approximately 230 to 500 msec. Since the opening or closing time is minimum compared to the time when the valve stays open or closed, the assumption to keep them at the open or closed location was suitable, especially when the ejection and injection took about 270 msec and 430 msec respectively (Frederic H.Martini and Judi L.Nath, 2009).

The model was meshed using an unstructured mesh, in order to optimize the computational time, and the spatial and temporal resolution of the results. A laminar solver was used to simulate fluid flow in this model, to check the mesh integrity, geometry, and the boundary conditions. The results from these simulations revealed a proper laminar flow patterns in both systolic (fluid from chamber through the valves) and diastolic (fluid flow from the channel through the valves) configurations. The maximum velocity estimated by the laminar solver (end of systole and diastole) in systolic configuration was 0.5086 m/s, while that in diastolic configuration was 0.4209 m/s. In both the configurations, the maximum velocity was found near the open valve. Estimation from turbulent solver showed the similar results - the maximum velocity was 0.5106 m/s in systolic configuration (end of systole and diastole), and 0.4321 m/s in diastole. Later, flow in the chamber was solved using k-ω solver in order to check for the existence of turbulence. The results revealed that the maximum Reynolds number was 2127.69 during systole. By comparing the flow fields, estimated by both laminar and turbulent models (Figure 4.11 and Figure 4.15), no turbulence was detected in both systolic and diastolic configurations. Also, similar maximum velocities were estimated by laminar and turbulent models (systolic: laminar-0.5086 m/s, turbulent-0.5106 m/s; diastolic: laminar-0.4209 m/s, turbulent-0.4321 m/s).

Combined, results obtained from the *in vitro* experiment and numerical simulations demonstrated that the structure of the testing fluid chamber did not induce complex flow conditions and the flow environment generated by the chamber was suitable for heart valve dynamic performance studies.

CHAPTER VI

CONCLUSIONS

A biocompatible flow chamber similar to left ventricular assist device was built to study the hemodynamic performance of prosthetic heart valves (PHVs). A detailed design of the flow chamber components was modeled using the computer aided design software (Pro-E Wildfire 4.0 PTC). The geometrical parameters of the major components (testing fluid chamber, water chamber, and transparent valve socket) were designed based on physiological conditions. The transparent part (transparent valve socket) of the flow chamber provided a direct visualization of the valve movement. The materials chosen were biocompatible and have been previously used in many medical devices. All together, the flow chamber provided a more economic and flexible experimental setup to study the performance of PHVs.

Biocompatibility of the flow chamber towards platelets and red blood cells were conducted under static and dynamic conditions. The static condition was conducted to check the surface contact induced platelet and red blood cell response, while dynamic condition, with St. Jude bileaflet mechanical heart valves, was to check the flow induced response. The results indicated that the flow chamber did not induce platelet activation and hemolysis under static or dynamic conditions. A computational fluid dynamic analysis of flow inside the chamber was conducted using ANSYS CFX-12.0.

Both systolic and diastolic conditions were simulated using laminar and turbulent solver (with ejection and injection volume of 20 ml, 40 ml, 60 ml, and 80 ml). A detailed velocity vectors distribution inside the flow chamber, and Reynolds number of each condition was reported. The results revealed that no turbulence was present in the flow chamber. Overall, the design of the flow chamber meets the materials and fluid dynamics requirements to conduct PHV study.

In the future, various novel designs of PHVs can be evaluated in the flow chamber that was built in this study. The performance of PHVs can be accessed through their effect on hemolysis and platelet activation under dynamic conditions. In addition, biocompatibility of PHV's made out of new material can be accessed under dynamic conditions. Techniques like Laser Doppler Velocimetry can be incorporated to the flow chamber to observe the platelet trajectory and to calculate other flow variables. The other recommendation is to involve a fluid solid interaction solver to improve the computational fluid dynamics simulation of flow conditions inside the chamber.

REFERENCES

Akutsu, T., Kantrowitz, A., (1967). Problems of materials in mechanical heart systems. J.Biomed.Mater.Res. 1**,** 33-54.

Alemu, Y., Bluestein, D., (2007). Flow-induced platelet activation and damage accumulation in a mechanical heart valve: numerical studies. Artif.Organs 31**,** 677-688.

Bjork, V. O., (1969). A new tilting disc valve prosthesis. Scand.J.Thorac.Cardiovasc.Surg. 3**,** 1-10.

Bluestein, D., Yin, W., Affeld, K., Jesty, J., (2004). Flow-induced platelet activation in mechanical heart valves. J.Heart Valve Dis. 13**,** 501-508.

Bortolotti, U., Milano, A., Mazzucco, A., Guerra, F., Magni, A., Thiene, G., Gallucci, V., (1988). Hancock bioprosthetic valve failure: causes, and results of reoperation. Tex.Heart Inst.J. 15**,** 25-30.

Butany, J., Ahluwalia, M. S., Munroe, C., Fayet, C., Ahn, C., Blit, P., Kepron, C., Cusimano, R. J., Leask, R. L., (2003). Mechanical heart valve prostheses: identification and evaluation (erratum). Cardiovasc.Pathol. 12**,** 322-344.

Daebritz, S. H., Fausten, B., Hermanns, B., Franke, A., Schroeder, J., Groetzner, J., Autschbach, R., Messmer, B. J., Sachweh, J. S., (2004). New flexible polymeric heart valve prostheses for the mitral and aortic positions. Heart Surg.Forum 7**,** E525-E532.

Davi, G., Patrono, C., (2007). Platelet activation and atherothrombosis. N.Engl.J.Med. 357**,** 2482-2494.

Frazier, O. H., (2010). Current status of cardiac transplantation and left ventricular assist devices. Tex.Heart Inst.J. 37**,** 319-321.

Frederic H.Martini, Judi L.Nath, (2009). The Heart. Fundamentals of Anatomy & Physiology. Pearson, pp. 681-718.

Garcia, M. J., Vandervoort, P., Stewart, W. J., Lytle, B. W., Cosgrove, D. M., III, Thomas, J. D., Griffin, B. P., (1996). Mechanisms of hemolysis with mitral prosthetic regurgitation. Study using transesophageal echocardiography and fluid dynamic simulation. J.Am.Coll.Cardiol. 27**,** 399-406.

Grunkemeier, G. L., Li, H. H., Naftel, D. C., Starr, A., Rahimtoola, S. H., (2000). Long-term performance of heart valve prostheses. Curr.Probl.Cardiol. 25**,** 73-154.

Hufnagel, C. A., Harvey, W. P., Rabil, P. J., McDermott, T. F., (1954). Surgical correction of aortic insufficiency. Surgery 35**,** 673-683.

King, M. J., David, T., Fisher, J., (1997). Three-dimensional study of the effect of two leaflet opening angles on the time-dependent flow through a bileaflet mechanical heart valve. Med.Eng Phys. 19**,** 235-241.

Krisnan B.Chandran, Ajit P.Yoganathan, Stanley E.Rittgers, (2007a). Cardiovascular Physiology. Biofluid Mechanics: The Human Circulation. CRC Press, pp. 69-112.

Krisnan B.Chandran, Ajit P.Yoganathan, Stanley E.Rittgers, (2007b). Prosthetic Heart Valve Fluid Dynamics. Biofluid Mechanics: The Human Circulation. CRC Press, pp. 277-313.

Kunadian, B., Vijayalakshmi, K., Thornley, A. R., de Belder, M. A., Hunter, S., Kendall, S., Graham, R., Stewart, M., Thambyrajah, J., Dunning, J., (2007). Meta-analysis of valve hemodynamics and left ventricular mass regression for stentless versus stented aortic valves. Ann.Thorac.Surg. 84**,** 73-78.

Maraj, R., Jacobs, L. E., Ioli, A., Kotler, M. N., (1998). Evaluation of hemolysis in patients with prosthetic heart valves. Clin.Cardiol. 21**,** 387-392.

Marchand, M. A., Aupart, M. R., Norton, R., Goldsmith, I. R., Pelletier, L. C., Pellerin, M., Dubiel, T., Daenen, W. J., Herijgers, P., Casselman, F. P., Holden, M. P., David, T. E., (2001). Fifteen-year experience with the mitral Carpentier-Edwards PERIMOUNT pericardial bioprosthesis. Ann.Thorac.Surg. 71**,** S236-S239.

Mecozzi, G., Milano, A. D., De, C. M., Sorrentino, F., Pratali, S., Nardi, C., Bortolotti, U., (2002). Intravascular hemolysis in patients with new-generation prosthetic heart valves: a prospective study. J.Thorac.Cardiovasc.Surg. 123**,** 550-556.

Oz, M. C., Gelijns, A. C., Miller, L., Wang, C., Nickens, P., Arons, R., Aaronson, K., Richenbacher, W., van, M. C., Nelson, K., Weinberg, A., Watson, J., Rose, E. A., Moskowitz, A. J., (2003). Left ventricular assist devices as permanent heart failure therapy: the price of progress. Ann.Surg. 238**,** 577-583.

Rodgers, B. M., Sabiston, D. C., Jr., (1969). Hemolytic anemia following prosthetic valve replacement. Circulation 39**,** I155-I161.

Shapira, Y., Vaturi, M., Sagie, A., (2009). Hemolysis associated with prosthetic heart valves: a review. Cardiol.Rev. 17**,** 121-124.

Simon, H. A., Ge, L., Borazjani, I., Sotiropoulos, F., Yoganathan, A. P., (2010). Simulation of the three-dimensional hinge flow fields of a bileaflet mechanical heart valve under aortic conditions. Ann.Biomed.Eng 38**,** 841-853.

Smadi, O., Hassan, I., Pibarot, P., Kadem, L., (2010). Numerical and experimental investigations of pulsatile blood flow pattern through a dysfunctional mechanical heart valve. J.Biomech. 43**,** 1565-1572.

Spilezewski, K. L., Anderson, J. M., Schaap, R. N., Solomon, D. D., (1988). In vivo biocompatibility of catheter materials. Biomaterials 9**,** 253-256.

Sun, J. C., Davidson, M. J., Lamy, A., Eikelboom, J. W., (2009). Antithrombotic management of patients with prosthetic heart valves: current evidence and future trends. Lancet 374**,** 565-576.

Yacoub, M. H., Takkenberg, J. J., (2005). Will heart valve tissue engineering change the world? Nat.Clin.Pract.Cardiovasc.Med. 2**,** 60-61.

Yoganathan, A. P., He, Z., Casey, J. S., (2004). Fluid mechanics of heart valves. Annu.Rev.Biomed.Eng 6**,** 331-362.

APPPENDIX A

CFX COMMAND LANGUAGE (CCL)

LAMINAR FLOW MODEL (80ml, DIASTOLE)

```
# State file created:  2010/11/21 02:57:58
# CFX-12.0.1 build 2009.04.14-23.02

LIBRARY:
  MATERIAL: Water
    Material Description = Water (liquid)
    Material Group = Water Data, Constant Property Liquids
    Option = Pure Substance
    Thermodynamic State = Liquid
    PROPERTIES:
      Option = General Material
      EQUATION OF STATE:
        Density = 997.0 [kg m^-3]
        Molar Mass = 18.02 [kg kmol^-1]
        Option = Value
      END
```

SPECIFIC HEAT CAPACITY:

Option = Value

Specific Heat Capacity = 4181.7 [J kg^-1 K^-1]

Specific Heat Type = Constant Pressure

END

REFERENCE STATE:

Option = Specified Point

Reference Pressure = 1 [atm]

Reference Specific Enthalpy = 0.0 [J/kg]

Reference Specific Entropy = 0.0 [J/kg/K]

Reference Temperature = 25 [C]

END

DYNAMIC VISCOSITY:

Dynamic Viscosity = 8.899E-4 [kg m^-1 s^-1]

Option = Value

END

THERMAL CONDUCTIVITY:

Option = Value

Thermal Conductivity = 0.6069 [W m^-1 K^-1]

END

ABSORPTION COEFFICIENT:

Absorption Coefficient = 1.0 [m^-1]

Option = Value

END

SCATTERING COEFFICIENT:

```
      Option = Value
      Scattering Coefficient = 0.0 [m^-1]
    END
    REFRACTIVE INDEX:
      Option = Value
      Refractive Index = 1.0 [m m^-1]
    END
    THERMAL EXPANSIVITY:
      Option = Value
      Thermal Expansivity = 2.57E-04 [K^-1]
    END
  END
 END
END
FLOW: Flow Analysis 1
 SOLUTION UNITS:
  Angle Units = [rad]
  Length Units = [m]
  Mass Units = [kg]
  Solid Angle Units = [sr]
  Temperature Units = [K]
  Time Units = [s]
 END
 ANALYSIS TYPE:
  Option = Steady State
```

```
  EXTERNAL SOLVER COUPLING:
    Option = None
  END
END
DOMAIN: Default Domain Modified
  Coord Frame = Coord 0
  Domain Type = Fluid
  Location = BODY_HOUSING,BODY_OUTLET_WALL
  BOUNDARY: Default Fluid Fluid Interface in Default Domain Modified Side 1
    Boundary Type = INTERFACE
    Location = HOUSING_OUTLET_1
    BOUNDARY CONDITIONS:
      MASS AND MOMENTUM:
        Option = Conservative Interface Flux
      END
    END
  END
  BOUNDARY: outlet
    Boundary Type = WALL
    Location = OUTLET
    BOUNDARY CONDITIONS:
      MASS AND MOMENTUM:
        Option = No Slip Wall
      END
    END
```

```
END
BOUNDARY: valve close
  Boundary Type = WALL
  Location = VALVE_INLET
  BOUNDARY CONDITIONS:
    MASS AND MOMENTUM:
      Option = No Slip Wall
    END
  END
END
BOUNDARY: wall
  Boundary Type = WALL
  Location = DIAPHRAGM,HOUSING,INLETWALL
  BOUNDARY CONDITIONS:
    MASS AND MOMENTUM:
      Option = No Slip Wall
    END
  END
END
DOMAIN MODELS:
  BUOYANCY MODEL:
    Option = Non Buoyant
  END
  DOMAIN MOTION:
    Option = Stationary
```

```
  END
  MESH DEFORMATION:
    Option = None
  END
  REFERENCE PRESSURE:
    Reference Pressure = 80 [mm Hg]
  END
END
FLUID DEFINITION: Fluid 1
  Material = Water
  Option = Material Library
  MORPHOLOGY:
    Option = Continuous Fluid
  END
END
FLUID MODELS:
  COMBUSTION MODEL:
    Option = None
  END
  HEAT TRANSFER MODEL:
    Option = None
  END
  THERMAL RADIATION MODEL:
    Option = None
  END
```

```
    TURBULENCE MODEL:
      Option = Laminar
    END
  END
END
DOMAIN: cylin
  Coord Frame = Coord 0
  Domain Type = Fluid
  Location = BODY_CYLINDER_INLET
  BOUNDARY: Default Fluid Fluid Interface in cylin Side 1
    Boundary Type = INTERFACE
    Location = CONNECTION_INLET_1
    BOUNDARY CONDITIONS:
      MASS AND MOMENTUM:
        Option = Conservative Interface Flux
      END
    END
  END
  BOUNDARY: inlet
    Boundary Type = INLET
    Location = INLET
    BOUNDARY CONDITIONS:
      FLOW REGIME:
        Option = Subsonic
      END
```

```
    MASS AND MOMENTUM:
      Normal Speed = 18.9458 [cm s^-1]
      Option = Normal Speed
    END
  END
END
BOUNDARY: wall cylin
  Boundary Type = WALL
  Location = CYLINDER_INLET
  BOUNDARY CONDITIONS:
    MASS AND MOMENTUM:
      Option = No Slip Wall
    END
  END
END
DOMAIN MODELS:
  BUOYANCY MODEL:
    Option = Non Buoyant
  END
  DOMAIN MOTION:
    Option = Stationary
  END
  MESH DEFORMATION:
    Option = None
  END
```

REFERENCE PRESSURE:

Reference Pressure = 80 [mm Hg]

END

END

FLUID DEFINITION: Fluid 1

Material = Water

Option = Material Library

MORPHOLOGY:

Option = Continuous Fluid

END

END

FLUID MODELS:

COMBUSTION MODEL:

Option = None

END

HEAT TRANSFER MODEL:

Option = None

END

THERMAL RADIATION MODEL:

Option = None

END

TURBULENCE MODEL:

Option = Laminar

END

END

```
END
DOMAIN: tube
  Coord Frame = Coord 0
  Domain Type = Fluid
  Location = BODY_INLET_WALL
  BOUNDARY: Default Fluid Fluid Interface in tube Side 2
    Boundary Type = INTERFACE
    Location = CONNECTION_INLET_2,HOUSING_OUTLET_2
    BOUNDARY CONDITIONS:
      MASS AND MOMENTUM:
        Option = Conservative Interface Flux
      END
    END
  END
  BOUNDARY: valve open
    Boundary Type = WALL
    Location = VALVE_OUTLET
    BOUNDARY CONDITIONS:
      MASS AND MOMENTUM:
        Option = No Slip Wall
      END
    END
  END
  BOUNDARY: wall tube
    Boundary Type = WALL
```

```
  Location = OUTLETWALL
  BOUNDARY CONDITIONS:
    MASS AND MOMENTUM:
      Option = No Slip Wall
    END
  END
END
DOMAIN MODELS:
  BUOYANCY MODEL:
    Option = Non Buoyant
  END
  DOMAIN MOTION:
    Option = Stationary
  END
  MESH DEFORMATION:
    Option = None
  END
  REFERENCE PRESSURE:
    Reference Pressure = 80 [mm Hg]
  END
END
FLUID DEFINITION: Fluid 1
  Material = Water
  Option = Material Library
  MORPHOLOGY:
```

```
    Option = Continuous Fluid
   END
  END
  FLUID MODELS:
   COMBUSTION MODEL:
    Option = None
   END
   HEAT TRANSFER MODEL:
    Option = None
   END
   THERMAL RADIATION MODEL:
    Option = None
   END
   TURBULENCE MODEL:
    Option = Laminar
   END
  END
END
DOMAIN INTERFACE: Default Fluid Fluid Interface
  Boundary List1 = Default Fluid Fluid Interface in Default Domain Modified \
   Side 1,Default Fluid Fluid Interface in cylin Side 1
  Boundary List2 = Default Fluid Fluid Interface in tube Side 2
  Interface Type = Fluid Fluid
  INTERFACE MODELS:
   Option = General Connection
```

```
    FRAME CHANGE:
      Option = None
    END
    MASS AND MOMENTUM:
      Option = Conservative Interface Flux
      MOMENTUM INTERFACE MODEL:
        Option = None
      END
    END
    PITCH CHANGE:
      Option = None
    END
  END
  MESH CONNECTION:
    Option = GGI
  END
END
INITIALISATION:
  Option = Automatic
  INITIAL CONDITIONS:
    Velocity Type = Cartesian
    CARTESIAN VELOCITY COMPONENTS:
      Option = Automatic
    END
    STATIC PRESSURE:
```

```
      Option = Automatic
    END
  END
END
OUTPUT CONTROL:
  RESULTS:
    File Compression Level = Default
    Option = Standard
  END
END
SOLVER CONTROL:
  ADVECTION SCHEME:
    Option = High Resolution
  END
  CONVERGENCE CONTROL:
    Length Scale Option = Conservative
    Maximum Number of Iterations = 250
    Minimum Number of Iterations = 1
    Timescale Control = Auto Timescale
    Timescale Factor = 1.0
  END
  CONVERGENCE CRITERIA:
    Residual Target = 1.E-4
    Residual Type = RMS
  END
```

```
    DYNAMIC MODEL CONTROL:
      Global Dynamic Model Control = On
    END
  END
END
COMMAND FILE:
  Version = 12.0.1
END
```

TURBULENT FLOW MODEL (80 ml, DIASTOLE)

```
# State file created:  2010/11/21 02:56:19
# CFX-12.0.1 build 2009.04.14-23.02

LIBRARY:
  MATERIAL: Water
    Material Description = Water (liquid)
    Material Group = Water Data, Constant Property Liquids
    Option = Pure Substance
    Thermodynamic State = Liquid
    PROPERTIES:
      Option = General Material
      EQUATION OF STATE:
        Density = 997.0 [kg m^-3]
        Molar Mass = 18.02 [kg kmol^-1]
```

Option = Value

END

SPECIFIC HEAT CAPACITY:

Option = Value

Specific Heat Capacity = 4181.7 [J kg^-1 K^-1]

Specific Heat Type = Constant Pressure

END

REFERENCE STATE:

Option = Specified Point

Reference Pressure = 1 [atm]

Reference Specific Enthalpy = 0.0 [J/kg]

Reference Specific Entropy = 0.0 [J/kg/K]

Reference Temperature = 25 [C]

END

DYNAMIC VISCOSITY:

Dynamic Viscosity = 8.899E-4 [kg m^-1 s^-1]

Option = Value

END

THERMAL CONDUCTIVITY:

Option = Value

Thermal Conductivity = 0.6069 [W m^-1 K^-1]

END

ABSORPTION COEFFICIENT:

Absorption Coefficient = 1.0 [m^-1]

Option = Value

```
      END
      SCATTERING COEFFICIENT:
        Option = Value
        Scattering Coefficient = 0.0 [m^-1]
      END
      REFRACTIVE INDEX:
        Option = Value
        Refractive Index = 1.0 [m m^-1]
      END
      THERMAL EXPANSIVITY:
        Option = Value
        Thermal Expansivity = 2.57E-04 [K^-1]
      END
    END
  END
END
FLOW: Flow Analysis 1
  SOLUTION UNITS:
    Angle Units = [rad]
    Length Units = [m]
    Mass Units = [kg]
    Solid Angle Units = [sr]
    Temperature Units = [K]
    Time Units = [s]
  END
```

```
ANALYSIS TYPE:
  Option = Steady State
  EXTERNAL SOLVER COUPLING:
    Option = None
  END
END
DOMAIN: Default Domain Modified
  Coord Frame = Coord 0
  Domain Type = Fluid
  Location = BODY_HOUSING,BODY_OUTLET_WALL
  BOUNDARY: Default Fluid Fluid Interface in Default Domain Modified Side 1
    Boundary Type = INTERFACE
    Location = HOUSING_OUTLET_1
    BOUNDARY CONDITIONS:
      MASS AND MOMENTUM:
        Option = Conservative Interface Flux
      END
      TURBULENCE:
        Option = Conservative Interface Flux
      END
    END
  END
  BOUNDARY: outlet
    Boundary Type = WALL
    Location = OUTLET
```

```
  BOUNDARY CONDITIONS:
    MASS AND MOMENTUM:
      Option = No Slip Wall
    END
    WALL ROUGHNESS:
      Option = Smooth Wall
    END
  END
END
BOUNDARY: valve close
  Boundary Type = WALL
  Location = VALVE_INLET
  BOUNDARY CONDITIONS:
    MASS AND MOMENTUM:
      Option = No Slip Wall
    END
    WALL ROUGHNESS:
      Option = Smooth Wall
    END
  END
END
BOUNDARY: wall
  Boundary Type = WALL
  Location = DIAPHRAGM,HOUSING,INLETWALL
  BOUNDARY CONDITIONS:
```

```
    MASS AND MOMENTUM:
      Option = No Slip Wall
    END
    WALL ROUGHNESS:
      Option = Smooth Wall
    END
  END
END
DOMAIN MODELS:
  BUOYANCY MODEL:
    Option = Non Buoyant
  END
  DOMAIN MOTION:
    Option = Stationary
  END
  MESH DEFORMATION:
    Option = None
  END
  REFERENCE PRESSURE:
    Reference Pressure = 80 [mm Hg]
  END
END
FLUID DEFINITION: Fluid 1
  Material = Water
  Option = Material Library
```

```
    MORPHOLOGY:
      Option = Continuous Fluid
    END
  END
  FLUID MODELS:
    COMBUSTION MODEL:
      Option = None
    END
    HEAT TRANSFER MODEL:
      Option = None
    END
    THERMAL RADIATION MODEL:
      Option = None
    END
    TURBULENCE MODEL:
      Option = k omega
    END
    TURBULENT WALL FUNCTIONS:
      Option = Automatic
    END
  END
END
DOMAIN: cylin
  Coord Frame = Coord 0
  Domain Type = Fluid
```

Location = BODY_CYLINDER_INLET

BOUNDARY: Default Fluid Fluid Interface in cylin Side 1

Boundary Type = INTERFACE

Location = CONNECTION_INLET_1

BOUNDARY CONDITIONS:

MASS AND MOMENTUM:

Option = Conservative Interface Flux

END

TURBULENCE:

Option = Conservative Interface Flux

END

END

END

BOUNDARY: inlet

Boundary Type = INLET

Location = INLET

BOUNDARY CONDITIONS:

FLOW REGIME:

Option = Subsonic

END

MASS AND MOMENTUM:

Normal Speed = 18.9458 [cm s^-1]

Option = Normal Speed

END

TURBULENCE:

```
      Option = Medium Intensity and Eddy Viscosity Ratio
    END
  END
END
BOUNDARY: wall cylin
  Boundary Type = WALL
  Location = CYLINDER_INLET
  BOUNDARY CONDITIONS:
    MASS AND MOMENTUM:
      Option = No Slip Wall
    END
    WALL ROUGHNESS:
      Option = Smooth Wall
    END
  END
END
DOMAIN MODELS:
  BUOYANCY MODEL:
    Option = Non Buoyant
  END
  DOMAIN MOTION:
    Option = Stationary
  END
  MESH DEFORMATION:
    Option = None
```

```
  END
  REFERENCE PRESSURE:
    Reference Pressure = 80 [mm Hg]
  END
END
FLUID DEFINITION: Fluid 1
  Material = Water
  Option = Material Library
  MORPHOLOGY:
    Option = Continuous Fluid
  END
END
FLUID MODELS:
  COMBUSTION MODEL:
    Option = None
  END
  HEAT TRANSFER MODEL:
    Option = None
  END
  THERMAL RADIATION MODEL:
    Option = None
  END
  TURBULENCE MODEL:
    Option = k omega
  END
```

```
    TURBULENT WALL FUNCTIONS:
      Option = Automatic
    END
  END
END
DOMAIN: tube
  Coord Frame = Coord 0
  Domain Type = Fluid
  Location = BODY_INLET_WALL
  BOUNDARY: Default Fluid Fluid Interface in tube Side 2
    Boundary Type = INTERFACE
    Location = CONNECTION_INLET_2,HOUSING_OUTLET_2
    BOUNDARY CONDITIONS:
      MASS AND MOMENTUM:
        Option = Conservative Interface Flux
      END
      TURBULENCE:
        Option = Conservative Interface Flux
      END
    END
  END
  BOUNDARY: valve open
    Boundary Type = WALL
    Location = VALVE_OUTLET
    BOUNDARY CONDITIONS:
```

```
    MASS AND MOMENTUM:
      Option = No Slip Wall
    END
    WALL ROUGHNESS:
      Option = Smooth Wall
    END
  END
END
BOUNDARY: wall tube
  Boundary Type = WALL
  Location = OUTLETWALL
  BOUNDARY CONDITIONS:
    MASS AND MOMENTUM:
      Option = No Slip Wall
    END
    WALL ROUGHNESS:
      Option = Smooth Wall
    END
  END
END
DOMAIN MODELS:
  BUOYANCY MODEL:
    Option = Non Buoyant
  END
  DOMAIN MOTION:
```

```
    Option = Stationary
  END
  MESH DEFORMATION:
    Option = None
  END
  REFERENCE PRESSURE:
    Reference Pressure = 80 [mm Hg]
  END
END
FLUID DEFINITION: Fluid 1
  Material = Water
  Option = Material Library
  MORPHOLOGY:
    Option = Continuous Fluid
  END
END
FLUID MODELS:
  COMBUSTION MODEL:
    Option = None
  END
  HEAT TRANSFER MODEL:
    Option = None
  END
  THERMAL RADIATION MODEL:
    Option = None
```

```
    END
    TURBULENCE MODEL:
      Option = k omega
    END
    TURBULENT WALL FUNCTIONS:
      Option = Automatic
    END
  END
END
DOMAIN INTERFACE: Default Fluid Fluid Interface
  Boundary List1 = Default Fluid Fluid Interface in Default Domain Modified \
    Side 1,Default Fluid Fluid Interface in cylin Side 1
  Boundary List2 = Default Fluid Fluid Interface in tube Side 2
  Interface Type = Fluid Fluid
  INTERFACE MODELS:
    Option = General Connection
    FRAME CHANGE:
      Option = None
    END
    MASS AND MOMENTUM:
      Option = Conservative Interface Flux
      MOMENTUM INTERFACE MODEL:
        Option = None
      END
    END
```

```
    PITCH CHANGE:
      Option = None
    END
  END
  MESH CONNECTION:
    Option = GGI
  END
END
INITIALISATION:
  Option = Automatic
  INITIAL CONDITIONS:
    Velocity Type = Cartesian
    CARTESIAN VELOCITY COMPONENTS:
      Option = Automatic
    END
    STATIC PRESSURE:
      Option = Automatic
    END
    TURBULENCE INITIAL CONDITIONS:
      Option = Medium Intensity and Eddy Viscosity Ratio
    END
  END
END
OUTPUT CONTROL:
  RESULTS:
```

```
    File Compression Level = Default
    Option = Standard
  END
 END
 SOLVER CONTROL:
  Turbulence Numerics = First Order
  ADVECTION SCHEME:
   Option = High Resolution
  END
  CONVERGENCE CONTROL:
   Length Scale Option = Conservative
   Maximum Number of Iterations = 250
   Minimum Number of Iterations = 1
   Timescale Control = Auto Timescale
   Timescale Factor = 1.0
  END
  CONVERGENCE CRITERIA:
   Residual Target = 1.E-4
   Residual Type = RMS
  END
  DYNAMIC MODEL CONTROL:
   Global Dynamic Model Control = On
  END
 END
END
```

COMMAND FILE:

Version = 12.0.1

END

APPENDIX B

CONFERENCE ABSTRACTS

Experimental Biology Conference, Anaheim, CA, April 2010

A flow chamber to study the performance of artificial heart valves

Abstract number: 1065.3

Wei Yin, Ek Ching Ngwe, David A. Rubenstein

School of Mechanical and Aerospace Engineering, Oklahoma State University

The goal of this study was to build a flow chamber to study the hemodynamic performance of a novel artificial heart valve made of cross-linked aerogels. This low density new material has a significantly improved mechanical strength and a promising biocompatibility with the cardiovascular system. The housing of the flow chamber was made of Teflon and clear PVC. Two aerogel heart valves were fixed oppositely in the chamber, controlling flow direction. Through a polyurethane diaphragm, flow was driven by a reciprocating pump through water. The flow rate of the chamber was fixed at 5L/min with a stroke volume of 80 ml and stroke rate of 72 min^{-1}. The systolic/diastolic ratio was 0.375. The performance of the system was examined using whole blood, platelet rich plasma (PRP) and washed platelets, under static and dynamic conditions. Hemolysis was measured with whole blood using a spectrophotometer. Platelet activation was measured by platelet surface P-selectin expression after PRP contact with the system. Platelet thrombogenecity was examined using a prothrombinase assay after washed platelets were placed into the chamber. Preliminary results indicate that the flow chamber does not induce hemolysis or platelet activation under static conditions, while its dynamic performance depends on the valves used. These results indicate it's feasible to use the flow chamber to study the hemodynamic performance of artificial heart valves.

Oklahoma Research Day, Lawton, OK, November, 2010

A Biocompatible Flow Device to Study the Hemodynamic Performance of Prosthetic Heart Valves

Ek Ching Ngwe, David A. Rubenstein, Wei Yin

School of Mechanical and Aerospace Engineering, Oklahoma State University

Heart valve diseases claim more than 250,000 victims each year in the United State and one treatment is to replace it with a prosthetic heart valve. The goal of this study was to build a biocompatible flow device (following the design of a left ventricular assist device) to study the hemodynamic performance of prosthetic heart valves. The flow device consists of two fluid chambers which made of Teflon and clear PVC, separated by a flexible latex diaphragm. One chamber was connected to a reciprocating pump which drives the diaphragm move and causes fluid in the other chamber to circulate through two heart valves. The biocompatibility of this flow device towards blood platelets and red blood cells were tested under static and dynamic conditions. For static testing, washed platelets and whole blood were placed in the test chamber for up to 6 hours. Platelet surface P-selectin expression and hemolysis were examined every hour using flow cytometry and spectrophotometer (at 540nm).For dynamic testing, two St. Jude bileaflet mechanical heart valves were placed into the test chamber to control the flow direction. Washed platelets and whole blood were circulated in the chamber for 90 minutes and examined every 15 minutes. The results demonstrated that the flow device did not induce hemolysis or platelet activation. In parallel, a 3D computational fluid dynamics model was built to study flow conditions and the results indicated that the flow device did not induce turbulence (maximum Reynolds number was ~2100), which is desirable to study cellular functions. These results demonstrated the feasibility of using this flow device to study the hemodynamic performance of prosthetic heart valves.

VITA

EK CHING NGWE

Candidate for the Degree of

Master of Science

Thesis: A BIOCOMPATIBLE FLOW CHAMBER TO STUDY THE HEMODYNAMIC PERFORMANCE OF PROSTHETIC HEART VALVE

Major Field: Mechanical and Aerospace Engineering

Biographical:

Personal Data: Born at Melaka, Malaysia, on July 16, 1983. Son of Kiow Pang and Lai Ngwe

Education:

Completed the requirements for the Master of Science in Mechanical Engineering at Oklahoma State University, Stillwater, Oklahoma in December, 2010.

Completed the requirements for the Bachelor of Science in Mechanical Engineering at Oklahoma State University, Stillwater, Oklahoma in 2008.

Experience: Research Assistant, Biomedical Engineering Lab (BELOS), from August 2009 to December 2010

Student Memberships: Member, Honor Society of Phi Kappa Phi; Member, Golden Key International Honor Society

Name: Ek Ching Ngwe Date of Degree: December, 2010

Institution: Oklahoma State University Location: Stillwater, Oklahoma

Title of Study: A BIOCOMPATIBLE FLOW CHAMBER TO STUDY THE HEMODYNAMIC PERFORMANCE OF PROSTHETIC HEART VALVES

Pages in Study: 117 Candidate for the Degree of Master of Science

Major Field: Mechanical and Aerospace Engineering

Heart valve diseases claim more than 250,000 victims each year in the United States. One option to treat a diseased heart valve is to replace it with a prosthetic heart valve. There are two main types of prosthetic heart valves, mechanical heart valves and bioprosthetic heart valves. The goal of this study was to build a biocompatible flow chamber (following the design of a left ventricular assist device) to study the hemodynamic performance of prosthetic heart valves. The flow chamber consists of two fluid chambers separated by a flexible latex diaphragm. One chamber is filled with water (water chamber) and connected to a Harvard reciprocating pump, which drives the diaphragm to move up and down and causes fluid in the other chamber (testing fluid chamber) to circulate through two heart valves. The biocompatibility of this flow chamber towards blood platelets and red blood cells were tested under static and dynamic conditions. For static testing, washed platelets were placed in the testing fluid chamber for up to 5 hours. Samples were taken out every hour and platelet surface P-selectin expression was measured using flow cytometry. To investigate the effect of the chamber on red blood cells, whole blood was placed in the test chamber for up to 6 hours. Hemolysis was measured every hour (at 540 nm). For dynamic testing, two St. Jude bileaflet mechanical heart valves were placed into the testing fluid chamber to control the flow direction. The flow rate of the system was fixed at 5 L/min with a stroke volume of 80mL and stroke rate of 72 min^{-1}. The systolic /diastolic ratio was 0.375. Washed platelets were circulated in the chamber for 90 minutes and platelet surface P-selectin expression was examined every 15 minutes. For hemolysis measurement, whole blood was circulated through the two heart valves for 90 minutes and blood samples were taken every 15 minutes. The results demonstrated that the flow chamber did not induce hemolysis and platelet activation under static or dynamic conditions, with or without the St. Jude bileaflet mechanical heart valves. In parallel, a 3D computational fluid dynamics model was built to study the flow conditions in the flow chamber. The results indicated that the design of the flow chamber did not induce any turbulence in the testing fluid chamber (maximum Reynolds number was ~2100), which is desirable to study cellular functions. These results demonstrated the feasibility of using this flow chamber to study the hemodynamic performance of prosthetic heart valves.

ADVISER'S APPROVAL: Dr. Wei Yin